Compressive Sensing Over TV White Space in Wideband Cognitive Radio

by

Zhijin Qin

Doctor of Philosophy

School of Electronic Engineering and Computer Science
Queen Mary University of London
United Kingdom

June 2016

Acknowledgments

Foremost, I would like to express my sincere gratitude to my primary supervisor, Dr. Yue Gao, for his wise guidance, patience and continuous support of my Ph.D research. With his profound knowledge on digital signal processing and wireless communication, he offered many constructive advices and suggestions on my Ph.D research and the directions for my future work. I could not have imagined having a better supervisor and mentor for my Ph.D research.

I would also like to thank Professor Mark D. Plumbley and Professor Clive G. Parini, for their invaluable suggestions and comments for my research and scientific writing. From them, I learnt not only the technical knowledge, but also the crucial aspects of being a good researcher, namely, meticulousness, passion, intelligence, and hard work.

I would also like to express my appreciation to Professor Laurie G. Cuthbert, Professor Andrea Cavallaro, and all the colleagues and friends in antenna group and network group including Qianyun Zhang, Xiang Li, Guangwei Jiang, Muhammad Rafaqat Ali Qureshi, Darryl Smith, Dr. Patrick Bradley, Shaker Alkaraki, Dr. Yangjie Liu, Dr. Oleksandr Sushko, Aleksandr Ageyskiy, Peter Alizadeh, Yuanwei Liu, Jie Deng, Dr. Yue Liu, Dr. Nan Wang, Dr. Fei Peng, Dr. Dantong Liu, for their constant encouragement, insightful comments, valuable discussions and kind help.

I would also like to thank the committee for my viva defense: Professor Kin K. Leung, and Professor Hugh Griffiths, for their encouragement and insightful comments.

Finally, and most importantly, I would like to thank my beloved family, especially my parents. Meanwhile, this thesis is specially dedicated to my father, and may his soul rest in peace.

Abstract

Spectrum scarcity is an important challenge faced by high-speed wireless communications. Meanwhile, caused by current spectrum assignment policy, a large portion of spectrum is underutilized. Motivated by this, cognitive radio (CR) has emerged as one of the most promising candidate solutions to improve spectrum utilization, by allowing secondary users (SUs) to opportunistically access the temporarily unused spectrum, without introducing harmful interference to primary users. Moreover, opening of TV white space (TVWS) gives us the confidence to enable CR for TVWS spectrum. A crucial requirement in CR networks (CRNs) is wideband spectrum sensing, in which SUs should detect spectral opportunities across a wide frequency range. However, wideband spectrum sensing could lead to unaffordably high sampling rates at energy-constrained SUs. Compressive sensing (CS) was developed to overcome this issue, which enables sub-Nyquist sampling by exploiting sparse property. As the spectrum utilization is low, spectral signals exhibit a natural sparsity in frequency domain, which motivates the promising application of CS in wideband CRNs.

This thesis proposes several effective algorithms for invoking CS in wideband CRNs. Specifically, a robust compressive spectrum sensing algorithm is proposed for reducing computational complexity of signal recovery. Additionally, a low-complexity algorithm is designed, in which original signals are recovered with fewer measurements, as geolocation database is invoked to provide prior information. Moreover, security enhancement issue of CRNs is addressed by proposing a malicious user detection algorithm, in which data corrupted by malicious users are removed during the process of matrix completion (MC). One key spotlight feature of this thesis is that both real-world signals and simulated signals over TVWS are invoked for evaluating network performance. Besides invoking CS and MC to reduce energy consumption, each SU is supposed to harvest energy from

radio frequency. The proposed algorithm is capable of offering higher throughput by performing signal recovery at a remote fusion center.

Table of Contents

List of Figures

List of Tables

List of Abbreviations

ADC	Analog-to-Digital Conversion
AOP	Adaptive Outlier Pursuit
AWGN	Additive White Gaussian Noise
CoSaMP	Compressive Sampling Matching Pursuit
CR	Cognitive Radio
CRN	Cognitive Radio Network
CS	Compressive Sensing/Compressed Sensing
CSS	Cooperative Spectrum Sensing
DNRLS	Data-Assisted Non-Iteratively Reweighted Least Squares
DSA	Dynamic Spectrum Access
DSO	Digital Switch-Over
DTT	Digital Terrestrial Television
DVB-T	Digital Video Broadcasting-Terrestrial
FFT	Fast Fourier transform
FCC	Federal Communications Commission
FC	Fusion Center
IDFT	Inverse Digital Fourier Transform
i.i.d.	Independent and Identically Distributed
IRLS	Iteratively Reweighted Least Squares
MC	Matrix Completion
MIMO	Multi-Input and Multi-Output

MP	Matching Pursuit
MWC	Modulated Wideband Converter
NGR	National Grid Reference
NOMA	Non-Orthogonal Multiple Access
Ofcom	Office of Communications
OFDM	Orthogonal Frequency Division Multiplexed
OMP	Orthogonal Matching Pursuit
PMSE	Programme Making and Special Events
PB	Power Beacon
PU	Primary User
QMUL	Queen Mary University of London
RIP	Restricted Isometry Property
RF	Radio Frequency
ROC	Receiver Operating Characteristics
RTRMC	Riemannian trust-region for MC
SNR	Signal-to-Noise Ratio
SU	Secondary User
TVWS	TV White Space
UHF	Ultra High Frequency
WSD	White Space Device
WPT	Wireless Power Transfer

List of Symbols

E_H	Harvested energy
E_S	Consumed energy for spectrum sensing
$\mathbf{d}$	Decision on spectrum occupancy
$\mathcal{F}^{-1}$	Inverse Discrete Fourier Transform
$h\,(t)$	Channel coefficients in time domain
$\mathbf{h_f}$	Channel coefficients in frequency domain
$\mathbf{H_f}$	Channel coefficients in frequency domain in matrix format
$\mathcal{I}$	Number of channels among the spectrum of interest
$I_{\max}$	Maximal iteration number
$\mathbf{I}_N$	$N \times N$ identity matrix
J	Number of SUs sensing the same channel at different locations
K	Number of occupied channels, or sparsity level, or rank order of a matrix
$K_{\max}$	Statistical upper bound of the rank order K
$\hat{K}$	Estimated sparsity level K
L	Number of channels in a channel group
L_c	Number of corrupted channels
$\hat{L}_c$	Estimated number of corrupted channels
$\mathbf{M}$	Low-rank matrix
$\hat{\mathbf{M}}$	Recovered low-rank matrix
N	Number of samples at Nyquist rates
p	Norm

p_{ij}	Uncorrupted power value of the ith channel sensed by the jth SU
$\tilde{p}_{ij}$	Corrupted power value of the ith channel sensed by the jth SU
$\hat{p}_{ij}$	Recovered power value of the ith channel sensed by the jth SU
P	Number of compressed measurements
P_{as}	Average received power of the wanted DTT signal
P_d	Probability of detection
$\bar{P}_d$	Target probability of detection
P_f	Probability of false alarm
$\bar{P}_f$	Target probability of false alarm
P_{IB}	Maximum allowable EIRP
P_s	Sensing power
P_t	Transmission power
P_{out}	Power outage probability
P_s^{out}	Power outage probability of spectrum sensing
P_t^{out}	Power outage probability of data transmission
$\mathbf{P^{\Omega}}$	Complete matrix constructed at the FC
q_1	DTT receiver's location probability in the absence of interference
q_2	DTT receiver's location probability with the interference from WSDs
$r\,(t)$	Received signal in time domain
$\mathbf{r_f}$	Received signal in frequency domain
$\mathbf{R_f}$	Received signal in frequency domain in matrix format
$s\,(t)$	Transmitted signal in time domain
$\mathbf{s_f}$	Transmitted signal in frequency domain
$\hat{\mathbf{s}}_\mathbf{f}$	Recovered signal
$\mathbf{S_f}$	Transmitted signal in frequency domain in matrix format
$\hat{\mathbf{S}}_\mathbf{f}$	Recovered signal in matrix format
$w\,(t)$	Additive white Gaussian noise in time domain
$\mathbf{w_f}$	AWGN in frequency domain
$\mathbf{W_f}$	AWGN in frequency domain in matrix format
$\mathbf{W}$	Weights matrix for IRLS

$\tilde{\mathbf{W}}$	Newly constructed weights matrix for DNRLS
$\mathbf{x}$	Compressed measurements
$\mathbf{X}$	Compressed measurements in matrix format
α	Fraction of energy harvesting in one frame period
β	Fraction of spectrum sensing in one frame period
γ	Compression ratio
κ	Malicious user ratio
λ	Threshold for energy detection
$\mathbf{\Lambda}$	Binary matrix denoting the uncorrupted channels
$\mathbf{\Omega}$	Index set of the complete matrix
$\mathbf{\Phi}$	Measurement matrix
$\mathbf{\Psi}$	Sparsifying matrix
σ_s	Standard signal derivation
σ_n	Standard noise derivation
τ	Throughput
ε	Error tolerance

Chapter 1

Introduction

Radio frequency (RF) spectrum is a valuable but tightly regulated resource due to its unique and important role in wireless communications. The demand for RF spectrum is increasing due to a rapidly expanding market of multimedia wireless services, while the usable spectrum is becoming scarce due to current rigid spectrum allocation policies. Specifically, according to reports from the Federal Communications Commission (FCC) and the Office of Communications (Ofcom), localized temporal and geographic spectrum utilization is extremely low in reality [1, 2]. Cognitive radio (CR) has become a promising solution to solve the spectrum scarcity problem, by allowing secondary users (SUs) to opportunistically access a licensed band when the primary user (PU) is absent [3]. Additionally, it is demonstrated that TV spectrum, which used to be allocated to analog TV signals, has been cleaned and opened to access due to the digital switch-over (DSO) around the world [1, 2]. These underutilized TV spectra are named as TV white space (TVWS). Lately, FCC issued a report and order for permitting the cognitive usage of TVWS spectrum [4]. Most recently, Ofcom has enabled licence exempt use of TVWS to harness the benefits of such an innovative wireless technology [5], which motivates the further research on the cognitive access to TVWS spectrum.

In order to avoid any harmful interference to the PUs in TVWS, SUs in CR networks

(CRNs) should be aware of the spectrum occupancy over TV band. Spectrum sensing is the first and one of the most challenging tasks in CR, which is performed to detect the spectrum holes over TV spectrum. As the radio environment changes over time and space, an efficient spectrum sensing technique should be capable of tracking these fast changes [6]. A good approach for detecting the primary transmitters is to adopt the traditional narrowband sensing algorithms, which include energy detection, matched-filtering, and cyclostationary feature detection. Here, the term "narrowband" implies that the frequency range is sufficiently narrow, such that the channel frequency response can be considered as flat. In another word, the bandwidth of interest is less than the coherence bandwidth of the channel [7].

While the present spectrum sensing algorithms have focused on exploiting spectral opportunities over narrow frequency range, CRNs will eventually be required to exploit spectral opportunities over wide frequency range from hundreds of megahertz (MHz) to several gigahertz (GHz), in order to improve spectrum efficiency and achieve higher opportunistic throughput. In wideband spectrum sensing, as driven by the Nyquist sampling theory, a simple approach is to acquire the wideband signal directly by a high-speed analog-to-digital converter (ADC). So far, wideband spectrum sensing has been investigated in [8–11] with the implementation of a high-speed ADC. However, the high-speed ADC is particularly challenging or even unaffordable for energy-constrained devices, such as smart phones or even battery-free devices in a wireless power transfer (WPT) model [12]. Subsequently, Landau [13] demonstrated that sampling rate should be no less than the measure of occupied part of the spectrum, with the purpose of guaranteeing the stable reconstruction of multiband signals. However, the energy consumption is still unaffordable for energy-constrained SUs in CRNs. Therefore, revolutionary wideband spectrum sensing techniques become more than desired to release the burden on high-speed ADCs .

Recent developments on compressive sensing (CS) theory inspires sub-Nyquist sampling, by utilizing the sparse nature of signals [14]. Driven by the inborn nature of

the signal sparsity in wireless communications, e.g., the sparse utilization of spectrum, CS theory is capable of enabling sub-Nyquist sampling possible for wideband spectrum sensing. More particularly, CS theory has been firstly applied to wideband spectrum sensing by Tian and Giannakis [8], where fewer compressed measurements are required on the basis of Nyquist sampling theory. Subsequently, the application of CS theory on wideband spectrum sensing in CRNs has attracted much attention.

1.1 Motivations and Contributions

Along with the developments on CS theory, my Ph.D spans the sub-Nyquist based wideband spectrum sensing with particular emphasis on CS technique. These proposed algorithms are capable of improving the robustness and security of CRNs, with low computational complexity at energy-constrained SUs. The specific motivations and contributions of my Ph.D research are summarized in the following.

1.1.1 Robust Compressive Spectrum Sensing

With the use of CS at SUs, each SU would only collect compressed samples at sub-Nyquist sampling rate. Subsequently, signal recovery would be performed at SUs or a fusion center (FC), where the data from the spatially located SUs are fused. It is noticed that the signal-to-noise ratio (SNR) of the CS measurements would be decreased by 3dB for every octave increasing in the subsampling factor for acquisition of a noisy signal with fixed sparsity level [15]. This makes the exact signal recovery more difficult for compressive spectrum sensing under heavy channel noise. Therefore, a robust spectrum sensing algorithm based on CS with low computational complexity is needed.

As motivated by this, two robust compressive spectrum sensing algorithms are designed for the single SU case and the case with multiple SUs, respectively. The proposed algorithms contain two phases. In the case with single SU, where signal recovery is to be

performed at the SU locally, a new wideband channel division scheme is proposed to reduce the computational complexity of signal recovery in the first phase. In the second phase, a denoising algorithm is performed to improve detection performance by enabling the compressive spectrum sensing algorithm being more robust to channel noise. For the case with multiple cooperative SUs, where spatial diversity among participating SUs is utilized to improve the sensing performance [16, 17], the sparse property of spectral signals can be transformed into a low-rank property [18]. In the first phase, the proposed wideband channel division scheme is invoked to reduce the costs of signal acquisition at SUs. Subsequently, only the compressed measurements are sent to the FC, which reduces amount of transmission overhead in CRNs. Matrix completion (MC), as a further development of CS, is invoked at the FC to recover the unsensed channels from the sensed channels. In the second phase, detection performance is further improved by the proposed denoising algorithm. To this end, the proposed robust compressive spectrum sensing algorithm is tested on the real-world signals over TVWS after being validated by the simulated TV signals.

1.1.2 Data-Assisted Low-Complexity Compressive Spectrum Sensing

Besides the robustness to channel noise, adaptive compressive spectrum sensing with low complexity has attracted much attention [7]. Theoretically, the required number of measurements will proportionally change when the sparsity level of wideband signal varies. However, in practice, the sparsity level of wideband signal is uncertainty, because of either the dynamic activities of PUs or the time-varying fading channels between PUs and SUs. Consequently, most of sub-Nyquist wideband sensing systems should pessimistically choose the number of measurements to ensure exact recovery, leading to more energy consumption at SUs. Moreover, the computational complexity of signal recovery may be unaffordable for the energy-constrained SUs as it is dependent on the number of collected compressed measurements. Therefore, a low-complexity compressive spectrum sensing algorithm is needed, which should be adaptive to the dynamic spectrum

occupancy.

Inspired by the geolocation database for TVWS, which is another approach to make SUs aware of spectrum occupancy, a hybrid framework combining compressive spectrum sensing and geolocation database is proposed to achieve adaptive CS with low complexity. More specifically, a geo-location database algorithm is proposed to be implemented at SUs locally to provide prior information on the spectrum occupancy. As a result, SUs collect samples at the minimum rate without loss any information. Additionally, with the availability of prior information, a data-assisted non-iteratively reweighted least squares (DNRLS) based compressive spectrum sensing algorithm is proposed to reduce the computational complexity of signal recovery. In order to further improve accuracy and efficiency of the geolocation database algorithm implemented at SUs, an efficient approach for calculating the maximum allowable equivalent isotropic radiated power (EIRP) is proposed. Furthermore, the proposed hybrid framework and algorithms are tested on the real-world signal and data over TVWS after being approved by the simulated data.

1.1.3 Malicious User Detection Based on Matrix Completion

Along with improving the robustness, adaption and reducing the complexity of compressive spectrum sensing algorithm, another challenge for CRNs comes from the malicious users, which will send out dishonest data to degrade system performance. In current CSS networks, all cooperative SUs are assumed to be honest and genuine. However, the existence of malicious users would severely degrade the performance of cooperative spectrum sensing (CSS) networks. Moreover, malicious users can degrade the detection performance heavily in sub-Nyquist based CSS networks. If part of the compressed measurements are corrupted by malicious users, signal recovery would be unstable at the FC.

In order to guarantee the security of CSS networks, a malicious user detection frame-

work is proposed by invoking the low-rank MC technique. More specifically, with the purpose of improving the detection accuracy and reducing the costs of data acquisitions at SUs, the data corrupted by malicious users are removed during the MC process at the FC. Additionally, in order to avoiding requiring any prior information of the CSS networks, a rank order estimation algorithm and a malicious user number estimation strategy are proposed. The proposed framework is tested on the real-world signals over TVWS after being validated by the simulated TV signals. Numerical results show that the proposed malicious user detection framework achieves higher detection accuracy with lower costs of data acquisition at SUs or less number of active SUs.

1.1.4 Wireless Powered Cognitive Radio Networks

Along with the invoking of CS technique to reduce the energy consumption at energy-constrained SUs, energy harvesting provides another approach to improve the energy efficiency at SUs. Different from harvesting energy from traditional energy sources (e.g., solar, wind, water, and other physical phenomena) [19], the emerging WPT further underpins the trend of green communications by harvesting energy from RF [20].

In wireless powered CRNs, CS and MC techniques are invoked for improving the energy efficiency and spectrum efficiency. With the purpose of optimizing the throughput in wireless powered CRNs, a new frame structure design is proposed, in which sub-Nyquist sampling is performed at SUs. The throughput of CRNs is optimized by scheduling the time slots for energy harvesting, spectrum sensing, data transmission and transmission power of SUs. As sub-Nyquist sampling is performed at SUs, time slot allocated to spectrum sensing would be reduced significantly, which allows more time for energy harvesting and data transmission. Additionally, CS and MC techniques are invoked to perform the signal recovery at a remote data FC, which allows SUs perform energy harvesting again before data transmission. Throughput optimization of the proposed frame structure is formulated into two linear constrained problems with the purpose of maximizing the throughput of a single SU and the whole cooperative networks,

respectively. The formulated problems are solved by using three different methods to obtain the maximal achievable throughputs. Numerical results show that the proposed frame structure design outperforms the traditional one in terms of throughput.

1.2 Publications

- Journal Papers

1. **Z. Qin**, Y. Gao and C. Parini, "Data-assisted Low Complexity Compressive Spectrum Sensing on Real-time Signals under Sub-Nyquist Rate," *IEEE Transactions on Wireless Communications*, pp.1174-1185, Feb. 2016.

2. **Z. Qin**, Y. Gao, M. Plumbley and C. Parini, "Wideband Spectrum Sensing on Real-time Signals at Sub-Nyquist Sampling Rates in Single and Cooperative Multiple Nodes," *IEEE Transactions on Signal Processing*, pp. 3106-3117, Jun. 2016.

3. Y. Gao, **Z. Qin**, Z. Feng, Q. Zhang, O. Holland and M. Dohler, "Scalable & Reliable IoT Enabled By Dynamic Spectrum Management for M2M in LTE-A," *IEEE Internet of Things*, 2016 (to appear).

4. **Z. Qin**, Y. Liu, Y. Gao, M. Elkashlan and A. Nallanathan, "Throughput Analysis of Wireless Powered Cognitive Radio Networks with Compressive Sensing and Matrix Completion," 2016 (under review).

5. Y. Liu, **Z. Qin**, M. Elkashlan, Y. Gao and L. Hanzo, "Enhancing the Physical Layer Security of Non-orthogonal Multiple Access in Large-Scale Networks," 2016 (under review).

6. **Z. Qin**, Y. Gao and M. Plumbley, "Malicious User Detection Based on Low-Rank Matrix Completion in Secure Cooperative Spectrum Sensing,"2016 (under review).

- Conference Papers

1. Y. Liu, **Z. Qin**, M. Elkashlan, Y. Gao, and A. Nallanathan, "Non-orthogonal Multiple Access in Massive MIMO Aided Heterogeneous Networks," in *Proc. IEEE Global Communications Conference (GLOBECOM'16)*, Washington, DC, 2016 (to appear).

2. Y. Gao, and **Z. Qin**, "Implementation of Compressive Sensing with Real-Time Signals over TV White Space Spectrum in Cognitive Radio", the IEEE Vehicular Technology Conference, VTC2016-Fall, Canada, 2016 (To appear)

3. **Z. Qin**, Y. Liu, Z. Ding, Y. Gao and M. Elkashlan, "Physical Layer Security for 5G Non-orthogonal Multiple Access in Large-scale Networks," in *Proc. IEEE International Conference on Communications (ICC'16)*, May 2016.

4. O. Holland, S. Wong, **Z. Qin** and Y. Gao, "Virtualized VHF/UHF Transmission Paired with Mobile Access for the Tactile Internet," in *Proc. International Conference on Telecommunications (ICT'16)*, Thessaloniki, 2016, pp. 1-5..

5. **Z. Qin**, Y. Liu, Y. Gao, M. Elkashlan and A. Nallanathan, "Throughput Analysis for Compressive Spectrum Sensing with Wireless Power Transfer," in *Proc. IEEE Global Communications Conference (GLOBECOM'15)*, San Diego, CA, Dec. 2015, pp.1-6.

6. O. Holland, S. Ping, A. Aijaz, J. Chareau, P. Chawdhry, Y. Gao, **Z. Qin** and H. Kokkinen, "To white space or not to white space: That is the trial within the Ofcom TV white spaces pilot," in *Proc. IEEE International Symposium on Dynamic Spectrum Access Networks (DYSPAN'15)*, Stockholm, Sweden, Sep. 2015, pp.11 - 22.

7. O. Holland, S. Ping, N. Sastry, P. Chawdhry, J. Chareau, J. Bishop, H. Xing, S. Taskafa, A. Aijaz, M. Bavaro, P. Viaud, T. Pinato, E. Angiuli, M. Akha-

van, J. McCann, Y. Gao, **Z. Qin**, Q. Zhang, R. Knopp, F. Kaltenberger, D. Nussbaum, R. Dionisio, J. Ribeiro, P. Marques, J. Hallio, M. Jakobsson, J. Auranen, R. Ekman, H. Kokkinen, J. Paavola, A. Kivinen, T. Solc, M. Mohorcic, H. Tran, K. Ishizu, T. Matsumura, K. Ibuka, H. Harada, K. Mizutani, "Some Initial Results and Observations from a Series of Trials within the Ofcom TV White Spaces Pilot", in *Proc. IEEE Vehicular Technology Conference (VTC-Spring'15)*, Glasgow, UK, May 2015, pp.1-7.

8. **Z. Qin**, L. Wei, Y. Gao and C. Parini, "Compressive Spectrum Sensing Augmented by Geo-location Database," in *Proc. IEEE Wireless Communications and Networking Conference Workshops (WCNC'15)*, New Orleans, Mar. 2015, pp.170-175.

9. **Z. Qin**, Y. Gao, M. Plumbley and C. Parini, "Efficient Compressive Spectrum Sensing Algorithm for M2M Devices," in *Proc. IEEE Global Conference on Signal and Information Processing (GlobalSIP'14)*, Atlanta, GA, Dec. 2014, pp. 1170-1174.

10. X. Zhang, **Z. Qin** and Y. Gao, "Dynamic Adjustment of Sparsity Upper Bound in Wideband Compressive Spectrum Sensing," in *Proc. IEEE Global Conference on Signal and Information Processing (GlobalSIP'14)*, Atlanta, GA, Dec. 2014, pp.1382-1386.

11. **Z. Qin**, Y. Gao, M. Plumbley, C. Parini and L. Cuthbert, "Low-Rank Matrix Completion based Malicious User Detection in Cooperative Spectrum Sensing," in *Proc. IEEE Global Conference on Signal and Information Processing (GlobalSIP'13)*, Austin, TX, Dec. 2013, pp.1186-1189.

12. **Z. Qin**, N. Wang, Y. Gao and L. Cuthbert, "Adaptive Threshold for Energy Detector Based on Discrete Wavelet Packet Transform," in *Proc. Wireless Technology Symposium (WTS'12)*, London, UK, April 2012, PP.1-5. (**Best Paper Award**)

1.3 Outline of the Thesis

Chapter 2 covers background of the CS and MC techniques, and their applications in CRNs. Additionally, the fundamental concept of TVWS is introduced.

Chapter 3 proposes a robust compressive spectrum sensing algorithm for the cases of a single SU and multiple cooperative SUs, respectively. Performance is verified by both the simulated signals and real-world signals to show the effectiveness and robustness of the proposed algorithm.

Chapter 4 presents a low-complexity compressive spectrum sensing framework with prior information from geolocation database for TVWS. Performance of the proposed framework is verified by both the simulated and the real-world data.

Chapter 5 designs malicious user detection framework based on low-rank MC. Numerical results validate the effectiveness and robustness of the proposed approach.

Chapter 6 investigates the throughput optimization of wireless powered CRNs, with invoking of CS and MC techniques for improving the achievable throughput. Numerical results are presented to show the effectiveness of the proposed frame structure.

Chapter 7 draws the conclusions and a plan for future work.

Chapter 2

Background

This chapter provides an overview of the background knowledge used in this thesis, including basic principles of CS and MC techniques, CR, compressive spectrum sensing, and dynamic spectrum access (DSA) to TVWS.

2.1 Compressive Sensing

CS theory, as proposed by David Donoho, Emmanuel J. Candes, Justin Romberg and Terence Tao, states that certain signals are able to be recovered from far fewer samples or measurements than the samples required by Nyquist sampling theory [14, 21–23]. The key concepts of CS theory include two principles: 1) sparsity, which requires the signals to be recovered should be able to be represented in a certain sparse domain; 2) Incoherence, which refers to extract the maximum information using the minimum number of measurements. In this following, the CS theory is introduced in detail.

2.1.1 Compressible Signals

Generally speaking, sparse signals are those that contain much less information than their ambient dimension suggests. Sparsity of a signal is defined as the number of non-zero elements in the signal under certain domain. Let us define $\mathbf{f}$ as an N-dimensional signal of interest, $\mathbf{\Psi} \in \mathcal{C}^{N \times N}$ is the orthonormal transformation basis where $\mathbf{f}$ is sparse, and $\mathbf{s}$ is the sparse representation of $\mathbf{f}$ over the basis $\mathbf{\Psi}$. Therefore, signal $\mathbf{f}$ can be given by

$$\mathbf{f} = \mathbf{\Psi}\mathbf{s}. \tag{2.1}$$

Apparently, $\mathbf{f}$ can be the time or space domain representation of a signal, and $\mathbf{s}$ is the equivalent representation of the same signal in the $\mathbf{\Psi}$ domain. Signal $\mathbf{f}$ is said to be K-sparse in $\mathbf{\Psi}$ domain as there are only K out of the N coefficients in $\mathbf{s}$ that are non-zero. The study of CS is mainly focused on the case where $K \leq N$. In practice, the condition for sparse signal is relaxed to the following: if the representation (2.1) has a few large coefficients and many small coefficients, signal $\mathbf{f}$ is considered as sparse. Here, the implication of sparsity is that one can discard the small coefficients without much perceptual loss, when a signal has a sparse expansion.

In traditional data acquisition systems (for example, digital cameras), the full signal $\mathbf{f}$ with N samples is acquired firstly. Subsequently, the complete set of transform coefficients is computed via $\mathbf{s} = \mathbf{\Psi}^T\mathbf{f}$. Then the K largest coefficients are located and the $(N - K)$ smallest coefficients are discarded. Meanwhile, the values and locations of the K largest coefficients are encoded. Unfortunately, this sample-then-compress framework suffers from three inherent areas of inefficiency. First, the initial number of samples N may be large even if the desired K is small. Second, the set of all N transformation coefficients in $\mathbf{s}$ must be computed even though all but K of them will be discarded. Third, the locations of the large coefficients must be encoded, thus introducing an overhead [24]. For such a case, it is naturally to think whether there is an approach to obtaining the compressed signal directly.

2.1.2 Compressed Measurements

If a signal is able to be represented in a certain sparse domain, CS technique can be invoked to obtain the compressed signal, by taking only a small amount of linear and non-adaptive measurements [21, 23]. Specifically, when an analog signal arrives, it should be processed by the measurement matrix to get the compressed version of the signal. Let us define $\mathbf{\Phi}$ as an $P \times N$ measurement matrix, where $P \leq N$. Then the compressed samples to be collected can be expressed as

$$\mathbf{x} = \mathbf{\Phi f} = \mathbf{\Phi \Psi s} = \mathbf{\Theta s}, \tag{2.2}$$

where $\mathbf{\Theta} = \mathbf{\Phi \Psi}$ is a $P \times N$ matrix. As $\mathbf{\Phi}$ is independent on signal $\mathbf{f}$, the projection process is non-adaptive. The key of CS theory is finding out a stable basis $\mathbf{\Theta}$ or measurement matrix $\mathbf{\Phi}$ to allow the exact recovery of the length-N signal from P measurements. This seems an undetermined problem. However, if $\mathbf{s}$ is K-sparse, and the restricted isometry property (RIP) is satisfied, as given in the following, the exact recovery is possible [22, 23].

Definition 1. *Restricted Isometry Property (RIP): For any vector $\boldsymbol{v}$ sharing the same K non-zero elements as $\boldsymbol{s}$, if*

$$1 - \varepsilon \leq \frac{\|\mathbf{\Theta v}\|_2}{\|\mathbf{v}\|_2} \leq 1 + \varepsilon. \tag{2.3}$$

for some ε, then the matrix $\mathbf{\Theta}$ preserves the information of the K-sparse signal.

An alternative approach to guarantee the stability of $\mathbf{\Theta}$ is to ensure that the measurement matrix $\mathbf{\Phi}$ is incoherent with the sparsifying basis $\mathbf{\Psi}$. More specifically, incoherence property requires that the rows of $\mathbf{\Phi}$ cannot sparsely represent the columns of $\mathbf{\Psi}$ and vice verse. However, in practice, the RIP condition and incoherence property are computationally complex to verify [24].

By following the RIP condition for exact recovery, different types of measurement matrices have been investigated, with consideration of the universality, recovery com-

plexity, recovery speed, minimum number of measurements required exact recovery, and the implementation costs. The common measurement matrices include random matrices and structured matrices, which are discussed in detail as following.

2.1.2.1 Random Matrices

It is pointed out that both the RIP and incoherence property can be achieved with high probability simply by selecting Φ as a random matrix [24]. The common random matrices include Gaussian matrix [25], Bernoulli matrix [26], or almost all others matrices which are independent and identically distributed (i.i.d.). It has been approved that an $P \times N$ Gaussian i.i.d. random measurement matrix guarantees exact recovery if $P \geq cK \log(N/K)$ [22, 23]. Besides, with the properties of Gaussian i.i.d distributed matrix $\mathbf{\Phi}$, the matrix $\mathbf{\Theta} = \mathbf{\Phi\Psi}$ also follows Gaussian i.i.d. distribution, regardless of the choice of $\mathbf{\Psi}$. Therefore, the random matrices are universal as they are random enough to be incoherent with any sparsifying matrix. Additionally, for Gaussian random matrices, the number of compressed measurements required for exact reconstruction is almost minimal. However, random matrices inherently have two major drawbacks in practical applications: huge memory buffering for storage of matrix elements, and high computational complexity due to their completely unstructured nature [27].

2.1.2.2 Structured Random Matrices

The classic structured random matrices include random demodulator [28], modulated wideband converter (MWC) [29] and multi-coset sampler [30], which are introduced in detail in the following. As they are well structured, the computational complexity is relatively low and physically implementable. However, the main drawbacks of structured random matrices are that they are harder to analyze.

- **Random demodulator** [28]: As shown in Fig. 2.1(a), the random demodulator consists of a pseudo-random number generator, a mixer, an accumulator, and a

low-rate sampler. When the signal $r(t)$ arrives, it is demodulated by the mixer, which multiples the signals with a high-rate pseudo-random sequence. As a result, the tones are smeared across the entire spectrum. Subsequently, the demodulated signal is summed by the accumulator for every $1/R$ seconds, where R is the sub-Nyquist sampling rate which is much lower than the Nqyuist sampling rate. Additionally, a low-rate ADC sampler is implemented to capture the signal by sampling it at a relatively low rate. The main advantage of this approach is that it bypasses the need for a high-rate ADC, thus allowing the use of robust, low-power and readily available components. Unfortunately, it has been identified that signal recovery performance of the random demodulator is computationally intensive, as the recovery process is highly nonlinear.

- **MWC** [29]: In the MWC, a parallel channel structure is proposed by implementing multiple sampling channels. Each sampling channel contains a general low-pass filter to replace the accumulator. As shown in Fig. 2.1(b), the analog signal is firstly multiplied with a periodic waveform, whose period corresponds to the multiband model parameters. Subsequently, the product is low-pass filtered and sampled uniformly at a low rate. One significant benefit of introducing a parallel channel structure is that the dimension of the measurement matrix is reduced, making the spectral reconstruction more computationally efficient. Besides the theory analysis, the implementation of MWC has been built on existing hardware devices as the first sub-Nyquist sampling demonstration system for handling wideband analog signals. However, the implementation is specifically designed for MWC, and it is difficult to extend the implementation to make it match well with the other existing CS algorithms.

- **Multi-coset sampler** [30]: An alternative multichannel sub-Nyquist sampling approach is multi-coset sampling. As shown in Fig. 2.1(c), multi-coset sampler chooses some samples from a uniform grid, which can be obtained by using a sampling rate f_s higher than the Nyquist rate. The uniform grid is then divided

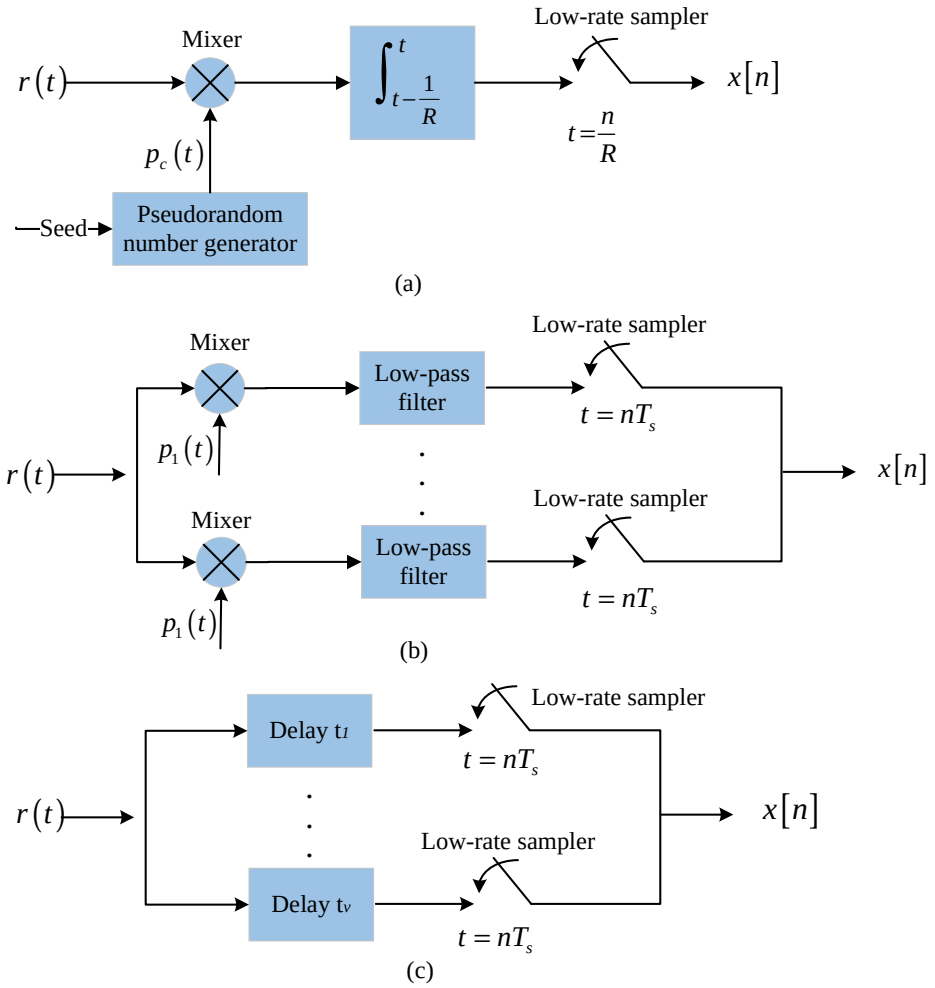

Figure 2.1: Block diagrams for measurement matrices: a) random demodulator; b) modulated wideband converter; c) multi-coset sampler.

into blocks of m consecutive samples, and in each block v ($v < m$) samples are retained, while the rest of samples are skipped. Thus, multi-coset sampler is normally implemented by using v sampling channels with sampling rate of f_s/m, which is m times lower than the Nyquist rate. Moreover, among the different sampling channels, different time offsets are invoked. To obtain a unique solution for the wideband spectrum from the partial measurements, the sampling pattern should be carefully designed. Therefore, one drawback of the multi-coset sampler is that accurate time offsets between sampling channels should be satisfied for robust spectral reconstruction.

2.1.3 Signal Reconstruction

After the compressed measurements are collected, the original signal should be recovered. For signal reconstruction, since most of the basis coefficients in $\mathbf{s}$ are negligible, an estimation of it can be obtained by finding out the minimum set of coefficients that match the set of compressed measurements $\mathbf{x}$. Therefore, if the RIP holds, the original signal is able to be reconstructed by solving

$$\min \|\hat{\mathbf{s}}\|_p, \text{ subject to } \boldsymbol{\Theta}\hat{\mathbf{s}} = \mathbf{x}, \tag{2.4}$$

where $p = 0$. Since the l_0-norm of vector $\mathbf{s}$ counts the number of non-zero elements, it is both numerically unstable and NP-hard [14].

Another classical approach to this type of inverse problems is to find the vector in the translated null space with the smallest l_2 norm. The closed-form solution can be given as $\hat{\mathbf{s}} = \boldsymbol{\Theta}^{\mathbf{T}}\left(\boldsymbol{\Theta}\boldsymbol{\Theta}^{\mathbf{T}}\right)^{-1}\mathbf{x}$. Unfortunately, l_2 minimization will almost never find a K-sparse solution, returning instead a non-sparse $\boldsymbol{\Theta}\hat{\mathbf{s}}$ with many non-zero elements [14].

So far, there are two types of relaxations to problem (2.4) to find a sparse solution. The first type is convex relaxation, which leads to l_1 minimization, also named as basis pursuit (BP) [31]. Another type of solution is to use greedy algorithms.

2.1.3.1 l_1-Norm Minimization

By invoking l_1-norm minimization, the original signal is able to be reconstructed by choosing $p = 1$ in (2.4). With the existence of noise, the signal reconstruction problem becomes

$$\min \|\hat{\mathbf{s}}\|_1, \text{ subject to } \|\boldsymbol{\Theta}\hat{\mathbf{s}} - \mathbf{x}\|_2 < \varepsilon, \tag{2.5}$$

where ε refers to the noise tolerance level. It has been proved that a length-N signal can be reconstructed from the P samples by BP, if $P \geq cK \log(N/K)$ for some absolute

Table 2-A: Compressive sensing solvers

Problems	Solvers
$\min \|\mathbf{s}\|_1,\ \text{subject to}\ \mathbf{\Theta s} = \mathbf{x}$	LP [35]
$\min \|\mathbf{s}\|_1,\ \text{subject to}\ \|\mathbf{\Theta s} - \mathbf{x}\|_2 \leq \varepsilon$	NESTA [36], SPGL1 [37]
$\min \left(\frac{1}{2} \|\mathbf{\Theta s} - \mathbf{x}\|_2^2 + \lambda \|\mathbf{s}\|_1 \right)$	FPC [38], Bregman [39], SpaRSA [40]
$\min \|\mathbf{\Theta s} - \mathbf{x}\|_2^2,\ \text{subject to}\ \|\mathbf{s}\|_1 \leq \varepsilon$	SPGL1 [37]

constant c [22, 23]. However, numerical experiments suggest that most K-sparse signals can be recovered exactly once $P \geq 4K$. Based on this, a strengthened RIP is proved by Candes and Tao [32]. It is supposed that $\mathbf{\Theta}$ obeys the RIP, if every collection of $4K$ columns of it are almost orthogonal and the top $4K$ singular values range from 0.9 to 1.1. In this case, any given K-sparse signal $\mathbf{s}$ can be recovered from $\mathbf{\Theta s}$ by BP. Therefore, it can be concluded that if the measurement matrix $\mathbf{\Theta}$ satisfies the RIP, the convex optimization problem with l_1-norm and that with l_0-norm have the same solution.

An easy way to solve the l_1-norm optimization is to use a general-purpose convex programming toolbox, such as the cvx toolbox maintained by Stanford [33]. However, when the problem size becomes large, such a toolbox normally requires a considerable length of computational time. To reduce the time, the proper structures of different optimization problems and the suitable solvers have been investigated and summarized in Table 2-A. The details of these CS solvers can be found in [34].

2.1.3.2 Greedy Algorithms

Greedy algorithms provide another approach for sparse recovery by finding out the supports of signal x iteratively. Existing greedy algorithms include various matching pursuits (MP) [41], orthogonal matching pursuits (OMP) [42], compressive sampling matching pursuit (CoSaMP) [43], etc. Taking OMP as an example, the residual $\mathbf{r_d}$ is defined as

$$\mathbf{r_d} = \mathbf{x} - \Phi \mathbf{s}. \tag{2.6}$$

At each iteration, the observation vector is set as $\mathbf{s} = \Phi^* \mathbf{r_d}$, based on that $\Phi^* \Phi \mathbf{s}$ is a good local approximation of $\mathbf{s}$. Then the coordinate of the observation vector's largest coefficient is added to index set $\mathbf{I}$. Subsequently, by solving a least-squares problem

$$\mathbf{s} = \arg \min_{\mathbf{s} \in R^I} \|\mathbf{x} - \Phi \mathbf{s}\|_2, \tag{2.7}$$

the residual is updated to remove this coordinate's contribution. These iterations are repeated K times, and then yields an index set of K coordinates corresponding to the support of signal $\mathbf{s}$. It is proved that OMP is capable of recovering a sparse signal with high probability [41].

In general, l_1-norm minimization outperforms greedy algorithms in the sense of recovered mean square error for sparse reconstruction. However, greedy algorithms are still popular and well accepted as they are straightforward for hardware implementations and thus suitable for embedded and real-time architectures. For example, [44] offered FPGA implementation examples.

2.1.3.3 Other Approaches Towards Sparse Recovery

Besides the aforementioned l_1-norm minimization and greedy algorithms, there are a number of computational approaches for solving the original sparse recovery problem (2.4).

1. l_p-norm minimization: One approach is to relax the l_0-norm to l_p-norm, where $p \in (0, 1)$. The l_p minimization problem is non-convex and it is more difficult to solve than l_1 optimization. However, it is able to recover the original sparse signal with fewer measurements [45, 46]. Meanwhile, l_p minimization can also increase the robustness against noise as well as signal recovery stability. Iteratively re-weighted least-square (IRLS) has been proposed to compute local minima of the l_p-norm minimization problem [47, 48].

2. Sparse Bayesian framework: Another approach is to adopt the Bayesian framework

to solve the CS problem. It has been pointed that the performance of l_1 minimization and greedy algorithms would become poor when the restrictions for CS are not satisfied well. Additionally, it has been proved that the iterative reweighted l_1 minimization can provide the sparsest solution [49, 50]. In order to obtain the sparsest solution, sparse Bayesian framework has been proposed to be invoked in CS as an equivalent to iterative reweighted l_1 minimization. More particularly, in sparse Bayesian framework, a prior distribution for the unknown vector is assumed to improve the recovery performance with fewer measurements, especially for the cases where the correlation of rows in the measurement matrix is high, noise level is high, or the sparsity of signal $\mathbf{s}$ is poor [51, 52]. The more details of sparse Bayesian framework based CS model is out of the scope of this thesis but can be found in [51, 52].

2.2 Compressive Sensing in Matrix Form

2.2.1 Distributed Compressive Sensing

In a typical setup, large groups of cheap and individually unreliable nodes may collaborate to perform a variety of data processing tasks, such as sensing, data collection, classification, modeling, tracking, and so on. In such type of networks, each individual node is normally energy-constrained. Therefore, they are sensitive to energy consumption and crucial to the reduction of data transmission costs. It is noted that, in most cases, the signal received at each individual sensor is itself sparse. Thus, the CS framework can be utilized to encode and decode each one separately. However, it is further noticed that data of sensors networks and arrays exhibit strong spatial correlations, which exhibits a joint sparsity property. Based on the concept of joint sparsity, distributed CS [53] is proposed to reduce the data transmission costs substantially, and thus enhancing battery life.

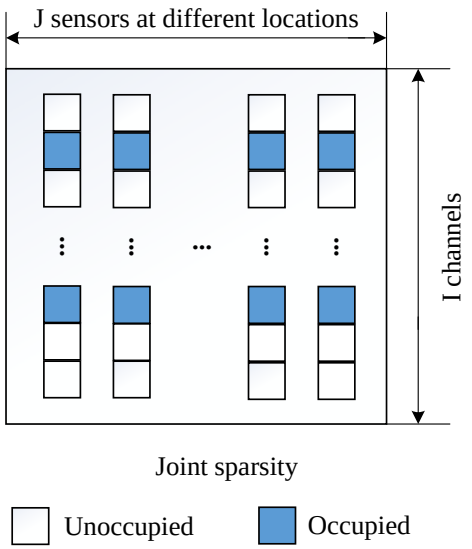

Figure 2.2: Joint sparsity illustration of a matrix.

An illustration of joint sparsity can be given as signals received at different sensors share common sparse supports. As shown in Fig. 2.2, the signal received at each sensor is supposed to be sparse in frequency domain, as only a few channels are occupied. For the matrix constructed at a data FC, the columns of it share the common sparse supports even though each sensor operates without cooperation. Additionally, it is noted that the samples of the same channel received at different locations are various, which is caused by the fading variance at different locations. Existing distributed CS solvers include Simultaneous Orthogonal Matching Pursuit (SOMP) [54] and multiple measurement vector (MMV) Order Recursive Matching Pursuit (M-ORMP) [55].

2.2.2 Matrix Completion

In many practical problems, one wants to recover a matrix from a sampling of its entries, in which some of the observations are missed or corrupted by malicious errors and noise. Normally, the matrix to be recovered is known to be structured in the sense that it is low-rank or approximately low-rank, e.g. matrix with I rows and J columns has rank K if its rows or columns span an K-dimensional space. Different from CS, which utilize the sparsity property of signals under ceratin basis, MC utilizes the sparsity property

of the matrix's singular values, which is named as low rank property. Furthermore, it is pointed out that the joint sparsity can be transformed into low-rank property of a matrix. Here, the low-rank MC model proposed by Candes in [56] is introduced.

The singular value decomposition of a $I \times J$ matrix $\mathbf{M}$ with rank K can be given by

$$\mathbf{M} = \sum_{k=1}^{K} \sigma_k u_k v_k^*, \tag{2.8}$$

where the u_k and v_k are the left and right singular vectors, and the σ_k are the singular values, which are square roots of eigenvalues of matrix $\mathbf{M}$. A generic low-rank matrix can be regard as: the family $\{u_k\}_{1 \leq k \leq K}$ is selected uniformly at random among all families of K orthogonal vectors, and similarly for the family $\{v_k\}_{1 \leq k \leq K}$. In a general MC problem, we try to recovery matrix $\mathbf{M}$ from a subset $\mathbf{\Omega}$ of its elements. The MC problem can be formulated as

$$\begin{aligned} &\min \ \text{rank}(\hat{\mathbf{M}}), \\ &\text{subject to } \ \hat{\mathbf{M}}_{ij} = \mathbf{M}_{ij} \quad (i,j) \in \mathbf{\Omega}, \end{aligned} \tag{2.9}$$

where $\hat{\mathbf{M}}$ is the reconstructed matrix, and rank $\left(\hat{\mathbf{M}}\right)$ is defined as the number of singular values of $\hat{\mathbf{M}}$. If the rank of a matrix is K, this matrix has exactly K non-zero singular values. Therefore, the rank function in (2.9) is simply counting the number of nonvanishing singular values. However, the matrix rank function is non-convex. As a result, the rank minimization in (2.9) is an NP-hard problem [14]. Similar as in CS model that l_1-norm minimization is considered as a good approximation of l_0-norm minimization, nuclear-norm minimization is taken as a good approximation for rank minimization. Accordingly, the MC problem can be formulated as

$$\begin{aligned} &\min \ \left\|\hat{\mathbf{M}}\right\|_*, \\ &\text{subject to } \ \hat{\mathbf{M}}_{ij} = \mathbf{M}_{ij} \quad (i,j) \in \mathbf{\Omega}, \end{aligned} \tag{2.10}$$

where $\left\|\hat{\mathbf{M}}\right\|_*$ is denoted as the sum of singular values of $\hat{\mathbf{M}}$.

So far, numerous MC solvers have been developed for solving problem (2.10). Existing MC solvers include, but not limited to, cvx [33], SVT [57], APGL [58] and FPCA [59].

If the rank K of the matrix $\mathbf{M}$ is known in advance, (2.9) can also be approximated by

$$\begin{aligned} &\min \ \left\| \mathcal{P}_{\mathbf{\Omega}} \left(\hat{\mathbf{M}} \right) - \mathcal{P}_{\mathbf{\Omega}} \left(\mathbf{M} \right) \right\|_F, \\ &\text{subject to } \operatorname{rank} \left(\hat{\mathbf{M}} \right) \leq K, \end{aligned} \tag{2.11}$$

where $\mathcal{P}_{\mathbf{\Omega}}$ stands for the projection onto the subspace of matrices with non-zeros restricted to the index subset $\mathbf{\Omega}$, and $\|\cdot\|_F$ refers to the Frobenius norm, which is defined as

$$\|\mathbf{A}\|_F = \sqrt{\sum_{i=1}^{I} \sum_{j=1}^{J} |\mathbf{A}_{ij}|^2}, \tag{2.12}$$

for any matrix $\mathbf{A} = (\mathbf{A}_{ij})_{I \times J}$. The existing MC solvers that are suitable for problem (2.11) include, but not limited to, OPTSPACE [60], ADMiRA [61], LMaFit [62] and RTRMC [63].

2.3 Applications of Compressive Sensing in Cognitive Radio

The last decade has witnessed the rapid explosion of wireless devices all over the world, which gives rise to the increasing demand for wireless spectral resource. As reported by FCC and Ofcom [1, 2], there are significant temporal and spatial variations in the allocated spectrum. Given this fact, CR has been proposed as an intelligent system to detect spectrum holes for unlicensed usage [3]. More specifically, the basic idea of CR is to match the requirements of higher layer applications or users with the available resources. The available resources include available power, spectrum and other resources that can be utilized by unlicensed SUs. CR is a radio that is capable of sensing the available resources and learning from the user behaviours and its previous decisions and mistakes, in order to provide a better response to the new resource request from SUs. So far, CR has been widely investigated [64].

2.3.1 Spectrum Sensing Methods

In CR, spectrum sensing is one of the most challenging tasks, which allows SUs to have the knowledge of spectrum occupancy. Once a spectrum hole is detected, SUs can make use of it for data transmission. Spectrum sensing requires high accuracy and low complexity for DSA [65]. There is extensive research work on spectrum sensing techniques being carried out. Many theoretical models for spectrum sensing techniques have been proposed, such as matched filter detection, cyclostationary feature detection, and energy detection. The matched filter detection is an optimal detection method that requires the prior information of PUs [66]. However, it requires SUs to have a dedicated sensing receiver for each type of PU signals. Cyclostationary feature detection can distinguish the PUs and noise by utilizing the periodicity in the received primary signal. However, it requires high computational complexity and prior information of the primary signals. Among these three approaches for spectrum sensing, energy detection is a non-coherent detection method, which avoids the requirement for prior knowledge of PUs. Additionally, energy detection approach does not require complicated receivers as the other two approaches do. Therefore, it is easy to be implemented, and the computational complexity is relatively low, but with a drawback of poor detection performance under low SNR scenarios. In this thesis, energy detection is adopted due to its simplicity.

2.3.2 Spectrum Sensing Model

In spectrum sensing, the received signal can be expressed as

$$r(t) = s(t) + w(t), \tag{2.13}$$

where $s(t)$ is the signal to be detected, $w(t)$ is the Additive White Gaussian Noise (AWGN) samples with noise variance σ_n^2. It is noted that $s(t) = 0$ when there is no

transmission by PU. The energy of sensed signals can be writhen as

$$E = \int_0^T |r(t)|^2 dt, \tag{2.14}$$

where T is the sensing period. When Nyquist sampling is performed, N samples are collected during one sensing period T. The decision on spectrum occupancy can be obtained by comparing the energy E of the received signal with a threshold λ. Particularly, the sensing decision can be formulated into a binary hypothesis problem

$$\begin{aligned} \mathcal{H}_0 &: r(t) = w(t), \\ \mathcal{H}_1 &: r(t) = s(t) + w(t), \end{aligned} \tag{2.15}$$

where $\mathcal{H}_0$ and $\mathcal{H}_1$ denote the hypothesis that PU is absent and present, respectively.

Additionally, the performance of energy detection algorithm can be measured by two probabilities: probability of detection P_d and probability of false alarm P_f. P_d is the probability of detecting a signal on the considered frequency when it actually is present. P_f is the probability that the test incorrectly decides that the considered frequency is occupied when it actually is not. With a target probability of false alarm $\bar{P}_f$, the threshold λ is given by

$$\lambda = \sigma_n^2 \left(1 + \frac{Q^{-1}\left(\bar{P}_f\right)}{\sqrt{N/2}} \right). \tag{2.16}$$

If the target probability of detection $\bar{P}_d$ is given, the threshold can be calculated as

$$\lambda = \left(\sigma_s^2 + \sigma_n^2\right) \left(1 + \frac{Q^{-1}\left(\bar{P}_d\right)}{\sqrt{N/2}} \right), \tag{2.17}$$

where σ_s^2 refers to the power of the transmitted primary signal.

2.3.2.1 Cooperative Spectrum Sensing

In practice, many factors such as multipath fading, shadowing may significantly degrade the detection performance in spectrum sensing [17]. To mitigate the impact of these issues, cooperative spectrum sensing has been shown to be an effective method to improve the detection performance by exploiting spatial diversity [67]. The common CSS schemes include the centralized [17] and decentralized structure [68], which are briefly introduced in the following.

1. Centralized Cooperative Spectrum Sensing: In a centralized CSS scheme, as shown in Fig. 2.3, an FC is implemented for data fusion. The mechanism of a centralized CSS scheme can be summarized into the following three steps [17].

   - The FC chooses spectrum of interest for sensing and all SUs (e.g. SU1 to SU5 in Fig. 2.3) in the CSS network conduct local sensing individually via sensing channels.
   - All the SUs send their local sensing information to the FC via reporting channel.
   - The FC combines all the information received from each SU to make a final decision on the spectrum occupancy, and then diffuses the final decision back to those participating SUs.

   This is a simple way to implement CSS networks, in which participating SUs do not need to make decisions on spectrum occupancy by themselves. Therefore, the energy consumption at each individual SU is reduced, which is really suitable for the energy-constrained SUs. However, the bandwidth required for reporting channels becomes large in the case of a large number of SUs, and the link failure between SUs and FC also causes loss of data.

2. Decentralized cooperative spectrum sensing: Different with the centralized CSS

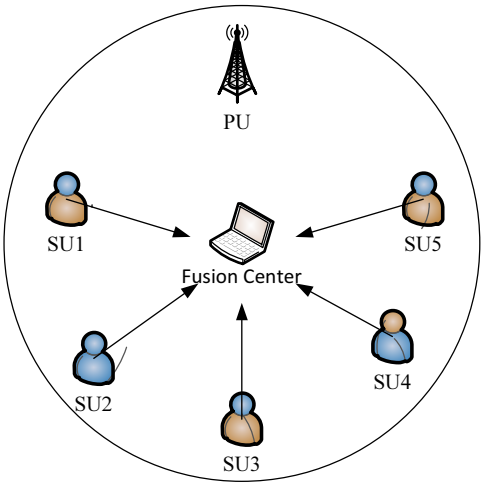

Figure 2.3: Centralized cooperative spectrum sensing.

scheme, the FC is removed in a decentralized CSS network. As shown in Fig. 2.4, each SU communicates with its neighbour SUs within the transmission range. Subsequently, each SU would make its local decision based on the received information when the network reaches global convergence. The decentralized scheme is robust to link failure in comparison with the centralized one, as it does not need a backbone infrastructure. However, the overhead in the reporting channel becomes very high when network scale becomes large. It is further proposed that SUs can transmit the local information only to their neighbour SUs within limited hops (e.g. one-hop) in the CSS network, in order to reduce the overhead during the convergence process. However, this type of scheme may cause longer convergence time.

2.3.3 Nyquist Wideband Spectrum Sensing

In CR, wideband spectrum sensing has attracted much attention. Wideband spectrum sensing techniques aim to sense a frequency bandwidth that exceeds the coherence bandwidth of the channel. For example, for exploiting spectral opportunities in the whole ultra-high frequency (UHF) TV band (between 300 MHz and 3 GHz), wideband spectrum sensing techniques should be employed. It is noted that narrowband sensing techniques

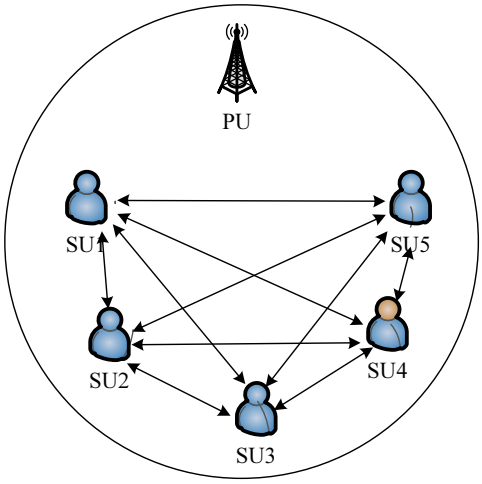

Figure 2.4: Decentralized cooperative spectrum sensing.

cannot be directly used for wideband spectrum sensing, as the narrowband technique normally makes a single binary decision for the whole spectrum, which cannot identify individual spectral opportunities that lie within the wideband spectrum [7]. Additionally, it is more efficient for spectrum detection if SUs could sense multiple channels simultaneously in a sensing period.

A direct approach of wideband spectrums sensing is to directly acquire the wideband signal by a standard ADC, and then digital signal processing techniques are utilized to detect spectral opportunities. So far, some research on wideband spectrum sensing have been done in [8–11] with the implementation of a high-speed ADC. Taking scheme proposed in [10] as an example, a multi-band joint detection algorithm sensing the PUs over multiple bands is as shown in Fig. 2.5. The wideband signal is directly sampled by a standard ADC. Subsequently, the received sinal is processed by a serial-to-parallel conversion circuit to divide sampled data into parallel data streams. Additionally, fast Fourier transform (FFT) is implemented to covert the wideband signals to frequency domain. As a result, the wideband spectrum signal is divided into series of narrowband channels labelled as $r_k\,(n)$. The energy of each channel is then calculated. Finally, spectrum occupancy of each narrow channel is determined by using an optimized threshold to achieve a better detection performance than the traditional narrowband spectrum

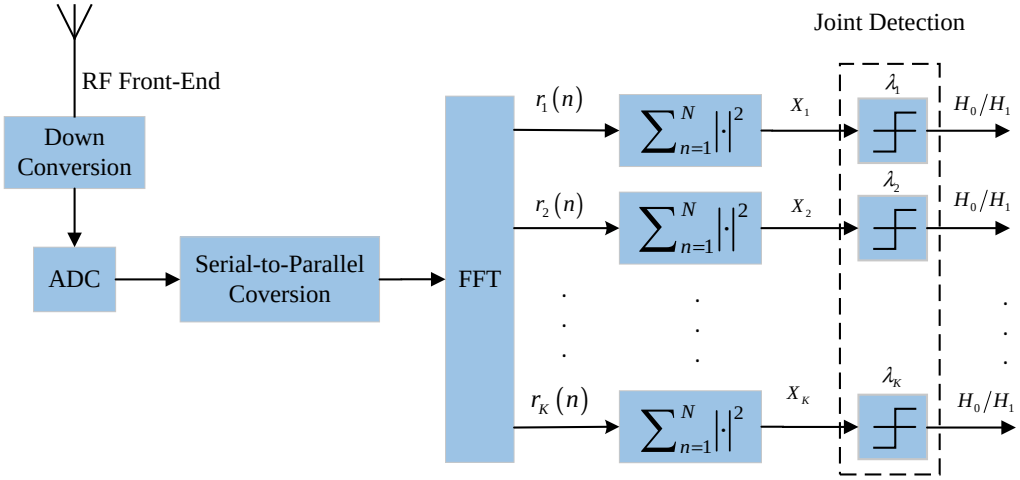

Figure 2.5: Multiband joint detection for wideband spectrum sensing.

sensing approaches.

However, special attention should be paid to the signal sampling procedure. As limited by the Shannon theorem, the sampling rate must be at least twice of the maximum frequency presented in the signal (known as Nyquist rate), in order to avoid spectral aliasing. Supposing that the wideband signal spans over frequency domain from 0 to 10 GHz, it should be uniformly sampled by a standard ADC at or above the Nyquist rate of 20 GHz. However, such an ADC is unaffordable for most of the devices in CRNs or sensor networks in terms of sampling rates and energy consumption. Therefore, wideband spectrum sensing presents significant challenges on hardware that operates at a sufficiently high rate. With current hardware technologies, high-rate ADCs with high resolution and reasonable power consumption (e.g., 20 GHz sampling rate with 16 bits resolution) are difficult to be achieved. Even if it were possible, the real-time digital signal processing of high-rate samples could be very expensive.

2.3.4 Compressive Wideband Spectrum Sensing

Inspiring by the most recent developments on CS and MC techniques, the bottleneck of Nyquist wideband sensing in CRNs can be broken through compressive spectrum

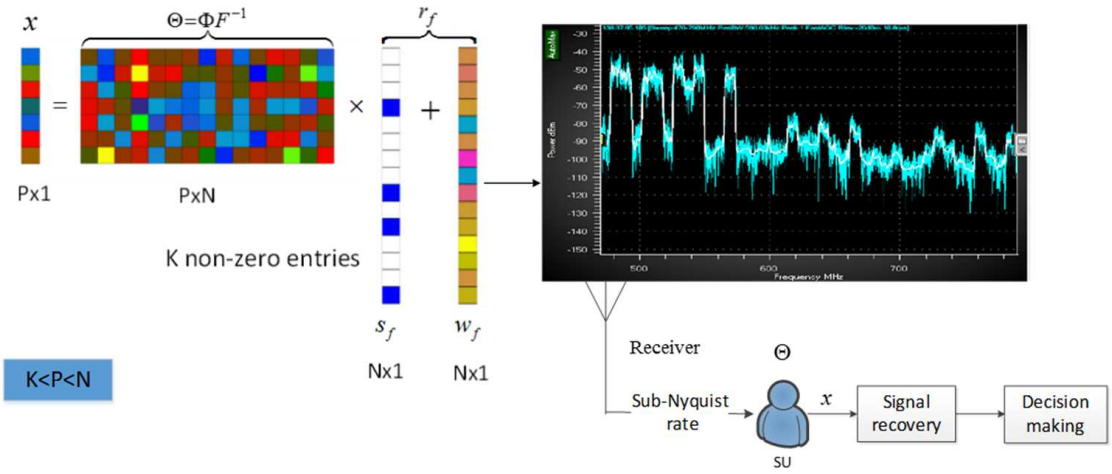

Figure 2.6: Block diagram for compressive spectrum sensing model.

sensing. The compressive spectrum sensing at a single SU is taken as an example. In the considered model, it is assumed that bandwidth of the whole spectrum is divided into I channels. A channel is either occupied by a PU or unoccupied. Meanwhile, there is no overlap between different channels. The number of occupied channels K is assumed to be much less than the total number of channels I. As shown in Fig. 2.6, the compressive spectrum sensing model includes the following four steps:

1. Signal arrives at SUs;
2. Compressed measurements collection at SUs;
3. Signal recovery;
4. Decision making for spectrum occupancy.

2.3.4.1 Signals Arrives at Secondary Users

The signals transmitting over the spectrum of interest are defined as $s(t) \in \mathcal{C}^{N\times 1}$, where N is the number of samples when $s(t)$ is sampled at or above Nyquist rate. Consequently,

the signals received at an SU is given by

$$r(t) = h(t) * s(t) + w(t), \tag{2.18}$$

where $h(t)$ is the channel gain between the transmitter and receiver, and $w(t) \sim \mathcal{CN}(0, \sigma_n^2 \mathbf{I}_N)$ refers to AWGN. Here, σ_n^2 refers to noise variance, and $\mathbf{I}_N$ is the identity matrix.

In order to make sure CS technique working well at SUs, the received signal $r(t)$ should be able to be expressed in a sparse domain. In spectrum sensing, as shown in Fig. 2.6, the signals $r(t)$ received at an SU are assumed to be sparse in the frequency domain, as the spectrum utilization is low in reality. Here, the sparse representation of the received signal can be expressed as

$$\mathbf{r_f} = \mathbf{h_f s_f} + \mathbf{w_f}, \tag{2.19}$$

where $\mathbf{r_f}$, $\mathbf{h_f}$, $\mathbf{s_f}$ and $\mathbf{w_f}$ refer to the discrete Fourier transform (DFT) of $r(t)$, $h(t)$, $s(t)$ and $w(t)$, respectively.

2.3.4.2 Compressed Measurements Collection

After the CS technique is invoked at an SU, the compressed measurements collected at the SU can be expressed as:

$$\mathbf{x} = \mathbf{\Phi} \mathcal{F}^{-1} \mathbf{r_f} = \mathbf{\Theta r_f} = \mathbf{\Theta} (\mathbf{h_f s_f} + \mathbf{w_f}), \tag{2.20}$$

where $\mathbf{\Phi} \in \mathcal{C}^{P \times N}$ $(P \leq N)$ is a measurement matrix to collect the compressed measurements $\mathbf{x} \in \mathcal{C}^{P \times 1}$, with $P/N \leq 1$ being the compression ratio. The measurement matrix can be a matrix which contains a single spike in each row. Then the case $P/N = 1$ corresponds to $\Phi = \mathbf{I}_N$. Additionally, $\mathbf{\Theta} = \mathbf{\Phi} \mathcal{F}^{-1}$, where $\mathcal{F}^{-1}$ is inverse DFT (IDFT) matrix which is used as the sparsifying matrix. In practical settings, structured random

matrices are often employed for improved implementation affordability.

2.3.4.3 Signal Recovery

With the available compressed measurements, the original signal should be recovered before making decision on spectrum occupancy. As l_0-norm minimization is an NP-hard problem, it has been proved in [14] that l_1-norm is a good approximation for l_0-norm. Taking the l_1-norm minimization as the CS solver, signal recovery can be performed at an SU by solving the following convex optimization problem

$$\begin{aligned} &\min \|\hat{\mathbf{s}}_\mathbf{f}\|_1, \\ &\text{subject to } \|\boldsymbol{\Theta} \cdot \mathbf{h}_\mathbf{f}\hat{\mathbf{s}}_\mathbf{f} - \mathbf{x}\|_2^2 \leq \varepsilon, \end{aligned} \tag{2.21}$$

where $\hat{\mathbf{s}}_\mathbf{f}$ refers to the recovered signal, and ε refers to the noise tolerance. In the case of CS based CSS, each participating SU sends the compressed measurements to the FC, which is the place to perform signal recovery.

2.3.4.4 Decision Making

When the reconstructed signal $\hat{\mathbf{s}}_\mathbf{f}$ is obtained, energy detection can be performed to determine the spectrum occupancy. More specifically, the energy density of each recovered channel is compared with a predefined threshold to determine whether the corresponding channel is occupied or not. The predefined threshold λ is as defined in (2.16) or (2.17), which is dependent on whether a target P_d or P_f is given.

In practice, the noise variance σ_n^2 can be calibrated in a given channel, which is known for sure to be idle. For example, some channels, such as channel 21 in TVWS, are supposed to be vacant currently in the UK [2]. If the energy density of the considered channel is higher than the threshold, the corresponding channel is determined as occupied by PUs. Consequently, SUs are forbidden to access it. Otherwise, the corresponding

channel is determined as vacant. Therefore, SUs can access it to transmit the unlicensed signals.

2.4 TV White Space

2.4.1 Overview of TV White Space

TVWS refers to the frequencies made available for unlicensed use at locations where the spectrum is not being utilized by the licensed broadcasting services. TVWS offers attractive features due to the large amount of spectrum resources and better propagation properties. FCC has published its final regulations to allow unlicensed radio devices to operate in the broadcast television spectrum at locations where that spectrum is vacant [69]. More recently, Ofcom has enabled licence exempt use of TVWS [5]. The opening of TVWS spectrum for cognitive access is one of the first tangible steps to solve spectrum scarcity problem in current wireless networks.

The reason for the arising of TVWS is the DSO movement from traditional analog to digital transmission. It is noticed that there is always a geographical zone for a given frequency channel, in which the use of high power broadcasting is impossible, due to the co-channel or adjacent channel interference caused by the high power broadcasting. Therefore, it is natural to think about the use of low or moderate powered devices, provided they are carefully designed to be compatible with the primary digital terrestrial television (DTT) station and programme making and special events (PMSE) users. An example of spectrum usage over TVWS spectrum at London is shown in Fig. 2.7. It can be observed that a large portion of TVWS spectrum can be utilized to conduct the unlicensed power transmission.

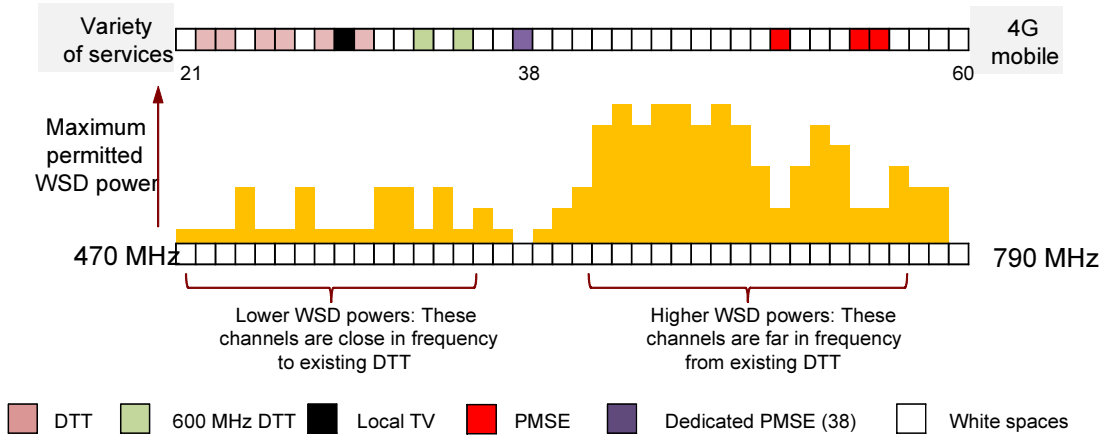

Figure 2.7: Illustration for the spectrum usage in London (Crystal Palace).

2.4.2 Geolocation Database Access to TV White Space Spectrum

The successful operation of CR in TV bands relies on the ability of white space devices (WSDs) to detect TVWS without causing harmful interference to primary services, such as TV broadcasting and wireless microphones. Besides the spectrum sensing approach, geolocation database access approach is regarded as the most important mechanism for TVWS spectrum detection as suggested by Ofcom [2] and FCC [70]. Specifically, geolocation database is a centralized database to output the maximum allowable EIRP for each TVWS channel at a specific location and time [1]. So far, several geo-location database providers such as Spectrum Bridge, Nominet, Google, etc. have been approved by Ofcom [71]. The advantages of geo-location database approach include easy implementation, high frequency utilisation in comparison with spectrum sensing techniques [72].

The operation of geo-location database access approach is described as follows: a geo-location database is firstly set up, which contains all the information of PUs (named as DTT database). Through the available DTT database, the geolocation database algorithm can compute the protected service contour for each DTT station, and determine the available frequency list at a specific location. A CR device would only need to report its location to the database, and in return receive information with regards to the maximum emission levels with which it can radiate. These devices would only radiate where

interference to the DTT service is deemed unlikely.

The framework developed in the UK, and being adopted more widely in Europe, is based on the premise that the impact of harmful interference on a DTT receiver is a function of the quality of DTT coverage in a geographical area, where the DTT receiver is located. In order to afford appropriate levels of protection to the DTT service, it is necessary for the database to specify the maximum permitted WSD emission levels across all DTT channels and in all geographic locations, where the DTT service is being used. DTT location probability is a measure for quantifying the quality of national DTT coverage [73, 74]. Location probability is widely used in the planning of DTT networks in order to quantify the quality of coverage. In the UK, it is typically calculated for every $100m \times 100m$ pixel across the country.

The DTT location probability is defined as the probability with which a DTT receiver could operate accurately at a specific location, i.e., the probability with which the average received wanted signal level is greater than a minimum required value. Fig. 2.8 shows the location probability model for the geo-location database. It is assumed that a DTT reception is located on the edge area of a DTT base station, which receives the lowest wanted power from the DTT base station. The average received power of the wanted DTT signal is labelled as P_{as}, and $P_{as(dBm)}$ is modeled as a Gaussian random variable with mean m_{as} and standard deviation σ_{as}. R is the coverage radius of the DTT base station and d is distance between the DTT receiver and the mobile WSD, which can be obtained from the DTT transmitter's database [75]. A mobile WSD radiates an in-bound EIRP P_{IB} with a power attenuation factor coupling gain (G). More particularly, DTT location probability can be expressed in linear domain as follows [76]:

$$q_1 = \Pr\left\{P_{as} \geq P_{as,\min} + \sum\nolimits_{k=1}^{\tilde{K}} r_{U,k} P_{U,k}\right\}, \tag{2.22}$$

$$q_2 = \Pr\left\{P_{as} \geq P_{as,\min} + \sum\nolimits_{k=1}^{\tilde{K}} r_{U,k} P_{U,k} + r\left(\Delta f, m_{as}\right) G P_{IB}\right\}, \tag{2.23}$$

where q_1 refers to the DTT receiver's location probability in the absence of interference

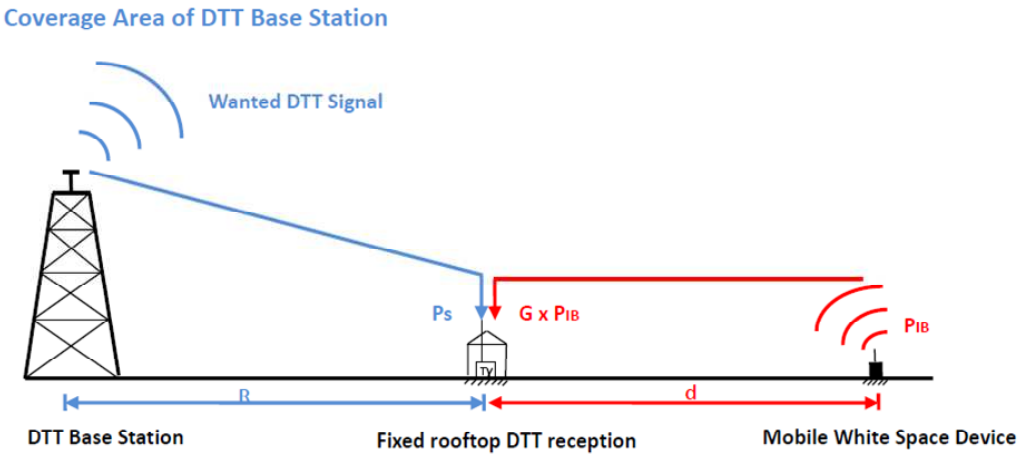

Figure 2.8: DTT location probability model.

from WSDs, and q_2 is the DTT receiver's location probability when considering the additional interference caused by WSDs. Here, $P_{as,\min}$ refers to DTT receiver's reference sensitivity level. Parameter $P_{U,k}$ refers to received power of the kth unwanted DTT signals, and $\tilde{K}$ is the total number of received unwanted DTT signals. The parameter $r_{U,k}$ is the protection ratio of the received wanted DTT power and received kth unwanted DTT power at the point where DTT receiver fails. The difference $\Delta f = f_{\text{WSD}} - f_{\text{DTT}}$, where f_{WSD} is the frequency in which a WSD operates and f_{DTT} is the DTT carrier frequency. When the interference from WSDs is considered, it results in a reduction in location probability $\Delta q = q_1 - q_2$. To identify the maximum allowable EIRP P_{IB} in (2.23), Δq is maximized by assigning a maximal allowable value Δq_T to Δq.

Equation (2.22) can be further expressed as follows [77]:

$$\begin{aligned} q_1 &= \Pr\left\{P_{as} \geq P_{as,\min} + \textstyle\sum_{k=1}^{\tilde{K}} r_{U,k} P_{U,k}\right\} \\ &= \Pr\left\{P_{as} \geq P_{as,\min} + V\right\} \\ &= \Pr\left\{1 \geq \tfrac{P_{as,\min}}{P_{as}} + \tfrac{V}{P_{as}}\right\} \\ &= \Pr\left\{1 \geq A + B\right\} \\ &= \Pr\left\{1 \geq X\right\}, \end{aligned} \tag{2.24}$$

where $V_{(dBm)}$ is modeled as a Gaussian random variable with mean m_V and standard

deviation σ_V. Furthermore, $A_{(dB)}$ and $B_{(dB)}$ can be modeled as Gaussian random variables. Additionally, $X_{(dB)}$ can be modeled as a Gaussian random variable with mean m_X and standard deviation σ_X. As a result, (2.24) can be given by

$$q_1 = \Pr\left\{0 \geq X_{(dB)}\right\} = \tfrac{1}{2}\mathrm{erfc}\left(\tfrac{m_X}{\sqrt{2}\sigma_X}\right). \tag{2.25}$$

Similarly, q_2 can be further expressed as follows:

$$\begin{aligned} q_2 &= \Pr\left\{P_{as} \geq P_{as,\min} + \textstyle\sum_{k=1}^{\tilde{K}} r_{U,k}P_{U,k} + r\left(\Delta f, m_{as}\right)GP_{IB}\right\} \\ &= \Pr\left\{P_{as} \geq P_{as,\min} + V + r\left(\Delta f, m_{as}\right)GP_{IB}\right\} \\ &= \Pr\left\{1 \geq \tfrac{P_{as,\min}}{P_{as}} + \tfrac{V + r(\Delta f, m_{as})GP_{IB}}{P_{as}}\right\} \\ &= \Pr\left\{1 \geq A + \tfrac{V+C}{P_{as}}\right\} \\ &= \Pr\left\{1 \geq A + \tfrac{D}{P_{as}}\right\} \\ &= \Pr\left\{1 \geq A + E\right\} \\ &= \Pr\left\{1 \geq Y\right\}, \end{aligned} \tag{2.26}$$

where C and V are two uncorrelated log-normal random variables. Additionally, $C_{(dBm)}$ and $V_{(dBm)}$ can be modeled as Gaussian random variables with mean m_C, m_V and standard deviation σ_C and σ_V, respectively. Furthermore, as D and P_S are both log-normal random variables, $E_{(dB)}$ is also Gaussian variable with $m_E = m_D - m_{as}$ and $\sigma_E = \sqrt{\sigma_D^2 + \sigma_{as}^2}$. Eventually, as A and E are both log-normal random variables, $Y_{(dB)}$ can be modeled as a Gaussian random variable with mean m_Y and standard deviation σ_Y. Furthermore, (2.26) can be expressed as

$$q_2 = \Pr\left\{0 \geq Y_{(dB)}\right\} = \tfrac{1}{2}\mathrm{erfc}\left(\tfrac{m_Y}{\sqrt{2}\sigma_Y}\right). \tag{2.27}$$

Once q_2 is obtained, the corresponding P_{IB} can be calculated to indicate the maximum allowable EIRP of each channel as the output of the geo-location database.

2.5 Summary

This chapter presents the fundamental concepts of CS and MC techniques, as well as model of CS based wideband spectrum sensing in CRNs. Additionally, the concept of TVWS is demonstrated in this chapter.

Chapter 3

Robust Compressive Spectrum Sensing

In this chapter, the existing work on compressive spectrum sensing in CRNs and the main contributions are firstly reviewed in Section 3.1. In Section 3.2, the proposed robust compressive spectrum sensing working at a single CR user is presented. Section 3.3 gives the related simulation results. Additionally, the proposed robust sub-Nyquist spectrum sensing algorithm for the CSS scenario is demonstrated in Section 3.4, in which the low-rank MC technique is invoked to perform signal recovery. The numerical results are presented in Section 3.5. Finally, Section 3.6 concludes this chapter.

3.1 Introduction

3.1.1 Related Work

CS theory was firstly applied to wideband spectrum sensing in CRNs by Tian and Giannakis [8] to perform sub-Nyquist sampling without loss any information. Subsequently, Wang *et al.* [78] proposed a two-step CS scheme for minimizing the sampling rates when

the sparsity level is varying. In this approach, the actual sparsity level is estimated firstly and the number of compressed measurements to be sampled are then adjusted before sampling. Subsequently, Sun *et al.* [79] proposed to adjust the number of compressed measurements adaptively without sparsity estimation by acquiring compressed samples step by step in continuous sensing slots. Signal acquisition is terminated once the number of collected samples were enough for successful spectral recovery. Along with these existing work on compressive spectrum sensing, it is noted that most of the existing algorithms [8, 18, 79–81] normally do not specify or quantify the noise. It is pointed that the SNR of the CS measurements would be decreased by 3dB for every octave increasing in the subsampling factor for acquisition of a noisy signal with fixed sparsity [15], which makes exact signal recovery more difficult for the case with high channel noise. Therefore, a robust compressive spectrum sensing algorithm with low computational complexity is more than desired.

Single node spectrum sensing faces the challenges that detection performance is significantly degraded if an SU experiences multipath fading and hidden terminals [17, 82]. This may cause miss detection. As a result, the SU may unwittingly transmit signals in channels with active PUs, which may cause serious interference to the PUs. In order to reduce the influence of imperfect channel environment, multiple nodes spectrum sensing, named as CSS, was proposed to efficiently combat fading problems by utilizing a spatial diversity of cooperative multiple SUs [10, 16, 81].

In CSS networks, there are two types of data fusion: centralized and decentralized fusion. In decentralized CSS, each SU only communicates with its neighbour SUs within one hop to reduce the transmission power consumed during sensing. After convergence, all SUs will have the fused sensing result without the implementation of an FC. Several decentralized CSS schemes [83–85] have been proposed where the average value of all the local spectrum sensing decisions is computed to get the final decision. As a result, the final decision obtained might be sub-optimal. Additionally, Zeng *et al.* [81] proposed a distributed CSS algorithm in which sensing samples rather than sensing decisions are

exchanged with the neighbour SUs within multi-hops to reach a global fusion at the cost of increasing network load. The convergence speed of decentralized CSS is an issue in large scale networks. In the centralized CSS scheme, all SUs report to an FC to make a final decision. In existing algorithms [86, 87], each SU makes a local decision about the spectrum of interest, and then the local decisions are sent to an FC to make a final decision. For a multi-channel sensing algorithm, such a separate approach of local spectrum estimation followed by a global decision fusion is suboptimal, which it does not take full advantage of the spatial diversity of the cooperative SUs [18]. In [81, 88, 89], an SU senses the whole spectrum of interest, and then the SU sends all the collected compressed measurements to an FC to get a global decision. As a result, the optimal decision can be obtained but the transmission load in the reporting channel between SUs and the FC is heavy. In [18], in order to reduce the sampling costs and transmission load between SUs and the FC, the length of received signal's frequency domain representations is set to be equal to the number of channels in the spectrum of interest rather than the original length of received signal in time domain, which results in a very poor resolution in the frequency domain and serious spectral leakage in each channel. Consequently, the P_f would increase and the P_d would decrease. Additionally, as aforementioned, the noise becomes critical after signals are collected at sub-Nyquist rate [15]. Therefore, a robust sub-Nyquist sampling based CSS algorithm with high spectrum resolution and low computational complexity is required.

3.1.2 Contributions

The main contributions of this chapter are summarized as follows:

1. A robust compressive spectrum sensing algorithm is proposed, in which the data acquisition and signal recovery are both conducted at a SU locally. In the proposed algorithm, the computational complexity is significant reduced by a new channel division scheme. Additionally, a denoising algorithm is performed to improve detection performance and make the algorithm robust to channel noise.

2. A robust sub-Nyquist sampling based CSS algorithm is proposed to reduce the signal acquisition costs at SUs, improve the spectrum resolution and the robustness to channel noise, by invoking the low-rank MC technique. In the considered system, signal recovery is performed at an FC. In the proposed algorithm, the computational complexity is reduced significantly by the new channel division scheme. Additionally, the robustness to channel noise is improved by the proposed denoising algorithm.

3. The proposed robust sub-Nyquist sampling based spectrum sensing algorithms are both tested on the real-world signals over TVWS after being validated by the simulated TV signals.

3.2 Robust Compressive Spectrum Sensing at Single User

3.2.1 System Model

In the single node case, the compressive spectrum sensing model is same as aforementioned in Section 2.3.4 of Chapter 2. As no prior information of PUs is required, l_1 norm minimization is invoked to perform signal recovery. In order to reduce the computational complexity during signal recovery process and enhance algorithm's robustness to imperfect channel noise, a robust spectrum sensing algorithm is proposed for the single node case based on CS. In the first phase, a new efficient channel division scheme is proposed to reduce the computation complexity for signal recovery. In the second phase, a denoising algorithm is proposed to make the algorithm robust against high channel noise.

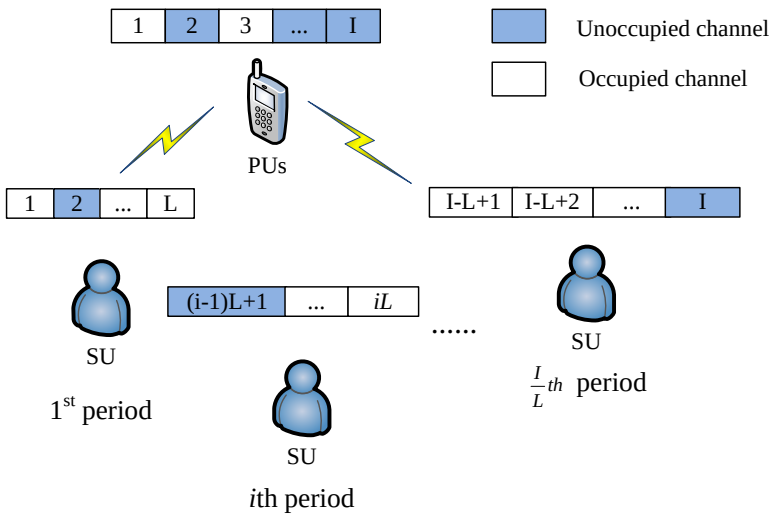

Figure 3.1: System model of the proposed channel division scheme in the single node spectrum sensing based on compressive sensing.

3.2.1.1 Proposed Channel Division Scheme

When an l_1 norm minimization based spectrum sensing algorithm is implemented at an SU, the computational complexity of signal recovery is dependent on the number of samples to be recovered. In the considered model, it is assumed that the spectrum of interest can be divided into $\mathcal{I}$ channels. A new channel division scheme is proposed, in which only $L\,(L < \mathcal{I})$ out of $\mathcal{I}$ channels are expected to be sensed in one sensing period at SUs to reduce the number of samples to be recovered. As shown in Fig. 3.1, each L-channel group is indexed by $i\left(i = 1, 2, \cdots, \frac{\mathcal{I}}{L}\right)$. If any vacant channel is detected, SU would stop sensing and start data transmission. Otherwise, SU begins to sense the next L-channel group in the next sensing period. As a result, the required sampling rates at SUs for exact recovery are further reduced by implementing the CS technique at SUs.

Once signal of the L-channel group $\mathbf{r_{fi}} = \mathbf{h_{fi}}\mathbf{s_{fi}} + \mathbf{w_{fi}} \in \mathcal{C}^{n\times 1}$ $(n = \frac{LN}{\mathcal{I}})$ arrives at the receiver, where N is the number of samples for the whole spectrum at Nyquist rates. The compressed measurements $\mathbf{x_i} \in \mathcal{C}^{\tilde{p}\times 1}$ are collected at sub-Nyquist sampling rates, with compression ratio is defined as $\gamma = \frac{\tilde{p}}{n}$. Here, $\mathbf{h_{fi}}$, $\mathbf{s_{fi}}$, $\mathbf{w_{fi}}$ refer to the frequency domain representations of channel coefficients, transmitted primary signal and channel noise in

the L-channel group channel. The noise variance is σ_n^2. Subsequently, the reconstructed frequency domain representations of the ith L-channel group $\hat{\mathbf{s}}_{\mathbf{fi}}$ can be obtained by solving l_1 norm minimization as:

$$\begin{aligned} &\min \ \|\hat{\mathbf{s}}_{\mathbf{fi}}\|_1, \\ &\text{subject to} \ \ \|\boldsymbol{\Theta}_{\mathbf{i}} \cdot \mathbf{h}_{\mathbf{fi}} \hat{\mathbf{s}}_{\mathbf{fi}} - \mathbf{x}_{\mathbf{i}}\|_2^2 \leq \varepsilon, \end{aligned} \tag{3.1}$$

where $\boldsymbol{\Theta}_{\mathbf{i}} \in \mathcal{C}^{\tilde{p} \times n}$, and ε is the tolerance for noise level.

3.2.1.2 Proposed Denoised Spectrum Sensing Algorithm

When making a decision for spectrum occupancy, the decision accuracy is influenced by the signal recovery errors. The recovery performance of traditional l_1 norm minimization algorithm is degraded by high channel noise and low compression ratio. Furthermore, it is noticed that the amplitudes of recovered signal $\hat{\mathbf{s}}_{\mathbf{fi}}$ may be negative with high absolute values. Here, the nonpositive power spectrum amplitudes are caused by the unsuccessful signal recovery after solving problem (3.1). The first possible reason for unsuccessful signal recovery is that the number of collected measurements $\tilde{p}$ is not enough for exact signal recovery. The second possible reason for unsuccessful signal recovery is caused by the high noise level that dominates the compressed measurements $\mathbf{x}_{\mathbf{i}}$. However, the power spectrum $\mathbf{s}_{\mathbf{fi}}$ is nonnegative. If those negative values are used to calculate the energy density, it would become higher than the real energy value. As a result, the P_f of spectrum sensing would increase, which means the vacant channels might be determined as occupied. In order to improve the recovery performance and detection performance, a denoising algorithm is proposed.

In the denoising algorithm, the amplitude of the bth sample in the recovered signal $\hat{\mathbf{s}}_{\mathbf{fi}}$ is compared with the corresponding noise level $\sigma_n(b)$, where b $(1 \leq b \leq n)$ is the index of the recovered signal. If $\hat{s}_{fi}(b)$ is higher than $\sigma_n(b)$, the compressed measurement collected at SUs $r_{fi}(b)$ is kept for the recovered signal. Otherwise, the corresponding

value will be set to zero to reduce the recovery error. Here, the recovery error may caused by the high channel noise or not enough number of compressed measurements. The denoised signal $\hat{\mathbf{s}}_{\mathbf{fi\_d}}$ can be expressed as:

$$\hat{s}_{fi\_d}(b) = \begin{cases} r_{fi}(b), & \text{if } \hat{s}_{fi}(b) \geq \sigma_n(b), \\ 0, & \text{otherwise.} \end{cases} \tag{3.2}$$

After the denoising algorithm is performed, the energy density of each considered L-channel group in the denoised signal is compared with the corresponding threshold as defined in (2.16) to determine the spectrum occupancy of the corresponding L-channel group. If any L-channel group are determined as vacant, they can be used by SUs to transmit the unlicensed signals. Otherwise, the SU should continue sensing the next L-channel group until any vacant channel is found out or the $\frac{\mathcal{T}}{L}$ sensing periods, named as a sensing loop, are run out. As there is a high probability that the spectrum vacant in last loop remains free in the current sensing loop, an SU should firstly sense the L-channel group determined as free in the last sensing loop at the beginning of a new sensing loop if any vacant L-channel group are detected in the most recent sensing loop. Otherwise, an SU should keep sensing from the first L-channel group. The whole process of the proposed robust spectrum sensing algorithm at single node based on CS is summarized as **Algorithm 1**.

3.2.2 Computational Complexity and Spectrum Usgae Analyses

In compressive spectrum sensing algorithm, the computational complexity mainly comes from the signal recovery process by solving the l_1 norm minimization problem. It is determined by the number of samples (N) to be recovered to represent the spectrum of interest. Specially, when the whole wideband spectrum of interest is sensed in one sensing period by an SU, the computational complexity of solving the l_1 norm minimization

Algorithm 1 Proposed Robust Compressive Spectrum Sensing Algorithm at Single User

Initialization: Set threshold λ as (2.16), $i = 1$.

1: **while** $i \leq \frac{\mathcal{I}}{L}$ or $E\left(\hat{\mathbf{s}}_{\mathbf{fi\_d}}\right) > \lambda_d$ **do**

Phase I:

2: The SU takes measurements at sub-Nyquist rate for the ith L-channel group to collect compressed measurements $\mathbf{x_i}$ in the ith sensing period.

3: Perform signal recovery by l_1 algorithm as (3.1) to get the recovered signal $\hat{\mathbf{s}}_{\mathbf{fi}}$.

Phase II:

4: Perform denoising to $\hat{\mathbf{s}}_{\mathbf{fi}}$ to get $\hat{\mathbf{s}}_{\mathbf{fi\_d}}$ according to (3.2).

5: Increase i by 1.

6: **end while**

7: **if** $E\left(\hat{\mathbf{s}}_{\mathbf{fi\_d}}\right) < \lambda$ **then**

8: **return** SU access the ith L-channel group.

9: **else**

10: **return** SU senses from the L-channel group vacant in last sensing loop or from the first L-channel group in the new sensing loop.

11: **end if**

problem can be expressed as:

$$C_1 = \mathrm{O}\left(N^3\right). \tag{3.3}$$

In the adaptive compressive spectrum sensing algorithm [79] for wideband CRs, the required computational complexity C_2 can be expressed as follows. In order to simplify the comparison, the spectrum sensed in each sensing period is assumed to be L out of $\mathcal{I}$ channels and the system starts data transmission after i sensing periods.

$$\begin{aligned} C_2 &= \mathrm{O}\left(\left(\tfrac{L}{\mathcal{I}} \times N\right)^3 + \left(\tfrac{2L}{\mathcal{I}} \times N\right)^3 + \ldots + \left(\tfrac{iL}{\mathcal{I}} \times N\right)^3\right) \\ &= \mathrm{O}\left(\left(1 + 2^3 + \ldots + i^3\right) \times \left(\tfrac{L}{\mathcal{I}}\right)^3 \times N^3\right) \\ &= \mathrm{O}\left(\left(\tfrac{(1+i)i}{2}\right)^2 \times \left(\tfrac{L}{\mathcal{I}}\right)^3 \times N^3\right), \end{aligned} \tag{3.4}$$

where $i = 1, \ldots, \frac{\mathcal{I}}{L}$ is the number of sensing periods that an SU needs to perform exact signal recovery to determine the accessible channels.

When the proposed new channel division scheme is used for single node wideband

spectrum sensing, computational complexity of the signal recovery process is expressed as:

$$C_3 = \mathrm{O}\left(i \times \left(\frac{L}{\mathcal{I}}\right)^3 \times N^3\right). \tag{3.5}$$

As analysed above, an SU may need multiple sensing periods to find out the accessible spectrum holes. Assuming there is at least one vacant channel in the spectrum of interest, the required sensing periods by the proposed channel division scheme is dependent on the number of channels in a L-channel group and the number of active PUs among the spectrum of interest. The worst case for the proposed scheme is that an SU does not find any vacant channel until the $\frac{\mathcal{I}}{L}$th sensing period. In such a case, $C_3 = \mathrm{O}\left(\left(\frac{L}{\mathcal{I}}\right)^2 \times N^3\right)$ as $i = \frac{\mathcal{I}}{L}$. In practice, there are multiple vacant channels in the spectrum of interest due to the low spectrum utilization. Therefore, the required sensing periods would be less than $\frac{\mathcal{I}}{L}$ in reality. As a result, $C_1 > C_3$ in all cases. The proposed channel division scheme relaxes the requirement on high speed ADC at the expense of compromised spectrum usage efficiency. This tradeoff is shown in the simulation part in Section 3.3. It seems the tradeoff is acceptable as the proposed algorithm is designed for networks in which SUs have limited computational power and infrequent low-speed transmission requirements. Comparing C_2 and C_3, it shows $C_2 = C_3$ if $i = 1$, which refers to the scenario that vacant channels can be found after signal recovery is only performed once. Otherwise, $C_2 > C_3$. Therefore, the proposed channel division scheme achieves a lower computational complexity than existing algorithms.

3.3 Numerical Analyses for Single User Case

3.3.1 Analyses on Simulated Signals

In the simulation, signals are orthogonal frequency division multiplexed (OFDM) generated as PUs, which are used in digital video broadcasting-terrestrial (DVB-T) over TVWS spectrum from 470MHz to 790MHz in the UK. There are $\mathcal{I} = 40$ channels in TVWS with bandwidth of 8MHz for each channel. P_f is set to be 0.01. $SNR = \sigma_s^2/\sigma_n^2$ is the ratio of signal power over noise power of a L-channel group. In the following simulations, the aforementioned tradeoff between spectrum usage efficiency and computational complexity is demonstrated firstly. Additionally, the influence of compression ratio, sparsity order and the classic receiver operating characteristics (ROC) curves are presented to validate the proposed algorithm.

Fig. 3.2 shows the average number of sensing periods which is required at SUs to find out the vacant channel for unlicensed usage. As aforementioned, the size of L-channel group which is sensed in each sensing period at SUs would influence the spectrum usage efficiency of the proposed channel division scheme. If $L = 1$, the case becomes a narrow band spectrum sensing which requires low-speed sampling rates at SUs. But the spectrum usage efficiency is low. With increasing L, it becomes a multichannel wideband spectrums sensing case in which the spectrum usage efficiency is increased with cost of expensive sampling acquisition. From Fig. 3.2, it can be observed that the vacant channels can be detected efficiently even with increasing L. Here, sparsity level refers to the ratio of occupied channels and the total number of channels. Higher sparsity level refers to higher spectrum occupancy, as the active PUs would result in nonzero amplitude in frequency domain. With higher sparsity level, the average required sensing periods to find the vacant spectrum holes increases. As the spectrum is underutilized in practice, the required number of sensing periods is relatively low. In the following simulation, it is assumed that the number of channels sensed by the SU in each sensing period is set to be $L = 8$.

Fig. 3.3 shows P_d for the traditional l_1 norm minimization based spectrum sensing

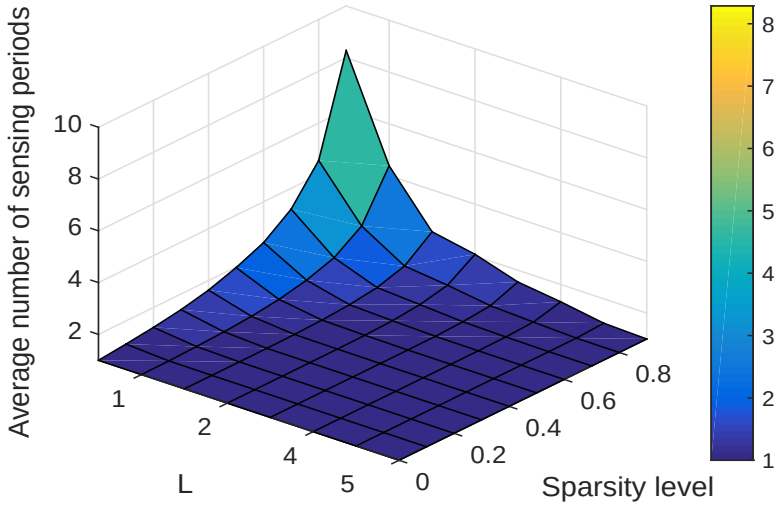

Figure 3.2: Average number of required sensing periods at SUs with different sparsity levels and number of channels L sensed in one sensing period, SNR=-5dB.

algorithm, and the proposed robust single node spectrum sensing algorithm based on CS under different number of compressed measurements with varying SNR values. Its detection performance is also compared with that of spectrum sensing algorithm without CS implemented, as well as the theoretical values derived from [90, 91]:

$$P_d = Q\left(\frac{\frac{\lambda}{\sigma_n^2} - \left(1+\frac{\sigma_s^2}{\sigma_n^2}\right)}{\left(1+\frac{\sigma_s^2}{\sigma_n^2}\right)/\sqrt{n/2}}\right), \tag{3.6}$$

where λ is the threshold for energy detection as calculated by (2.16), and σ_s^2 refers to the power of transmitted primary signal. Here, n refers to the number of samples sampled from a L-channel group at Nyquist rate.

Fig. 3.3 shows that the performance of l_1 norm minimization based spectrum sensing algorithm (labeled as traditional CS based SS) and the proposed robust single node spectrum sensing algorithm based on CS (labeled as robust CS based SS) are both the same with that of spectrum sensing algorithm without CS implemented at the SU (labeled as no CS) and the theoretical curves obtained by (3.6). In Fig. 3.3, SS is the abbreviation for spectrum sensing which is only used in the legend. In this case, the number of

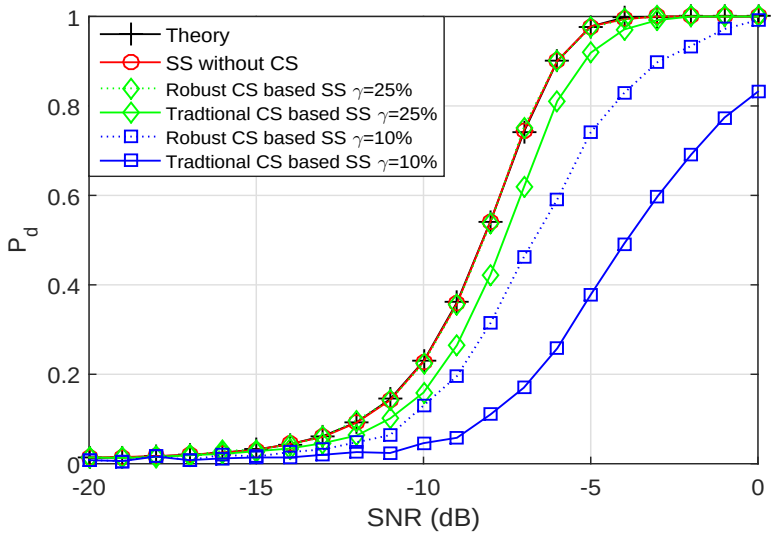

Figure 3.3: Proposed robust compressive spectrum sensing algorithm at a single user achieves higher P_d than the traditional algorithms with simulated signals under different compression ratios γ and different SNR values.

occupied channels is 1 among 8. Therefore, the sparsity level is set to be 12.5%. When the number of collected measurements decreases, the detection performance degrades. It also shows that performance of the proposed robust single node spectrum sensing based on CS is better than that of the CS based spectrum sensing without denoising when the compression ratio is 25% and 10%. This gain benefits from the proposed denoising algorithm which can improve the signal recovery accuracy. As the recovery accuracy becomes higher with the higher compression ratio, detection performance of the proposed robust spectrum sensing algorithm gets closer to the theoretical curves. The simulation result shows that the proposed robust spectrum sensing algorithm can reduce the sampling rates by 75% without degrading detection performance.

Fig. 3.4 shows the detection performance of the proposed robust single node spectrum sensing based on CS with different sparsity levels and different compression ratios. In this scenario, the different sparsity levels refer to different number of active PUs in the spectrum of interest. The positions of these active PUs are set to be random. The detection performance becomes worse with increasing sparsity level and decreasing

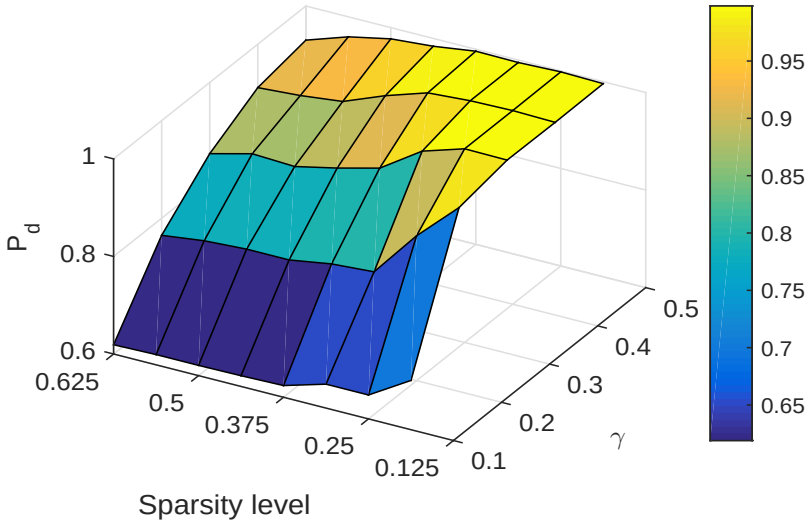

Figure 3.4: P_d comparison with different sparsity levels and different compression ratios γ, SNR=-5dB.

compression ratio as shown in Fig. 3.4. As the sparsity level increases, sparse property of signal to be recovered becomes less sparse, and therefore more compressed measurements should be collected for signal recovery to make sure the detection performance not being degraded. It is noticed that the detection performance would only be slightly degraded when the proposed algorithm is applied to the practical signals in TVWS spectrum as the its occupancy ratio is normally 15% to 20% in practice [1, 2].

The ROC curves under different SNR values are shown in Fig. 3.5, where the compression ratio is set to be 25%. In this case, the sparsity level is set to be 12.5%. It can be observed that the proposed robust spectrum sensing algorithm based on CS exhibits better performance than the traditional spectrum sensing algorithm based on CS. Meanwhile, it is also noticed that the performance of the proposed robust spectrum sensing algorithm is almost as good as that of spectrum sensing algorithm without CS applied. This gain arises from the proposed denoising algorithm. This result matches with Fig. 3.3 when compression ratio is set to be 25%. It should be pointed that the increasing P_f refers to decreasing threshold level if the number of samples is fixed as defined in (2.16). Therefore, the detection performance becomes degraded with increasing threshold level

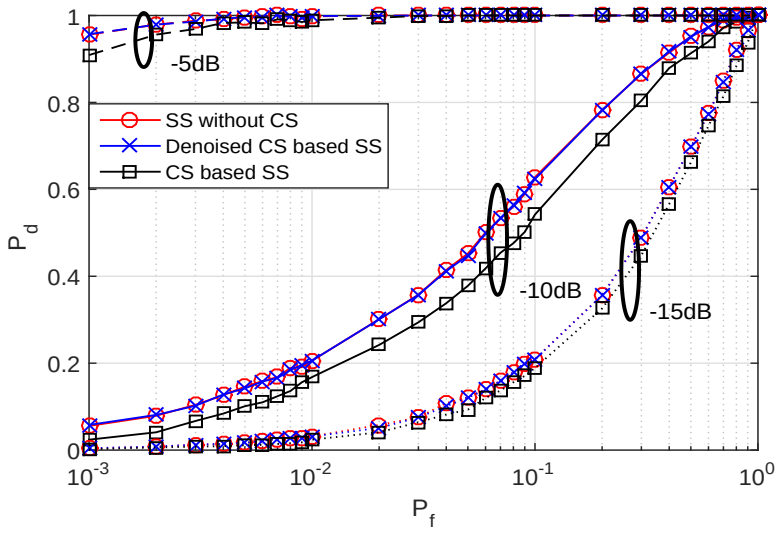

Figure 3.5: Proposed robust compressive spectrum sensing algorithm at a single node achieves higher ROC curves than the traditional algorithms with simulated signals, and compression ratio $\gamma = 25\%$.

as shown in Fig. 3.5.

3.3.2 Analyses on Real-World Signals

After the proposed robust single node spectrum sensing algorithm has been validated with simulated signals, it is further tested on the real-world signals recorded by the RFeye node [92]. The RFeye node is a scalable and cost-effective node which can provide real-time 24/7 monitoring of radio spectrum. It is capable of sweeping spectrum from 10MHz to 6GHz, and can capture signals of all types, including transient transmission such as pulsing or short-burst signals. It is even sensitive to very low power signals. The RFeye node used for measurement is located at Queen Mary University of London (QMUL) (51.523021°N 0.041592°W) as shown in Fig. 3.6 with the height about 15 meters above ground. The real-world signal recorded by the RFeye node is for TVWS ranging from 470MHz to 790MHz.

When the recorded real-world signal is used as source signal for the proposed robust single node spectrum sensing algorithm, Fig. 3.7 shows P_d and P_f of the spectrum sensing

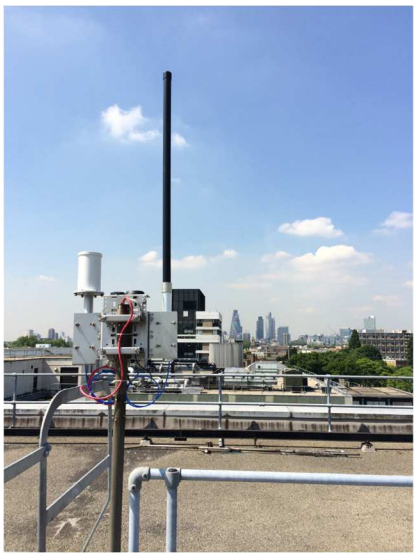

(a). Measurement setup at Queen Mary University of London

(b). RFeye sensing node

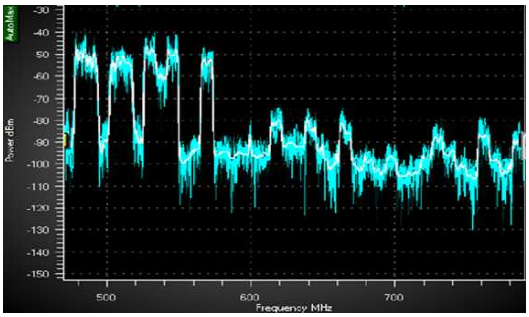

(c). Real-time TVWS signal observed by RFeye sensing node

Figure 3.6: Measurement setup for real-world TVWS signals recorded at Queen Mary University of London.

without CS implemented, traditional CS based spectrum sensing, and the proposed robust spectrum sensing algorithms under different threshold values. Here, the thresholds are experimental values. In this scenario, the compression ratio is set to be 15%. It can be observed that both P_d and P_f decrease with increasing threshold values. IEEE 802.22 demands a stringent sensing requirement. For the maximum P_f of 10%, a sensing algorithm should achieve 90% for P_d [93]. According to the Fig. 3.7, it shows that the detection performance of the spectrum sensing without CS implemented can achieve the target performance required in IEEE 802.22 when threshold is set to be -73.5 dBm or higher. However, the P_d of the algorithms with CS would be degraded with increasing threshold. Therefore, -73.5 dBm is chosen as the suitable threshold to get a better tradeoff of P_d and P_f in the following analyses. From Fig. 3.7, it is also noticed that the proposed robust single node spectrum sensing algorithm outperforms the traditional one when threshold is 1.5. It can be observed that the P_d increases with decreasing threshold level which is matched with the simulation results shown in Fig. 3.5.

Fig. 3.8 shows the P_d and P_f of the traditional spectrum sensing algorithm based on

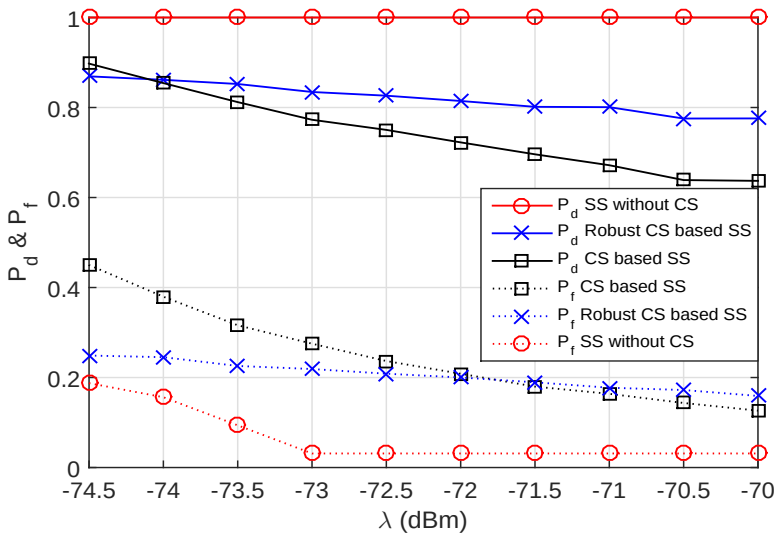

Figure 3.7: P_d and P_f comparison of single node spectrum sensing with real-world signals under different thresholds λ, and compression ratio $\gamma = 15\%$.

CS and the proposed robust spectrum sensing algorithm with real-world signals under different compression ratios from 1% to 100%. In this scenario, the threshold value is set to be -73.5 dBm according to Fig. 3.7. It can be observed that the detection performance gets better with increasing number of compressed measurements collected at the SU, and the proposed robust spectrum sensing algorithm outperforms the traditional one, which is similar with the results of simulated signals as shown in Fig. 3.3. It is further noticed that there is sharp dropping for P_f when the compression ratio γ is increased from 20% to 30%. This is caused by that the signal recovery becomes exact when the compression ratio γ is no less than 20%. Once the signal recovery is exact, P_f caused by recovery errors would be alleviated.

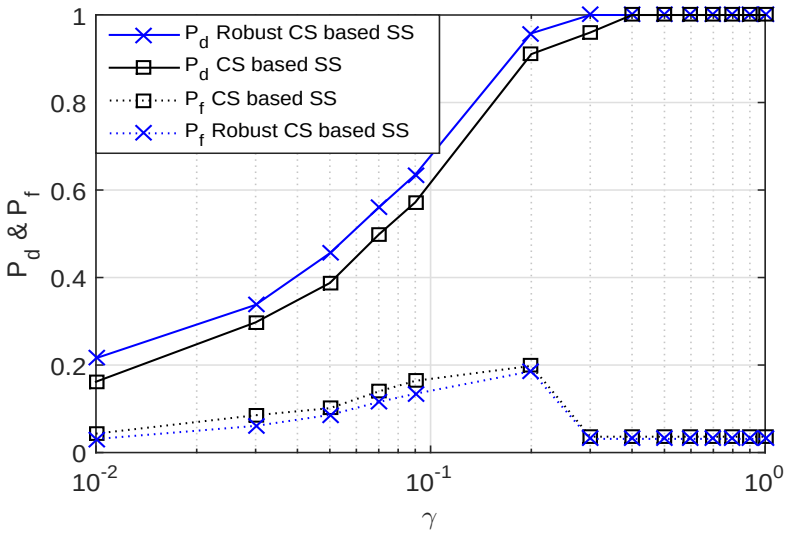

Figure 3.8: Proposed robust compressive spectrum sensing algorithm at single node achieves higher P_d and lower P_f than the traditional algorithm with real-world signals under different compression ratios γ, and threshold λ is -73.5 dBm.

3.4 Matrix Completion Based Robust Spectrum Sensing at Cooperative Multiple Users

Based on the proposed robust spectrum sensing algorithm for single node in CRNs, a new robust CSS algorithm based on low-rank MC is proposed to overcome the deep fading problem. In the considered network, the whole spectrum of interest can be divided into $\mathcal{I}$ channels, and K out of the I channels are occupied by PUs. It is assumed that the positions of active PUs are random among the whole spectrum of interest. The proposed algorithm includes two phases. In the first phase, the proposed channel division scheme is extended to the CSS scenario, in which each SU is implemented to sense a L-channel group of the $\mathcal{I}$ channels to reduce sampling rates. Here, each L channels are sensed by the same SU. As a result, at least $S(S = \frac{\mathcal{I}}{L})$ SUs should be implemented to sense the whole spectrum in one sensing period. Due to deep fading, J SUs are spatially implemented to sense the same L-channel group. Therefore, the jth SU implemented to sense the ith L-channel group is labeled as SU_{ij}. The whole scenario is shown in Fig. 3.9. In the

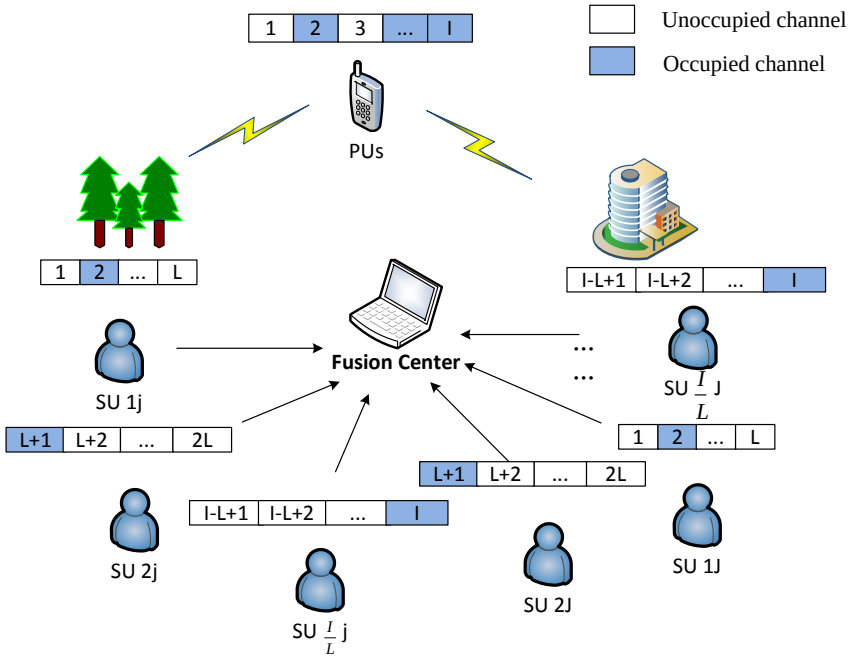

Figure 3.9: System model of the proposed channel division scheme in cooperative spectrum sensing based on low-rank matrix completion.

second phase, a denoising algorithm is proposed to improve the detection performance of CSS, which is introduced in Section 3.4.2.

3.4.1 System Model

Based on the scenario shown in Fig. 3.9, the CSS algorithm based on low-rank MC can be formulated into a four-step model:

1. Sparse signals received at SUs.

2. Incomplete matrix generation at an FC.

3. MC at the FC.

4. Decision making at an FC.

3.4.1.1 Signals Arrives at Secondary Users

As noise exists in the transmission channels, signals received at SU_{ij} is $r_{ij}(t) = h_{ij}(t) * s_{ij}(t) + w_{ij}(t)$, where $s_{ij}(t) \in \mathcal{C}^{n\times 1}$ refers to time domain signals of the ith L-channel group received at the jth receiver SU_{ij}, $h_{ij}(t)$ refers to the channel gain for the ith L-channel group between transmitter and SU_{ij}, $w_{ij}(t)$ refers to AWGN in the related transmission channels. The frequency domain representations of signals in the ith L-channel group which is received by SU_{ij} can be expressed as:

$$\mathbf{r_{fij}} = \mathbf{h_{fij}}\mathbf{s_{fij}} + \mathbf{w_{fij}}, \tag{3.7}$$

where $\mathbf{r_{fij}}$, $\mathbf{h_{fij}}$, $\mathbf{s_{fij}}$ and $\mathbf{w_{fij}}$ are the DFT of $r_{ij}(t)$, $h_{ij}(t)$, $s_{ij}(t)$ and $w_{ij}(t)$.

At SU_{ij}, a random demodulator $\hat{\mathbf{\Phi}}_{\mathbf{ij}} \in \mathcal{C}^{\tilde{p}\times n}$ is implemented to collect the compressed measurements as follows:

$$\begin{aligned}\mathbf{x_{ij}} &= \hat{\mathbf{\Phi}}_{\mathbf{ij}}\left(\mathbf{h_{fij}}\mathcal{F}^{-\mathbf{1}}\mathbf{s_{fij}} + \mathcal{F}^{-\mathbf{1}}\mathbf{w_{fij}}\right) \\ &= \hat{\mathbf{\Theta}}_{\mathbf{ij}}\left(\mathbf{h_{fij}}\mathbf{s_{fij}} + \mathbf{w_{fij}}\right).\end{aligned} \tag{3.8}$$

3.4.1.2 Incomplete Matrix Construction at Fusion Center

As spectrum utilization is low, the stack of received frequency domain representations $\mathbf{r_{fj}} = \sum_{i=1}^{S} \mathbf{r_{fij}}$ are approximately sparse. Each SU only sends $\tilde{p}$ compressed measurements to an FC where $\tilde{p} < n$. At the FC, the matrix $\mathbf{R_f} \in \mathcal{C}^{N\times J}$ $(N = S \times n)$ to be recovered shows a low-rank property transformed from the sparse property of signals received at SUs as shown in Fig. 3.10. In Fig. 3.10, the circled items refer to the observed measurements as the CS technique is implemented at each SU. In order to avoid poor spectrum resolution in frequency domain and high spectral leakage in each channel, the number of the rows N is set to be equal to the original number of samples for the whole spectrum of interest $S \times n$ rather than the number of channels $\mathcal{I}$, which is invoked

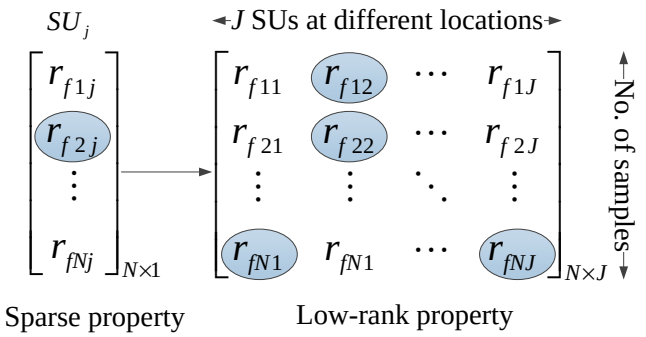

Figure 3.10: Matrix to be recovered at the fusion center.

in [18, 94].

At the FC, only a subset $\mathbf{\Omega} \subseteq \mathcal{C}^{M\times J}$ of $\mathbf{R_f}$ are collected where $P = S \times \tilde{p}$. Here, the compression ratio is defined as $\gamma = \frac{P}{N}$. We stack all columns $\mathbf{r_j}$ of $\mathbf{R_f}$ into a long vector as vec $(\mathbf{R_f})$. The incomplete matrix $\mathbf{X}$ is obtained by:

$$\text{vec}\,(\mathbf{X}) = \hat{\mathbf{\Theta}}\text{vec}\,(\mathbf{R_f}) = \hat{\mathbf{\Theta}}\mathbf{H}\text{vec}\,(\mathbf{S_f}) + \hat{\mathbf{\Theta}}\mathbf{H}\text{vec}\,(\mathbf{W_f})\,, \tag{3.9}$$

where $\mathbf{h_f} = \text{diag}(\text{diag}(h_{f11}, ..., \mathbf{h_{f1J}}), ..., \text{diag}(\mathbf{h_{f\mathcal{I}1}}, ..., \mathbf{h_{f\mathcal{I}J}}))$, $\mathbf{H} = \text{vec}(\mathbf{h_f})$, and $\hat{\mathbf{\Theta}} = diag\left\{\hat{\mathbf{\Theta}}_{11}, \ldots, \hat{\mathbf{\Theta}}_{\mathbf{ij}}, \ldots \hat{\mathbf{\Theta}}_{\mathcal{I}\mathbf{J}}\right\}$ is the block diagonal matrix. It is assumed $\mathbf{S_f}$ is the corresponding noiseless matrix of $\mathbf{R_f}$, and $\mathbf{W_f} = \mathbf{R_f} - \mathbf{S_f}$ is the matrix of the corresponding noise contained in $\mathbf{R_f}$. The unobserved measurements in $\mathbf{S_f}$ should be recovered from $\mathbf{X}$.

3.4.1.3 Matrix Completion at Fusion Center

The size of the matrix and the computational cost would increase when the number of the rows N is equal to the length of samples $S \times n$, which is the samples size of the whole spectrum of interest, to improve the frequency resolution. The signal recovery process is normally performed at SUs in the single node spectrum sensing algorithm, and SUs are normally power limited devices [95]. Therefore, the signal recovery process may cause long delay which will make the final decision invalid for the dynamic spectrum. However,

in a CSS network, the MC process can be performed by a powerful device such as the FC to replace the power limited SUs.

With the low-rank property, the complete matrix $\mathbf{S_f}$ can be recovered from a random subset of its elements in $\mathbf{X}$ at the FC. This MC problem is defined as [96]

$$\begin{aligned} &\min\ \text{rank}\left(\hat{\mathbf{S}}_\mathbf{f}\right), \\ &\text{subject to}\ \left\|\hat{\mathbf{\Theta}}\cdot\mathbf{H}\text{vec}(\hat{\mathbf{S}}_\mathbf{f})-\text{vec}(\mathbf{X})\right\|_2^2 \leq \varepsilon, \end{aligned} \tag{3.10}$$

where $\hat{\mathbf{S}}_\mathbf{f}$ refers to the reconstructed matrix. Here, solving problem (3.10) refers to find a matrix with the minimal singular values but satisfies the constraints.

However, (3.10) is an NP-hard problem [96]. It has been proved that such an NP-hard problem can be well approximated by nuclear norm minimization problem. Then, the MC problem can be formulated as

$$\begin{aligned} &\min\ \left\|\hat{\mathbf{S}}_\mathbf{f}\right\|_*, \\ &\text{subject to}\ \left\|\hat{\mathbf{\Theta}}\cdot\mathbf{H}\text{vec}(\hat{\mathbf{S}}_\mathbf{f})-\text{vec}(\mathbf{X})\right\|_2^2 \leq \varepsilon. \end{aligned} \tag{3.11}$$

Here, $\left\|\hat{\mathbf{S}}_\mathbf{f}\right\|_*$ refers to the sum of singular values of $\hat{\mathbf{S}}_\mathbf{f}$.

3.4.1.4 Decision Making at an Fusion Center

When the complete matrix $\hat{\mathbf{S}}_\mathbf{f}$ is obtained by solving (3.11), the average energy density of each L-channel group can be calculated and compared with the threshold λ defined in (2.16) to make the final decision on spectrum occupancy. Once the final decision is made, it should be sent back to each SU participating the cooperative networks to enable them getting access to the vacant channels.

3.4.2 Denoised Cooperative Spectrum Sensing Algorithm

Similarly to the denoising algorithm in the proposed robust single node spectrum sensing algorithm in (3.2), the bth sample in the recovered signal $\hat{\mathbf{s}}_{\mathbf{fij}}$ is compared with the corresponding noise level $\sigma_n(b)$. If $\hat{s}_{fij}(b)$ is higher than $\sigma_n(b)$, the measurement observed at the FC $r_{fij}(b)$ is kept. Otherwise, the corresponding value is set to be zero to eliminate the influence of noise. Here, the recovery error may caused by the high channel noise or not enough number of compressed measurements. This process can be illustrated as:

$$\hat{s}_{fij\_d}(b) = \begin{cases} r_{fij}(b), & \text{if } \hat{s}_{fij}(b) \geq \sigma_n(b), \\ 0, & \text{otherwise.} \end{cases} \tag{3.12}$$

3.4.3 Computational Complexity and Performance Analyses

In the low-rank MC based CSS scenario, the computational complexity of solving the MC problem is at the level of $\mathrm{O}\left(N^3\right)$, and the MC is performed at a very powerful FC. As a result, the complexity introduced by MC would not be a key issue to be considered. In such a case, the key issue is the high sampling requirement for wideband spectrum at SUs with limited sensing capability.

In the proposed robust CSS algorithm based on low-rank MC, the bandwidth to be sensed at each SU is reduced to L out of $\mathcal{I}$ channels. Additionally, each SU performs sub-Nyqusit sampling and only the collected samples p are sent to the FC which would lower the transmission load in the networks in comparison with the scenario where all the n samples are sent to an FC. Meanwhile, $\frac{\mathcal{I}}{L}$ SUs are needed to employ at different locations to sense the whole spectrum of interest. As the spatial diversity of SUs are utilized to avoid the deep fading problem in CSS network, the more SUs participating in the CSS network, the better detection performance can be achieved. In such a case, if each SU only senses part of the spectrum, detection performance will be degraded. This tradeoff is illustrated in the following simulations. In large scale CRNs, such kind

of performance degradation can be compensated as the number of participating SUs are large.

3.5 Numerical Analyses for Cooperative Multiple Users Case

3.5.1 Analyses on Simulated Signals

In the multiple node scenario, the spectrum of interest is TVWS with $\mathcal{I} = 40$ channels. Each SU is assumed to sense a non-overlapping L-channel ($L = 8$) group which is the same as the simulation setup of the single node spectrum sensing scenario in Section 3.3. The target P_f is set to be 0.01. Transmission channels between the transmitters to the SUs experience frequency-selective fading. In each sensing period, the fading on each channel is time-invariant and it is modeled by setting a random delay and independent Rayleigh fading gains for the multipath fading channels. Without loss of generality, the first SU participating in the cooperative networks is assumed to experience deep fading and the rest of SUs are experiencing Rayleigh fading. In the following simulations, the performance of proposed robust CSS algorithm is presented by considering the influence of multipath deep fading, different number of measurements observed at the FC and different network sizes are analyzed.

The detection performance of single node spectrum sensing under deep fading channels in comparison with CSS algorithm with fading channels, AWGN channels, and the theoretical curves defined in (3.6) are shown in Fig. 3.11. It can be seen that P_d of the single node spectrum sensing, which can be considered as the number of SU implemented to sense each L-channel group is $J = 1$, becomes much lower than the theoretical curves when the transmission channels experience deep fading. As the spatial diversity gain

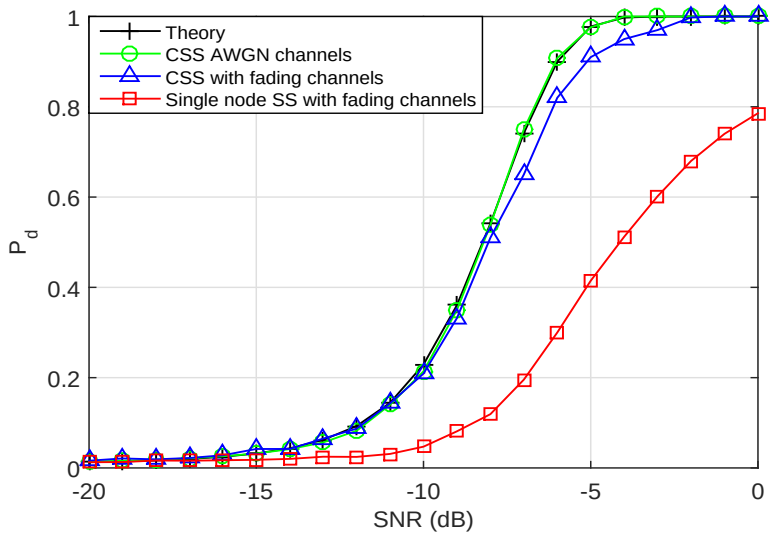

Figure 3.11: P_d comparison of theoretic curves, CSS under AWGN channels and deep fading channels, and single node spectrum sensing under deep fading channels with simulated signals.

of CSS, the detection performance of CSS algorithm is much improved even though the SUs experiencing deep fading are also in the cooperative network. In the CSS network, the number of SUs being implemented to sense each L-channel group is $J = 10$. It can be observed that the detection performance of CSS experiencing deep fading is still a bit lower than that of the theoretical curves and the CSS under AWGN channels.

Furthermore, it is noticed that the signal recovery step introduces most of the computational complexities among the four-step process for the single node spectrum sensing and the CSS algorithms. In the single node spectrum sensing algorithm based on CS, the signal recovery process is performed at the SU. However, in the CSS algorithm based on low-rank MC, signal recovery process is performed at the FC. SU devices, such as mobile phones and the slave WSDs, are normally battery powered [95] or even battery free for those nodes in WPT model in which the energy is harvested from power beacons. Therefore, the computation complexity should not be too high at the SUs. Otherwise, SUs cannot afford the sensing and signal recovery locally, and the delay caused by signal recovery would be intolerable. As a result, the spectrum sensing decision may not be meaningful since spectrum occupancy may have changed during the period of signal

recovery. However, for the FC, they are normally powerful devices such as base stations and master WSDs. In fact, size of the to be solved matrix at the FC is much greater than the number of samples to be recovered at SUs in the single node spectrum sensing, and the size of the matrix to be solved at the FC would also influence the performance of the proposed algorithm.

Fig. 3.12 illustrates the detection performance comparison of the proposed robust CSS algorithm based on low-rank MC, low-rank MC based CSS without denoising algorithm, CSS algorithm without CS technique implemented at SUs and the theoretical values as defined in (3.6) under different number of observed measurements at the FC. In this scenario, the number of SUs being implemented to sense the same L-channel group is $J = 10$. The number of active PUs in each L-channel group is 1 with random position, corresponding to the sparsity level of 12.5% in the whole spectrum of interest, which is close to the real spectrum occupancy scenario [1, 2]. It is noticed the P_d increases when the number of observed measurements at the FC increases from 10% to 25%. As the MC error becomes lower with more observed measurements at the FC, the detection performance of proposed robust MC based CSS algorithm can almost match with that of CSS algorithm without CS implemented at SUs when the observed measurements at the FC is increased to 25%.

Fig. 3.13 presents the P_d of the proposed robust CSS algorithm under different network sizes. In this scenario, the number of SUs being implemented to sense the same L-channel group is $J = 1$, 2, 5, 10, 20 and $J = 25$, respectively. In this scenario, the number of observed measurements at the FC is set to be 25% of the total measurements. With decreasing number of SUs participating in the CSS networks, the cooperative gain of CSS networks degrades. When the number of SUs implemented to sense the same L-channel group is decreased to $J = 1$, it becomes a single node spectrum sensing scenario, and the cooperative gain for CSS networks is decreased to zero. In such a case, it becomes a single node case which provides a benchmark for the comparison. It shows that the detection performance increases with increasing number of SUs implemented

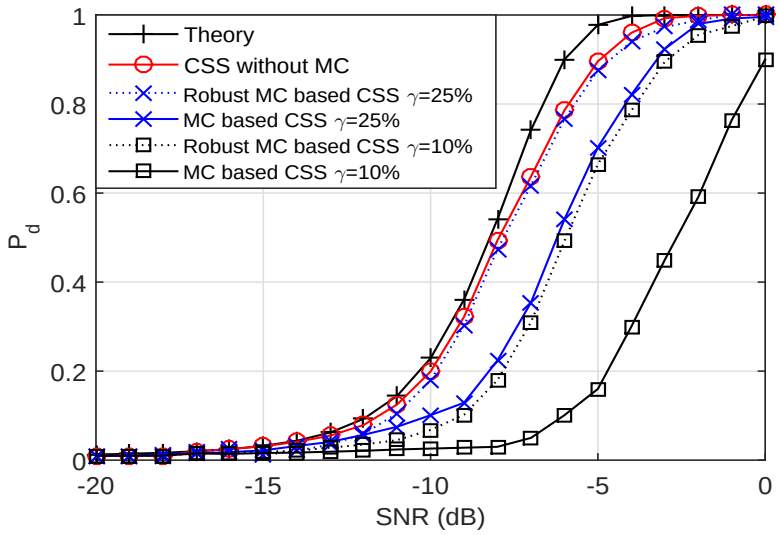

Figure 3.12: P_d comparison of the proposed robust cooperative spectrum sensing algorithm with simulated signals under different compression ratios γ.

to sense the same L-channel group. It is also noticed that the performance gap for the number of SUs implemented to sense the same L-channel group increased from 5 to 10 is higher than that of the number of SUs changing from 10 to 20. As more information about the spectrum is sent to the FC for the final decision making, which refers to more SUs implemented to sense the same L-channel group, the detection performance becomes closer to the theoretical curves. However, when the network size is enlarged, the computational complexity of MC increases. Therefore, it is a balance between the detection performance and the computational complexity of MC. In addition, in the case $J = 5$, there are 25 SUs participating in the CSS network as each $\frac{\mathcal{I}}{L} = 5$ SUs are implemented to sense the whole spectrum of interest at the same location. It can be observed that the detection performance reaches the theoretic curves with increasing number of SUs. Therefore, the performance degradation caused by the proposed channel division scheme would not be an issue in large scale networks.

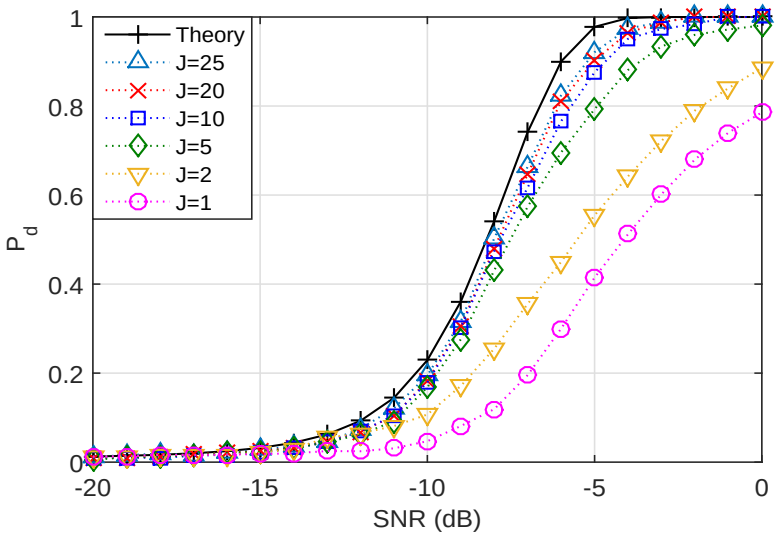

Figure 3.13: P_d comparison of the proposed robust cooperative spectrum sensing algorithm with simulated signals under different network sizes, compression ratio $\gamma = 25\%$.

3.5.2 Analyses on Real-WorldSignals

When the performance of proposed robust CSS algorithm based on low-rank MC is verified by the simulated signals, it is further tested on real-world signals collected by the RFeye sensing node installed in our lab as shown in Fig. 3.6 and a portable RFeye sensing node implemented at different locations in London.

Fig. 3.14 shows the detection performance comparison of the traditional and the proposed robust CSS algorithms under different compression ratios when the real-world signals recorded by the RFeye node are utilized as the signal resources. In this scenario, the number of SUs used to sense the same channels is $J = 5$ and the threshold is set to be -73.5 dBm. It is noticed that detection performance of the proposed algorithm would reach the target performance (P_d is higher than 90% and P_f is lower than 10%) when the compression ratio γ is no lower than about 25%. In addition, the detection performance of the proposed robust CSS algorithm is better than the traditional one with increasing compression ratio at the SU, which is the benefit of the proposed denoising algorithm. When compared with Fig 3.12, it can be observed that the detection perfor-

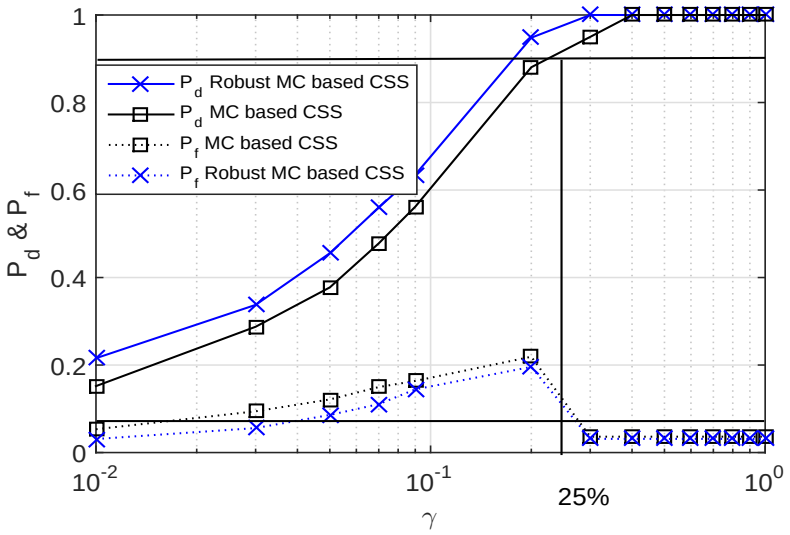

Figure 3.14: Proposed robust cooperative spectrum sensing algorithm achieves higher P_d and lower P_f than the traditional algorithm with real-world signals under different compression ratios γ, and threshold λ is -73.5 dBm.

mance becomes better when the compression ratio increases. This is also matched with the single node spectrum sensing algorithm based on CS in Fig. 3.8. Similar as the single node case shown in Fig. 3.8, there is a sharp dropping on P_f when the compression ratio γ becomes higher than 20%. The reason for the drop is that the MC becomes exact when the compression ratio is increased to be more than 20%, which lower the probability to falsely determine the unoccupied channels as occupied.

3.6 Summary

In this chapter, two algorithms for wideband spectrum sensing at sub-Nyquist sampling rates were proposed to reduce the computational complexity and improve the robustness to channel noise, which are designed for the cases of single SU and cooperative multiple SUs, respectively. The proposed algorithms were further tested on real-world signals after being validated by the theoretical results and the simulated signals. The analyses results showed that computational complexity of the proposed algorithms is much less

than other state-of-the-art methods. Furthermore, simulation results demonstrated that the detection performance of the proposed spectrum sensing algorithms on both single and multiple nodes were more robust to channel noise than the traditional algorithms.

Chapter 4

Data-Assisted Compressive Spectrum Sensing

In this chapter, the related work and the main contributions are firstly introduced in Section 4.1. In Section 4.2, the proposed data-assisted compressive spectrum sensing framework is presented, in which geolocation database is used to provide prior information for signal recovery. Additionally, Section 4.3 gives the numerical results of the proposed framework. Finally, Section 4.4 concludes this chapter.

4.1 Introduction

In order to avoid any harmful interference to primary services in TVWS, SUs, also named as WSDs, should have the knowledge of spectrum occupancy. Two approaches have been proposed to make SUs aware of the spectrum occupancy. One approach is geolocation database which is a centralized database to output the maximum allowable EIRP for each vacant TVWS channel for a specific location and time [1]. Geolocation database typically calculates the interference generated in wireless communication systems through theoretical propagation models rather than actual measurements, which

may result in inaccurate results for spectrum occupancy [97]. Furthermore, geolocation database approach can only protect the registered users. However, some SUs may not be registered, which may pose significant challenges to a geolocation database. For example, PMSE devices such as wireless microphone operate mostly on an unlicensed basis, without any record in TVWS [98]. The approach to protect unregistered applications is spectrum sensing. Spectrum sensing requires SUs to have the capability to detect spectrum holes that are not occupied by PUs. This approach provides instant channel occupancy information, but it may cause interference to some reserved channels which would be determined as vacant by sensing only. Therefore, a geolocation database can be utilized to improve the accuracy of spectrum sensing.

4.1.1 Related Work

So far, some work has been researched on the combination of spectrum sensing and geolocation database. Wang *et al.* [99] proposed a framework combining spectrum sensing with geolocation database was proposed, in which the utilization of spatial-temporal spectrum hole is maximized. Wang and Gao *et al.* [100] proposed to combine the advantages of spectrum sensing and geolocation database, in which different spectrum sensing modules are performed based on the output of geolocation database. Furthermore, Ribeiro *et al.* [98] implemented a framework into an experimental platform by combining wireless microphone sensors with a web-based geolocation database access for PMSE. However, all the existing frameworks required that SUs should build a direct link to the remote geolocation database. This direct link causes increasing loads in CR networks.

Besides the work on framework combining spectrum sensing and geolocation database, wideband spectrum sensing has attracted much attention. As limited by the Nyquist sampling theory, CS has been proposed to achieve sub-Nyquist rate by utilizing the natural sparse property of signals [14]. So far, amount of work has been done on compressive spectrum sensing [8, 18, 78, 79]. Many of the existing algorithms utilize l_1-norm minimization. However, as pointed out in [49], large coefficients are penalized more heavily

than smaller coefficients in l_1 minimization, which may lead to performance degeneration. In order to rectify a key difference between l_0 and l_1 minimization and balance the penalty on large coefficients and smaller coefficients of the sparse signal, Candes *et al.* [49] proposed an iteratively reweighted l_1 minimization algorithm by introducing weight for each bin of the signal to be recovered. Another approach to recover a sparse signal with fewer measurements is to replace the l_1 norm with l_p norm. In order to solve the l_p norm problem, an IRLS algorithm was proposed to perform sparse signal reconstruction [45, 46, 48, 101–103].

Moreover, recovering signals from compressed measurements by utilizing prior information has been studied in [104–107]. More specifically, Oscar *et al.* [104] proposed the prior information assisted sparse signal approximation algorithms: weighted basis pursuit denoising and weighted match pursuit. Additionally, two partial support information assisted CS algorithms were proposed respectively in [105] and [106], in which the weighted l_1 minimization approach with fixed weights on the known support is utilized to find the sparse solution for CS problems. Furthermore, Miosso *et al.* [107] proposed an IRLS based CS recovery algorithm utilizing the prior information, in which the weights are updated in each iteration of the IRLS algorithm. The different iterative approaches for weight setting in IRLS were compared in [50]. However, the iterative weight updating approach in IRLS introduces extra computational complexities for signal recovery.

4.1.2 Contributions

Motivated by the challenges identified above, the main contributions of this chapter are listed as follows:

1. A data-assisted compressive spectrum sensing framework is proposed, in which a geolocation database algorithm is implemented at SUs locally to provide prior information for the compressive spectrum sensing.

2. In the proposed framework, a DNRLS based compressive spectrum sensing algo-

rithm with lower computational complexity and fewer compressed measurements is proposed. In the proposed DNRLS, data generated by the locally stored geolocation database algorithm is utilized to replace the iterative process of weights updating in IRLS algorithm. Convergence and computational complexity of the proposed DNRLS are analysed.

3. Additionally, an efficient approach for calculating the maximum allowable EIRP is proposed to further improve the accuracy and efficiency of the geolocation database algorithm stored at SUs.

4. Furthermore, based on recent work on the trial within the Ofcom TVWS pilot [108], the proposed framework and algorithms are tested on real-world signals and data after being validated by the simulated signals and data.

4.2 Data-Assisted Compressive Spectrum Sensing Framework

In the wideband spectrum sensing scenario, as shown in Fig. 4.1 (a), multiple PUs exist in the multiband spectrum of interest and each SU is capable to detect the active PUs accurately and efficiently. The traditional hybrid frameworks with geolocation database and spectrum sensing proposed in [98–100] require a direct link to the remote geolocation database as shown in Fig. 4.1 (b). Dynamic changes of the spectrum would not be reflected unless the users are registered and updated in the centralized geolocation database. This process introduces several information exchanges such as the two-way transmissions between the SU and the geolocation database. Additionally, each transmission link introduces extra energy consumption at SUs and requires bandwidth for information exchange.

In order to reduce the necessary sampling rates at SUs and alleviate both the network load and the transmission errors between geolocation database and SUs, a framework is

proposed by combining compressive spectrum sensing with geolocation database algorithm, which is named as DNRLS framework as shown in Fig. 4.1 (c). In the proposed framework, the DTT database is maintained at the SU locally, which includes the DTT transmitter (TV base station) information. The geolocation database calculation algorithm is employed locally at the SU to calculate the maximum allowable EIRP P_{IB} of each TV channel based on the DTT database and geography location information of the SU. Before starting a new sensing period, the SU firstly collects its own geography location information by GPS. Then the location information is utilized as the input of geolocation database calculation algorithm to calculate P_{IB} of each TV channel at the SU locally. Subsequently, the obtained P_{IB} of each channel is mapped to the instant spectrum occupancy information and then fused with the historical spectrum occupancy information. The fused results can provide an estimation on the sparsity level of the spectrum of interest. According to the estimated sparsity level, SU can determine the minimal sampling rate to collect compressed measurements that can guarantee exact signal recovery. After the compressed measurements are obtained, fused channel occupancy information is utilized as the prior information for solving signal recovery problem for compressive spectrum sensing. As a result, necessary sampling rates for exact signal recovery and computational complexities are reduced at SUs. After the original signal is recovered, the decision on spectrum occupancy can be made by employing energy detection method. Furthermore, in order to further relax the SU, a Wilkinson's method [109] is adopted to calculate the maximum allowable EIRP P_{IB} of each TV channel efficiently.

4.2.1 Iteratively Reweighted Least Square Based Compressive Sensing

Before introducing the proposed DNRLS based compressive spectrum sensing algorithm, the IRLS algorithm is introduced. As aforementioned, l_1-norm has been proved as a good approximation for the NP-hard l_0-norm problem. However, as pointed out in [49], large coefficients are penalized more heavily than smaller coefficients in l_1 minimization,

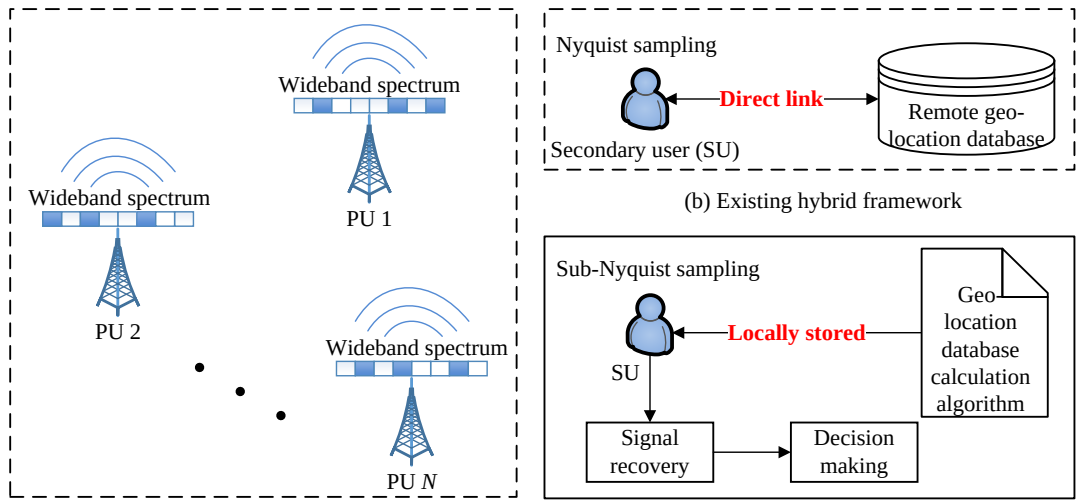

(a) Multiple primary users (PUs) with wideband spectrum

(b) Existing hybrid framework

(c) The proposed hybrid framework

Figure 4.1: (a). Scenario of wideband spectrum sensing with multiple primary users (PUs); (b). the existing framework with a conventional spectrum sensing at Nyquist rate and a direct link to remote database; and (c). the proposed DNRLS framework.

which may lead to performance degeneration. In order to balance the penalty on large coefficients and small coefficients in the signal to be recovered, an iterative process to construct the weights is introduced. Additionally, l_p-norm ($0 < p < 1$) is utilized to lower the computational complexity of signal recovery process caused by solving the l_1-norm optimization problem. Furthermore, IRLS based compressive sensing has been proposed to utilize the l_p-norm to reduce computational complexity of signal recovery [45, 46, 48, 101–103]. Meanwhile, the signal recovery performance is improved by introducing the iteratively updated weights.

Based on the compressive spectrum sensing model introduced in Section 2.3.4 of Chapter 2, with the IRLS algorithm, the original signal $\hat{\mathbf{s}}_\mathbf{f}$ can be obtained by solving the following problem in Lagrangian form

$$\min \quad \|\mathbf{\Theta} \cdot \mathbf{h_f}\hat{\mathbf{s}}_\mathbf{f} - \mathbf{x}\|_2^2 + \lambda_L \mathbf{W}\hat{\mathbf{s}}_\mathbf{f}{}^2, \tag{4.1}$$

where $\hat{\mathbf{s}}_\mathbf{f}$ refers to the signal to be reconstructed, and $\mathbf{h_f}$ refers to the related channel coefficients. $\mathbf{W} = diag\left\{\frac{1}{w_1}, \ldots, \frac{1}{w_n}, \ldots, \frac{1}{w_N}\right\}$ is a diagonal matrix which is computed

from the previous iteration and updated in each iteration. Here, w_n refers to the weight for the sample indexed by n, and $\mathbf{x} \in \mathcal{C}^{P\times 1}$. The compression ratio is defined as $\gamma = \frac{P}{N}$. Additionally, λ_L is the Lagrangian factor. In the lth ($l = 0, 1, \ldots, I_{\max}$) iteration of the IRLS algorithm, the weights are calculated with the recovered signal $\hat{\mathbf{s}}_{\mathbf{f\_n}}^{(l-1)}$ in the $(l-1)$th iteration as

$$w_n^{(l)} = \left(\left(\hat{\mathbf{s}}_{\mathbf{f\_n}}^{(l-1)} \right)^2 + \zeta^{(l)} \right)^{\frac{p}{2}-1}. \tag{4.2}$$

In (4.2), $\zeta^{(l)}$ is updated in each iteration, and it is a positive value to make sure that a zero-valued component in $\hat{\mathbf{s}}_{\mathbf{f}}$ does not strictly prohibit a non-zero estimate in the next iteration of weights update. Additionally, the solution of (4.1) at the lth iteration can be expressed as

$$\hat{\mathbf{s}}_{\mathbf{f\_n}}^{(l)} = \mathbf{W}^{(l)}\mathbf{\Theta}^{\mathrm{T}} \left(\mathbf{h_f}\mathbf{\Theta}\mathbf{W}^{(l)}\mathbf{\Theta}^{\mathrm{T}} + \lambda_L \mathbf{I}_P \right)^{-1} \mathbf{x}, \tag{4.3}$$

where the initial value for the weights w_n in $\mathbf{W}$ is 1, and then $\mathbf{W}^{(0)} = \mathbf{I}_N$. As a result, $\hat{\mathbf{s}}_{\mathbf{f\_n}}^{(0)} = \mathbf{\Theta}^{\mathrm{T}}(\mathbf{h_f} + \lambda_L \mathbf{I}_P)^{-1} x$. It is noted that (4.1) is a convex optimization problem when $p = 1$, and a non-convex optimization problem when $0 < p < 1$. As such, the solution to (4.1) can be local minima when $0 < p < 1$. Even though no theoretic guarantee, the numerical results in [45, 46, 48] has shown that the computed local minimizer of (4.1) is global minimizer when it is solved by IRLS.

Definition 2. *The RIP guarantees the stable and robust recovery by solving the optimization problem (2.21). We say that a matrix* $\mathbf{\Theta}$ *satisfies the property* (a, K, p) *if it satisfies*

$$\delta_{aK} + a^{\frac{2}{p}-1}\delta_{(a+1)K} < a^{\frac{2}{p}-1} - 1, \tag{4.4}$$

where $a > 1$*, and* K *is sparsity level of the spectrum of interest.*

Theorem 1. *Let* $0 < p \leq 1$*. If a* $P \times N$ *matrix satisfies* $P\,(a, K, p)$*, then [102]*

$$\|\hat{\mathbf{s}}_{\mathbf{f}} - \mathbf{s_f}\|_2^p \leq C^1\eta + C^2 \frac{\|\mathbf{s_f} - \mathbf{s_{f,K}}\|_p^p}{K^{\frac{2}{p}-1}}, \tag{4.5}$$

where $C^1 = 2^p \frac{1+a^{\left(\frac{p}{2}-1\right)}\left(\frac{p}{2}-1\right)^{-\frac{p}{2}}}{\left(1-\delta_{(a+1)K}\right)^{\frac{p}{2}}-(1+\delta_{aK})^{\frac{p}{2}}a^{\left(\frac{p}{2}-1\right)}}$, *and*
$C^2 = \frac{2\left(\frac{p}{2-p}\right)^{\frac{p}{2}}}{a^{\left(1-\frac{p}{2}\right)}}\left(1+\frac{\left(\left(\frac{p}{2}-1\right)^{-\frac{p}{2}}+a^{\left(\frac{p}{2}-1\right)}\right)(1+\delta_{aK})^{\frac{p}{2}}}{\left(1-\delta_{(a+1)K}\right)^{\frac{p}{2}}-(1+\delta_{aK})^{\frac{p}{2}}a^{\left(\frac{p}{2}-1\right)}}\right)$.

4.2.2 Non-Iteratively Reweighted Least Square Based Compressive Sensing

In the traditional IRLS based CS given by (4.1), the key challenge is to find the optimal set of weights $\mathbf{W}$ in an iterative process for a better estimate of the original signals. It should be noted that the iterations generate more computational complexities during the signal recovery process. When part of the maximum allowable EIRP is available in advance, the iterative process can be removed without degrading the recovery performance heavily. In this chapter, a DNRLS based compressive spectrum sensing algorithm is proposed. In the proposed algorithm, a geolocation database algorithm is implemented at SUs locally to provide data for weights calculation. It is achieved by a non-iterative method, so that SUs do not need any additional link to a centralized geolocation database. Based on (4.2), the proposed calculation yields the weights as

$$w_n = \left(|\bar{\gamma}_n|^2 + \zeta\right)^{\frac{p}{2}-1}, \tag{4.6}$$

where ζ is a positive value same as $\zeta^{(l)}$ in (4.2), and $\bar{\boldsymbol{\gamma}} = \{\bar{\gamma}_1, \ldots \bar{\gamma}_n, \ldots \bar{\gamma}_N\}$ is constructed by the channel historical data and the output of geolocation database algorithm. By introducing weights to solving the optimization problem (4.1), the samples with high power density will be penalty by relative light weights. While for the samples with low power density, the weighted penalty will be relative large. By doing so, the optimization result of (4.1) will be more close to the solution of the original l_0-norm problem. The construction of $\bar{\boldsymbol{\gamma}}$ in detail is introduced in the following.

In the $(t+1)$th sensing period, the maximum allowable EIRP $P_{IB}(t+1)$ is calculated for the current period by the proposed Wilkinson's method based DTT location proba-

bility calculation algorithm introduced in Section 4.2.3. Subsequently, the $P_{IB}(t+1)$ is mapped to $\boldsymbol{\gamma}(t+1)$. Furthermore, the averaged $\bar{\boldsymbol{\gamma}}(t+1)$ is updated by fusing $\bar{\boldsymbol{\gamma}}(t+1)$ with $\bar{\boldsymbol{\gamma}}(t)$ as

$$\bar{\boldsymbol{\gamma}}(t+1) = \xi\bar{\boldsymbol{\gamma}}(t) + (1-\xi)\boldsymbol{\gamma}(t+1), \tag{4.7}$$

where $\bar{\boldsymbol{\gamma}}(t)$ is the historical data for the weights construction at the tth sensing period with $t = \{0, 1, \ldots, T\}$, and $\xi\,(0 < \xi < 1)$ is the weight for $\bar{\boldsymbol{\gamma}}(t)$. Herein T is the window size for SUs to fuse the current allowable maximum P_{IB} with the historical data. At a SU, only the $\bar{\boldsymbol{\gamma}}(t)$ is stored locally after the tth sensing period. If there is any new unregistered user showing up in the spectrum of interest in tth period, the related DTT transmitter information used for geolocation database calculation algorithm is updated locally. This makes the proposed weights calculation robust to the new unregistered users. Meanwhile, the geolocation database at other SUs would not be influenced. In the $(t+1)$th period, the $\boldsymbol{\gamma}(t+1)$ provided by the local geolocation database calculation algorithm would be updated accordingly by considering the unregistered users. After $\bar{\boldsymbol{\gamma}}(t+1)$ for the current sensing period is obtained to calculate the weights, a more accurate spectrum estimation can be obtained by solving the following non-iterative problem

$$\hat{\mathbf{s}}_{\mathbf{f}} = \tilde{\mathbf{W}}\boldsymbol{\Theta}^{\mathrm{T}}\left(\mathbf{h}_{\mathbf{f}}\hat{\mathbf{s}}_{\mathbf{f}}\tilde{\mathbf{W}}\boldsymbol{\Theta}^{\mathrm{T}} + \lambda_L \mathrm{I}_P\right)^{-1}\mathbf{x}. \tag{4.8}$$

In (4.8), $\tilde{\mathbf{W}} = diag\left(\frac{1}{w_1}, \ldots, \frac{1}{w_n}, \ldots, \frac{1}{w_1}\right)$ is a diagonal matrix in which w_n is calculated by (4.6) to replace the iterative update process in (4.2). In the proposed DNRLS based compressive spectrum sensing algorithm, the accuracy of $\bar{\boldsymbol{\gamma}}$ would affect the recovery performance.

4.2.2.1 Convergence Analyses

If there is no unregistered user in the spectrum of interest, which means the values of $\bar{\boldsymbol{\gamma}}$ used to construct the weights are accurate, the recovery performance of DNRLS is

very good. When the unregistered users show up in the spectrum of interest at the 1st sensing period, the $\bar{\boldsymbol{\gamma}}(1)$ becomes inaccurate on the corresponding bins as the output of the local geolocation database algorithm $\boldsymbol{\gamma}(1)$ for the 1st period is inaccurate. As a result, the signal recovery and detection performance would be degraded accordingly. In the tth period after the unregistered user shows up in the spectrum of interest, $\boldsymbol{\gamma}(t)$ is fused with the historical data $\bar{\boldsymbol{\gamma}}(t-1)$ of the $(t-1)$th period. The accuracy of weights $\bar{\boldsymbol{\gamma}}(T)$ are dependent on the window size T for the weights fusion at SUs. The weights fusion process is shown as follows:

$$\begin{aligned}
\bar{\boldsymbol{\gamma}}(1) &= \xi\bar{\boldsymbol{\gamma}}(0) + (1-\xi)\boldsymbol{\gamma}(1), \qquad \text{(1st period)} \\
\bar{\boldsymbol{\gamma}}(1) &= \xi\bar{\boldsymbol{\gamma}}(1) + (1-\xi)\boldsymbol{\gamma}(2), \qquad \text{(1st period)} \\
\bar{\boldsymbol{\gamma}}(T) &= \xi\bar{\boldsymbol{\gamma}}(T-1) + (1-\xi)\boldsymbol{\gamma}(T), \quad \text{(Tth period)}
\end{aligned} \tag{4.9}$$

where $\bar{\boldsymbol{\gamma}}(0)$ is the historical data for weights construction before unregistered user showing up, and $\boldsymbol{\gamma}(1)$ is the output of the locally implemented geolocation database algorithm for the period when unregistered users show up in the spectrum of interest. As $\boldsymbol{\gamma}(2) = \cdots = \boldsymbol{\gamma}(T) = \boldsymbol{\gamma}$, which represents the real spectrum status with consideration of the unregistered users in the spectrum of interest, $\bar{\boldsymbol{\gamma}}(T)$ can be expressed as

$$\begin{aligned}
\bar{\boldsymbol{\gamma}}(T) &= \xi^T \times \bar{\boldsymbol{\gamma}}(0) + (1-\xi)\,\xi^{T-1} \times \boldsymbol{\gamma}(1) + \frac{(1-\xi) \times \boldsymbol{\gamma} \times \left(1-\xi^{T-1}\right)}{1-\xi} \\
&= \xi^T \times \bar{\boldsymbol{\gamma}}(0) + (1-\xi)\,\xi^{T-1} \times \boldsymbol{\gamma}(1) + \left(1-(\xi)^{T-1}\right) \times \boldsymbol{\gamma}.
\end{aligned} \tag{4.10}$$

It is noted that $\bar{\boldsymbol{\gamma}}(T)$ will converge fast to $\boldsymbol{\gamma}$ after unregistered users show up in the spectrum of interest. The smaller ξ, the convergence speed goes faster. Additionally, part of channels in TVWS are fixed and utilized by DTV signals, and some of the channels are reserved for other purposes. As result, at least the weights for those fixed channels in $\bar{\boldsymbol{\gamma}}(0)$ and $\boldsymbol{\gamma}(1)$ are accurate. This characteristic provides a guarantee that the recovery performance would not be degraded heavily when unregistered users show up in the spectrum of interest. With increasing window size T, the influence of inaccurate weights

in $\bar{\boldsymbol{\gamma}}(0)$ and $\boldsymbol{\gamma}(1)$ degrades. The influence of the window size T is shown in the numerical analyses part in Section 4.3.

4.2.2.2 Complexity Analyses

The computational complexity reduction of the proposed DNRLS based compressive spectrum sensing comes from following three parts. Firstly, in the traditional IRLS algorithm, the inverse of $\left(\mathbf{h_f}\boldsymbol{\Theta}\mathbf{W}^{(l)}\boldsymbol{\Theta}^{\mathbf{T}} + \lambda_L \mathbf{I}_P\right)$ takes $\mathrm{O}\left(P^3\right)$ and it is required in each iteration. In large size CS problem, solving a problem with complexity $\mathrm{O}\left(P^3\right)$ $I_{\max}$ times is unacceptable. As summarized in **Algorithm 2**, the proposed DNRLS based CS algorithm solves the signal recovery problem in a non-iterative approach. Therefore, the computational complexity is $1/I_{\max}$ of the traditional IRLS based compressive spectrum sensing in which $I_{\max}$ iterations are required to get an accurate estimation of the spectrum. Secondly, the computational complexity reduction is contributed by the fewer measurements required by the proposed DNRLS algorithm to achieve exact signal recovery. In the proposed DNRLS algorithm, the minimal number of measurements P for exact recovery is reduced to $\tilde{P}\left(\tilde{P} < P\right)$. It leads to a large computational complexity reduction as the complexity of solving the inverse of $\left(\mathbf{h_f}\boldsymbol{\Theta}\mathbf{W}^{(l)}\boldsymbol{\Theta}^{\mathbf{T}} + \lambda_L \mathbf{I}_P\right)$ is $\mathrm{O}\left(\tilde{P}^3\right)$. The performance analyses are further shown in numerical analyses. Thirdly, the computational complexity reduction comes from the calculation of P_{IB} in the proposed DNRLS framework. Specifically, to minimize the necessary computational complexity at SUs, the Wilkilson's method is utilized to calculate the P_{IB} for each TVWS channel. The details of the Wilkilson's method based DTT location probability calculation algorithm are introduced in section 4.2.3.

Algorithm 2 Data-assisted non-iteratively reweighted least squares based compressive spectrum sensing

Input: p, λ, $\mathbf{\Theta}$, $\mathbf{x}$, ζ, $\bar{\boldsymbol{\gamma}}(t)$.

1: Calculate $P_{IB}(t+1)$ by the proposed Wilkinson's method based DTT location probability model introduced in Section 4.2.3.
2: Map $P_{IB}(t+1)$ to $\boldsymbol{\gamma}(t+1)$.
3: Calculate $\bar{\boldsymbol{\gamma}}(t+1)$ by $\bar{\boldsymbol{\gamma}}(t)$ and $\boldsymbol{\gamma}(t+1)$ based on (4.7).
4: Perform signal recovery by (4.8) to get $\hat{\mathbf{s}}_{\mathbf{f}}$.
5: Make decision $\mathbf{d}$ on spectrum occupancy by comparing $\hat{\mathbf{s}}_{\mathbf{f}}$ with λ defined in (2.16).
6: **return** $\mathbf{d}$.

4.2.3 Proposed Wilkinson's Method Based DTT Location Probability Calculation Algorithm

At a SU, the calculation of maximum allowable EIRP P_{IB} of each channel in TVWS should be efficient and accurate. Monte Carlo method and Schwartz-Yeh's method are the two algorithms approved by regulators to calculate the maximum allowable EIRP P_{IB}. Schwartz-Yeh's method is an approximate algorithm in which infinite loops are used to calculate the mean and standard deviation of log-normal distribution variables such as variables A, B and E in (2.24) and (2.26) [74]. However, the large computational complexity and low efficiency of the Schwartz-Yeh's method are difficult to overcome at power-limited SUs. In this chapter, the Wilkinson's method is invoked to calculate q_1, q_2 and P_{IB} in a much more efficient way.

4.2.3.1 Maximum Allowable Equivalent Isotropic Radiated Power Calculation

Based on the Wilkinson's method given in Appendix A, q_1 and q_2 can be calculated accordingly. Taking the calculation of q_1 as an example, as shown in (2.24), $\frac{P_{as,\min}}{P_{as}}+\frac{V}{P_{as}} = A+B \leq 1$. $10\log_{10}(A+B) \leq 0$, which is equivalent to $X_{(dB)} = 10\log_{10}\left(10^{\frac{A_{dB}}{10}}+10^{\frac{B_{dB}}{10}}\right) \leq 0$. It can be fitted into the precondition of Wilkinson's method to get $10^{\frac{A_{dB}}{10}}+10^{\frac{B_{dB}}{10}} = 10^{X_{dB}} = e^{\Lambda_1}+e^{\Lambda_2}$. Therefore, $\Lambda_1 = \rho \times A_{(dB)}$ and $\Lambda_2 = \rho \times B_{(dB)}$. The relevant

correlation coefficient of A and B can be given as

$$r_{A,B} = \frac{\text{cov}\left(A_{(dB)},\, B_{(dB)}\right)}{\sqrt{\text{var}\left(A_{(dB)}\right)\text{var}\left(B_{(dB)}\right)}} = \frac{\sigma_{as}}{\sqrt{\sigma_{as}^2 + \sigma_V^2}}, \tag{4.11}$$

where σ_{as} and σ_V can be calculated based on the DTT transmitter information used for geolocation database calculation algorithm. Based on (A.1) and (A.2), μ_1 and μ_2 can be obtained. Furthermore, m_X and σ_X can be calculated according to (A.3) and (A.4), and then q_1 is obtained by (2.25) consequently.

Similarly, q_2 can be calculated by the Wilkinson's method by the following procedure:

1. Input m_{as}, σ_{as}, m_V, σ_V, m_C and σ_C as shown in (2.26), which can be calculated based on the DTT transmitter information used for geolocation database calculation algorithm;

2. Calculate m_D and σ_D by Wilkinson's method based on m_V, σ_V, m_C and σ_C;

3. Calculate m_A, σ_A, m_E and σ_E by Wilkinson's method based on m_{as}, σ_{as}, m_D and σ_D;

4. Calculate m_Y and σ_Y by Wilkinson's method based on m_A, σ_A, m_E and σ_E;

5. Calculate q_2 by (2.27) based on m_A, σ_A, m_E and σ_E.

With q_1 and q_2 calculated by the Wilkinson's method, the procedure of calculating P_{IB} is shown in Fig. 4.2. Firstly, input the mean and standard derivation of the received power of wanted DTT signal, i.e., P_{as}, and the minimum required power of wanted DTT signal, i.e., V, which can be obtained from the DTT transmitter information used for geolocation database calculation algorithm. As defined in IEEE 802.22 standard, the maximum allowable EIRP that can be utilized in TV frequency band is 4 watts [93]. Therefore, the predefined maximum allowable value (4 watts) is assigned to P_{IB} for each TVWS channel. Subsequently, the mean and standard derivation of C can be calculated based on initial value of P_{IB}. Additionally, q_1 and q_2 are calculated by the Wilkinson's

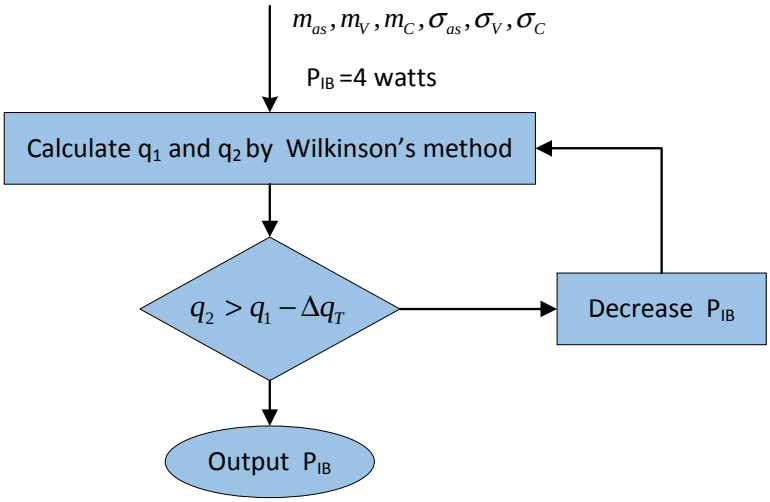

Figure 4.2: The procedure of calculating maximum allowable P_{IB}.

method with inputs m_{as}, m_V, m_C, σ_{as}, σ_V, σ_C. Consequently, the corresponding P_{IB} is updated, which is utilized to calculate the new q_1 and q_2 until $q_2 \leq q_1 - \Delta q_T$. The output of this procedure is the maximum allowable EIRP P_{IB} for each TVWS channel.

4.3 Numerical Analyses

The analyses of the proposed stand-alone DNRLS framework on the simulated signals and data are presented in this section. Furthermore, the proposed framework is tested on the real-world signals collected by RFeye node and the data obtained from the geolocation database provided by Nominet.

4.3.1 Numerical Analyses on Simulated Signals and Data

In the simulations, OFDM signals are simulated as PUs, which is used by the DVB-T signals in TVWS from 470MHz to 790MHz in the UK. There are a total of 40 channels in TVWS with a bandwidth of 8MHz for each channel. It is assumed that each PU is independent and only locates at one channel. The transmission channel for signals is modeled as an AWGN channel. The target P_f is set to be 0.01.

Table 4-A: Error rates comparison.

	q_1	q_2	P_{IB}
Schwartz-Yeh's method	31.25%	4.76%	7.87%
Wilkinson's method	9.36%	1.31%	1.54%

The comparison of the proposed and traditional methods for calculating maximum allowable EIRP are presented firstly. Since Monte Carlo simulation is based on no assumption and approximation, its results can be considered precise as long as the number of trials is large enough. With 10,000 points, Monte Carlo simulation shows a relatively stable performance. By taking the results obtained by Monte Carlo simulation as a benchmark, the accuracy of the Schwartz-Yeh's method and Wilkinson's method can be measured by the error rate $\Delta Q(\cdot)/Q_{(\text{MonteCarlo})}(\cdot)$, where $Q_{(\text{MonteCarlo})}(\cdot)$ refers to values calculated by Monte Carlo simulation and $\Delta Q(\cdot)$ refers to the absolute difference of parameters' values between Schwartz-Yeh's method or Wilkinson's method and the Monte Carlo simulation. More specifically, $\Delta Q(q_1) = \left|q_1^{S,W} - q_1^M\right|$, $\Delta Q(q_2) = \left|q_2^{S,W} - q_2^M\right|$ and $\Delta Q(P_{IB}) = \left|P_{IB}^{S,W} - P_{IB}^M\right|$, where $q_1^{S,W}$, $q_2^{S,W}$ and $P_{IB}^{S,W}$ refer to the corresponding values calculated by the Schwartz-Yeh's method or Wilkinson's method respectively, and q_1^M, q_2^M and P_{IB}^M refer to the corresponding values calculated by Monte Carlo simulation. The error rates of q_1, q_2 and P_{IB} calculated by the Schwartz-Yeh's method and Wilkinson's method are shown in Table 4-A. It shows that the proposed Wilkinson's method outperforms the Schwartz-Yeh's method in terms of the calculation accuracy.

Similarly as the error rate calculation, running time of Monte Carlo simulation with 10,000 points is chosen as a benchmark when measuring the running time for the calculation of q_1, q_2 and q_{IB}. Table 4-B shows the running time comparison of the Schwartz-Yeh's and Wilkinson's methods. It can be observed that the Wilkinson's method reduces the running time significantly in comparison with the Schwartz-Yeh's method. Therefore, the proposed Wilkinson's method is very suitable for SUs with limited power to obtain the q_1, q_2 and P_{IB} efficiently.

Table 4-B: Running time comparison.

	q_1	q_2	P_{IB}
Schwartz-Yeh's method	15966.04%	153278.65%	75462.57%
Wilkinson's method	99.06%	98.89%	99.47%

Table 4-C: Comparison of actual maximum allowable EIRP P_{IB} in Oxford.

	Actual Maximum Allowable EIRP P_{IB} (Watt)			
	The latest release of Ofcom TV white space model by Wilkinson's method			Power control model
Available Channel	Open	Suburban	Urban	
22	0	4.0000	4.0000	4.0000
25	0	4.0000	4.0000	4.0000
28	0	4.0000	4.0000	4.0000
29	0.0025	4.0000	4.0000	4.0000
40	0	4.0000	4.0000	4.0000
43	0	4.0000	4.0000	4.0000
46	0	4.0000	4.0000	4.0000
49	0.0013	4.0000	4.0000	4.0000
51	0.3981	1.2589	4.0000	0.0002
54	0.0013	4.0000	4.0000	4.0000
58	0.0013	4.0000	4.0000	4.0000

After validating the accuracy and efficiency, a national grid reference (NGR) based geolocation database is built with the proposed Wilkinson's method. By utilizing the DTT transmitter information for geolocation database calculation algorithm, P_{IB} can be calculated by the proposed Wilkinson's method based DTT location probability model for any specific location. Taking an NGR number of SP515065 in Oxford as a test location, the maximum allowable EIRP calculated by the power control and the proposed location probability model are shown in Table 4-C.

As shown in Table 4-C, there are 11 available channels at SP515065 in total. In the proposed location probability model, the transmission environment is classified into three situations: open, suburban and urban. Coupling gain in different situations is treated differently, leading to different interference toleration levels of DTT receivers. It is obvious that the power attenuation in open areas is much lower than suburban and urban areas. As a result, the actual maximum allowable EIRP P_{IB} in open areas is

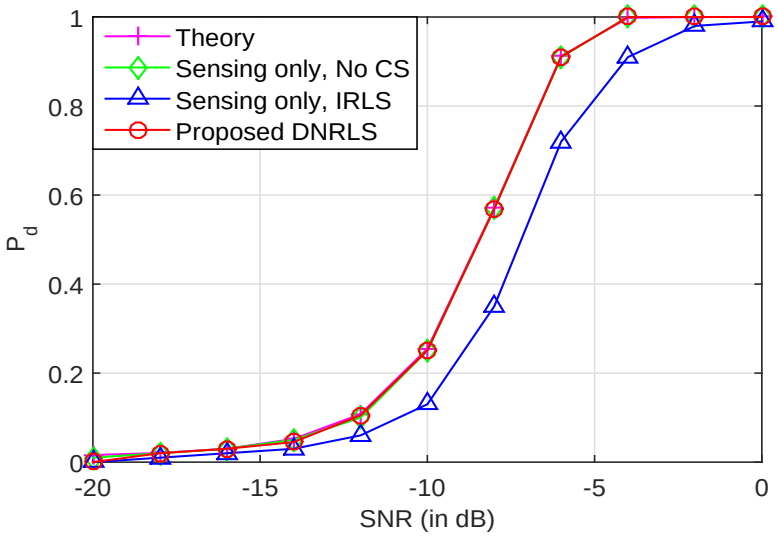

Figure 4.3: Detection performance on the simulated signals and data under different SNR values, $p = 0.1$, compression ratio $\gamma = 20\%$.

smaller than the other two situations at a certain NGR location. Taking channel 51 as an example, the P_{IB} is 0.0002 watts in power control model. However, the spectrum of interest could be utilized more effectively if the transmission environment is classified, which is 0.3981 watts in open areas, 1.2589 watts in suburban areas and 4.0000 watts in urban areas.

Based on the obtained P_{IB} from the local geolocation database algorithm, the weights are constructed by fusing the current P_{IB} with historical data in the proposed DNRLS based compressive spectrum sensing. Fig. 4.3 shows detection performance of the sensing only approach and the proposed DNRLS framework implemented at SUs, where p is set to be 0.1. It is observed that the detection performance of the sensing only approach without CS implemented at a SU is matched with the theoretical curve, which is presented as a benchmark and expressed as (3.6).

Fig. 4.3 shows that detection performance of the sensing only approach with IRLS is smaller than the theoretic curve due to the signal recovery errors caused by the sub-Nyquist sampling ($\gamma = 20\%$). When the proposed DNRLS framework is performed, detection probability increases greatly which can almost match with the theoretic curve.

The reason for the large performance improvement is that the data used to construct the weights is the exact representation of the spectrum of interest if there is no unregistered user. Additionally, it is noted that the sensing only approach with IRLS requires an iterative process to update the weights. This iterative process introduces a higher computational complexity. As a result, the proposed DNRLS based compressive spectrum sensing can achieve better detection performance with $(I_{\max}-1)/I_{\max}-1$ of computational complexity reduced in comparison with the sensing only approach with IRLS.

Fig. 4.4 shows detection probability of the sensing only approach with IRLS and the proposed DNRLS framework with varying compression ratios. In this scenario, the spectrum occupancy ratio is assumed to be 12.5%, p is 0.1 and the SNR value is -5dB. It is noted that there is a big difference on the necessary number of measurements between the proposed DNRLS framework and the sensing only approach to achieve the same detection probability. Specifically, as shown in Fig. 4.4, the proposed DNRLS framework can achieve 90% detection probability when the compression ratio is no higher than 7%. However, the sensing only approach requires the compression ratio to be about 20% in order to achieve the same performance. As a result, the sampling rates can be reduced by 13% without degrading the detection performance.

The detection performance of the proposed DNRLS framework is shown in Fig. 4.5 with different spectrum occupancy ratios in TVWS and different p values for l_p. In this scenario, SNR is set to be -5dB and the positions of these active PUs are set to be random. In compressive spectrum sensing, increasing spectrum occupancy in spectrum of interest refers to higher sparsity levels of the signal to be recovered. It can be observed that the detection performance becomes improved with decreasing value of p and fixed sparsity level. Meanwhile, the detection performance is degraded slightly with increasing sparsity level increases when the value for p is fixed. As a result, more compressed measurements should be collected at SUs to avoid performance degradation when sparsity level increases.

Fig. 4.6 shows the detection probability of the proposed DNRLS framework under

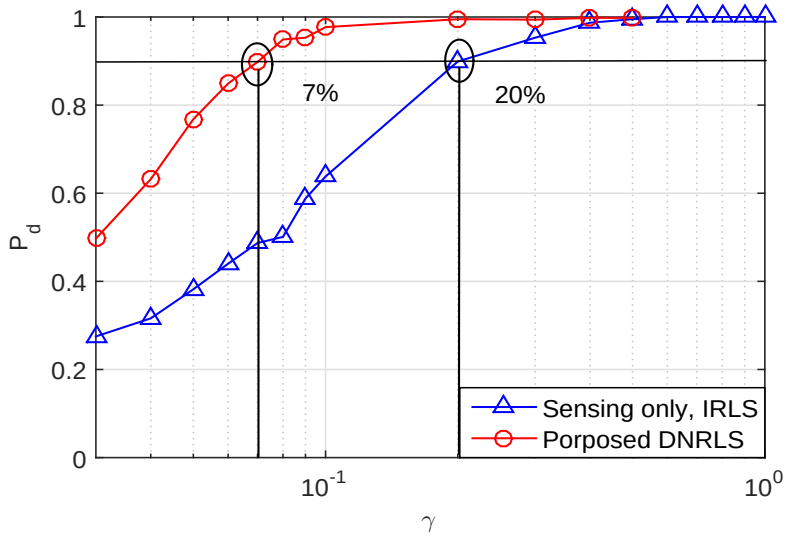

Figure 4.4: Detection performance on the simulated signals and data under different compression ratios γ, $p = 0.1$, SNR=-5dB.

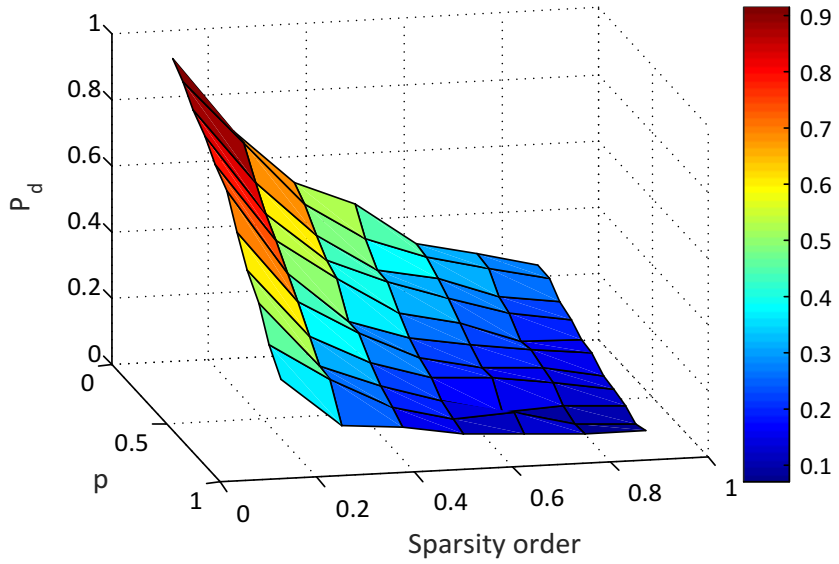

Figure 4.5: Detection performance on the simulated signals and data under different sparsity levels and p values, compression ratio $\gamma = 10\%$, SNR=-5dB.

different window sizes T with new unregistered users showing up in the spectrum of interest. In this scenario, the spectrum occupancy is 12.5%, p is 0.1 and compression ratio is 10%. With unregistered users in TVWS, only half of the weights for the channels with active PUs are exact. It can be observed that the detection performance is degraded from 98% to 85% in the first sensing period after a new unregistered user

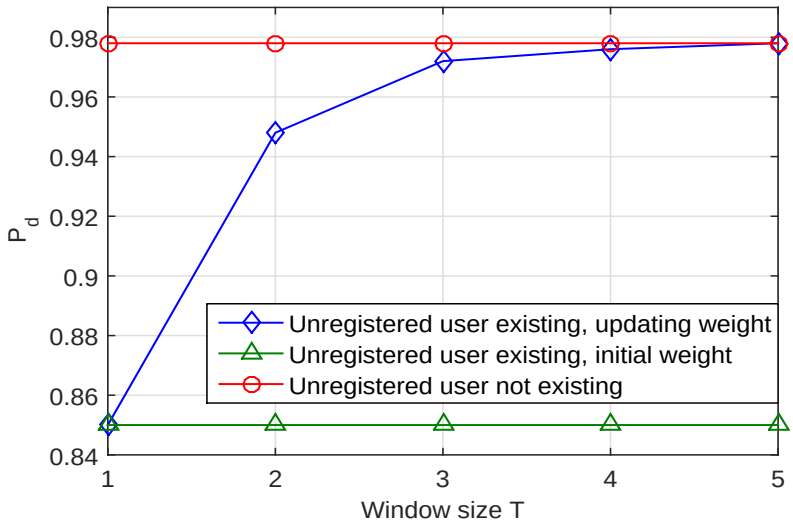

Figure 4.6: Detection performance on the simulated signals and data under different window sizes T with unregistered users existing, compression ratio $\gamma = 10\%$, $p = 0.1$, SNR=-5dB.

shows up in TVWS. However, after one sensing period has passed, which refers to $T = 2$, the detection performance is improved to about 95%. This improvement benefits from the weights are constructed by fusing the output of the geolocation database algorithm with the historical data. The geolocation database algorithm utilizes the self-maintained geolocation database at SU locally which contains the new unregistered users' information. Furthermore, the detection performance converges to 98% after four updates of the weights. With increasing window size T, the improvement on detection performance becomes slower after the first updating on the weights. However, if the unregistered user shows up again in the same position of TVWS, detection probability of the proposed DNRLS framework falls between 85% and 95%, which is dependent on the window size T. If T is large enough, the detection probability would get close to 95%.

4.3.2 Numerical Analyses on Real-World Signals and Data

After the proposed DNRLS compressive spectrum sensing algorithm is validated by the simulated signals and data, the proposed framework is tested on real-world signals col-

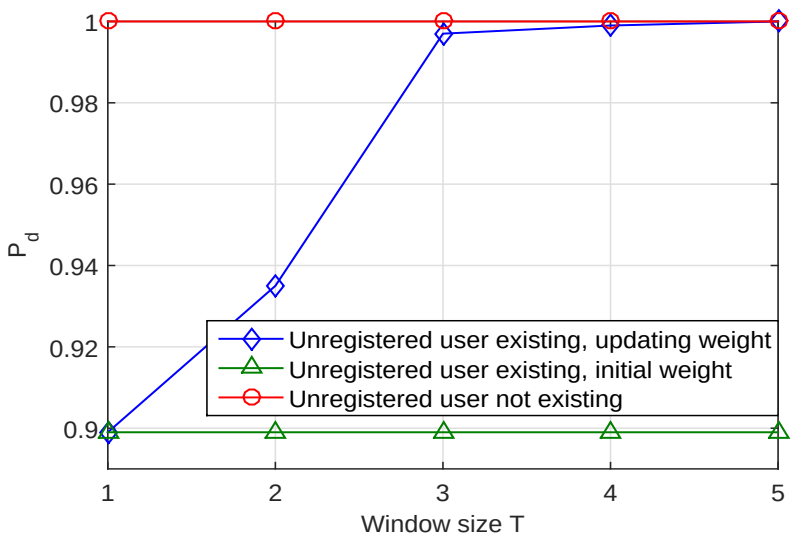

Figure 4.7: Detection performance on the real-world signals under different window sizes T with unregistered users existing, compression ratio $\gamma = 10\%$, $p = 0.1$.

lected by the CRFS RFeye node and the real data provided by the geolocation database from Nominet qualified by Ofcom. The setup for RFeye node as shown in Fig. 3.6 in Section 3.3.2 of Chapter 3. Some pilots in TVWS have been undertaken in the UK as launched by the Ofcom. In the trials run at QMUL, an unregistered user is transmitted in TVWS channel 27 (518MHz to 526MHz). In this case, the historical data and P_{IB} from the geolocation database would not be exact for the channel 27 as it is the first time for the unregistered user showing up in TVWS. As a result, the output of the geolocation database would still allow a high EIRP in channel 27. The simulation results for the case with unregistered users under different window sizes T are shown in Fig. 4.7. It can be observed that the detection performance would be degraded once the unregistered user shows up in TVWS. This is caused by the inexact weights constructed by the inaccurate P_{IB} in channel 27. Similarly as Fig. 4.6, the detection performance is increased largely after window size T is increased to 2. With increasing window size, the detection performance of the proposed DNRLS framework converges efficiently.

Based on the fast convergence performance shown in Fig. 4.6 and Fig. 4.7, it can be indicated the practicability of the proposed DNRLS framework is reasonable. The

implementation of compressive spectrum sensing with a geolocation database algorithm can improve the energy efficiency at SUs by reducing its computational complexities. Therefore, such an energy efficient algorithm could be applied to multiple scenarios with energy-constrained devices.

4.4 Summary

This chapter introduced a stand-alone DNRLS framework combining compressive spectrum sensing with geolocation database for wideband spectrum. In particular, a DNRL based compressive spectrum sensing algorithm was proposed to reduce the sampling rates and lower the computational complexities by invoking geolocation database. Additionally, the proposed framework was tested on the real-world signals and data after having been validated by the simulated signals and data over TVWS. The numerical results showed that the computational complexities of signal recovery process were reduced with improved detection performance. Furthermore, it is noted the proposed framework can also provide benefits to relax the requirement on sparsity level estimation in compressive spectrum sensing. More specifically, the compression ratio at SUs is difficult to determine in existing CS algorithms, as the sparsity level is unknown before the compressive spectrum sensing is performed. By the proposed framework, an estimation of the sparsity level can be easily obtained by invoking of geolcoation database. As a result, the lowest compression ratio guaranteing exact recovery can be determined by the well-known relationship between necessary measurements and the sparsity level, which further leads to lower complexity and less energy consumption at SUs.

Chapter 5

Malicious User Detection Based on Low-Rank Matrix Completion

In this chapter, a malicious user detection model is proposed to improve the security of CSS networks. The low-rank MC technique is invoked in the proposed model. More specifically, Section 5.1 introduces the related work and main contributions of the work in this chapter. Section 5.2 describes the system model of CSS networks with malicious users. Section 5.3 presents the proposed low-rank MC based malicious user detection framework along with the proposed rank estimation algorithm and the estimation strategy for the number of malicious users. Section 5.4 shows the numerical analyses of the proposed framework on both simulated and real-world signals. Section 5.5 concludes this chapter.

5.1 Introduction

In CRNs, CSS is an effective approach to offer significant performance gain in incumbent detection by exploiting the spatial diversity of the collaborative SUs [16, 17]. However, due to the openness of low-layer protocol stacks, CSS networks are vulnerable to endure

attacks from spectrum sensing data falsification (SSDF). This characteristic of CSS networks blocks the application of CR technique in large-scale networks.

In CSS networks, SUs that launch SSDF attackers are named as malicious users. The main goals of malicious attacks come from two aspects: 1) decreasing detection probability for disturbing the normal operations of PUs; 2) increasing false alarm probability to deprive access opportunities of the honest SUs [110]. In decentralized CSS networks, sensing results are exchanged between neighbor SUs for improving the network reliability to link failure. However, this characteristic makes decentralized CSS more vulnerable to malicious attacks [111], as the observations at honest SUs would be known by malicious users during the convergence process. Furthermore, fake data can be integrated into the decisions of honest neighbor SUs, which eventually brings significant performance degradation of the whole CSS networks [112]. In centralized CSS networks, all SUs report their local sensing data to an FC, at which the final decision on spectrum occupancy is made. By doing so, all participating SUs including malicious users can only obtain the spectrum occupancy knowledge from the FC. Thus, the observations at honest SUs in CSS networks would not leak to malicious users directly. However, as the fake data are still considered in decision making process, existence of malicious users may lead to false decisions at the FC. Generally, regardless of the types of malicious attacks and CSS networks, malicious users have posed significant challenges on the security in CSS networks. As a result, detection accuracy of malicious users is quite essential to guarantee the security of CSS networks.

Along with improving the security of CSS networks through malicious user detection, another key challenge for secure CSS networks comes from the data acquisition costs reduction at SUs. As the spectrum is normally underutilized, spectral signal exhibits a sparse property [8] in the frequency domain. It is further noted that this sparse property can be transformed to a low-rank property of the matrix constructed by spectral signals received at spatially distributed SUs [18], since nearby locations or adjacent channels are supposed to share the similar spectrum occupancies. The MC technique [96] can

be applied to recover the complete matrix with only partial of observable elements. Specifically, by invoking MC technique at the FC, SUs in CSS networks can sense less number of channels as the unsensed channels can be reconstructed from the sensed channels based on the low-rank property.

5.1.1 Related Work

So far, malicious user detection has been widely researched for enhancing the security of CSS networks [113–121]. Specifically, the performance of CSS networks with single and multiple malicious users were investigated by Wang *et al.* in [113, 114], respectively. Particularly, based on the historical reports from SUs, the suspicious level of each SU as well as consistency values were calculated to alleviate the influences of malicious users. Chen *et al.* [115] proposed a reputation-based mechanism to defense the malicious attacks. However, these historical data based algorithms take a long time to build a reliable reputation. Additionally, Kaligineedi *et al.* [117] proposed a robust outlier detection to identify "Always Yes" malicious users by utilizing outlier factors and spatial information of SUs. Kalamkar *et al.* [118] proposed an outlier detection scheme to detect malicious users sending true or false power values randomly to confuse other SUs in CSS networks. Furthermore, some work has been done on the attacks detection from intelligent malicious users. Li *et al.* [119] proposed an abnormality-detection approach for secure CSS networks, in which the attack strategy adopted by malicious users is unknown. Wang *et al.* [120, 121] constructed a moral hazard principal-agent framework for malicious user detection. More specifically, an incentive compatible mechanism was designed for thwarting the malicious behaviors from rational and irrational intelligent malicious users. By doing so, the proposed approach was more practical to be implemented in CR networks.

Besides the existing work on malicious user detection, the MC based CSS networks have been studied in [18, 89, 122], with the purpose of alleviating the costs of data acquisition at SUs. Meng *et al.* [89] firstly introduced the concept of MC to CSS networks.

It was proposed that each SU linearly combined the information of multiple channels at sub-Nyquist sampling rates. Subsequently, each SU sent a small number of such linear combinations to a FC to perform MC. Additionally, Wang *et al.* [18] proposed a robust wideband spectrum sensing algorithm with sub-Nyquist sampling performed at each active SU in the considered CSS networks. Once the compressed measurements were sent to the FC, nuclear norm minimization was adopted to solve the low-rank MC problem. By doing so, the costs of data acquisition at SUs are reduced significantly. Furthermore, Li [122] firstly applied belief propagation framework to MC for making it implementable and efficient on reconstructing spectrum occupancies in wideband CSS networks.

5.1.2 Motivations and Contributions

The aforementioned work has played a vital role and laid solid foundation for developing new strategies on malicious user detection. However, many of them are trust based, which utilizes the historical information of malicious users' behaviours. In practice, reliable reputation information is not always available since well-established historical statistics may be too expensive or even unrealistic in a fast-changing CR environment. Additionally, intelligent malicious users sending random values are more challenging than the types of malicious users considered in [117, 118]. Motivated by these, a malicious user detection dealing with malicious users sending random values is desirable for secure CSS networks. Another motivation of the work comes from reducing the number of active SUs in CSS networks and data acquisition costs at SUs without loss any information. Here, the active SUs refer to SUs send data to the FC. All the aforementioned work on MC based CSS focus on reducing the costs of data acquisition at SUs without considering any secure issue in CSS networks. Therefore, a malicious user detection algorithm with energy efficiency at SUs is extremely challenging and desired.

In this chapter, compared to the CSS network without MC,a malicious user detection model with fewer number of active SUs is considered. To the best of my knowledge, this

is the first work which invokes MC technique to achieve the malicious user detection in CSS networks. The contributions of this chapter are summarized as follows:

- A malicious users detection framework is proposed without requiring prior information of networks. In the proposed framework, along with the reduction of the number of active SUs and the data acquisition costs at SUs, the accuracy of malicious user detection is improved.

- In the proposed framework, compared to the CSS network without MC, fewer number of sensed channels is required, as MC technique is invoked at the FC to recover the information of unsensed channels. As a result, less number of active SUs are required. If there are enough active SUs in CSS networks, with the invoking of MC technique, each active SU can sense less number of channels without degrading the recovery performance. At the FC, sensed channels but corrupted by malicious users are removed during the MC process by utilizing the adaptive outlier pursuit (AOP) algorithm [123].

- A dynamic rank estimation algorithm is proposed to provide the rank order as one of the inputs for AOP algorithm. By doing so, the proposed framework does not require any prior information of the considered CSS networks for malicious user detection at the FC.

- An estimation strategy on the number of malicious users is proposed for the malicious user detection framework. With the new strategy, the estimated number of malicious users can be used as one of the inputs for AOP algorithm to make the malicious user detection algorithm completely blind.

- The proposed framework is tested on the real-world signals after being validated by the simulated signals. Numerical results show that the proposed malicious user detection framework can achieve high detection accuracy with low costs of data acquisition at SUs or less number of active SUs.

5.2 System Model of Cooperative Spectrum Sensing with Malicious Users

5.2.1 Networks Description

We take a typical CSS scenario as the considered network model, as shown in Fig. 5.1(a). It is assumed that the whole spectrum of interest with bandwidth $\mathcal{D}$ can be divided into $\mathcal{I}$ channels. A channel is either occupied by a PU or unoccupied. There is no overlap between different channels. The number of occupied channels K is assumed to be much less than the total number of channels, i.e. $K \ll \mathcal{I}$. Each channel is sensed by SUs at J different locations, which are spatially randomly distributed. At an arbitrary location indexed by j $(1 \leq j \leq J)$, it is assumed that B_j $(1 \leq B_j \leq \mathcal{I})$ SUs, indexed by $\mathbf{b}$ $(1 \leq \mathbf{b} \leq B_j)$, are implemented to sense the spectrum of interest. In a conventional CSS network, the whole spectrum is sensed by an SU at each location, which results in $B_j = 1$. However, high sampling rates are challenging for SUs in a CSS network, as the SUs are normally energy-constrained with limited sensing capabilities.

In this chapter, a few SUs are implemented at each location j of the CSS network $(B_j > 1)$, where each SU only needs to sense a segment of the whole spectrum at Nyquist rates, which means that some of the channels are unsensed at one location as shown in Fig. 5.1(a). Consequently, costs of data acquisition at SUs can be reduced significantly, in comparison with the case that each SU senses the whole spectrum. After sampling is performed, each SU calculates the power values of the sensed channels, and then sends this information to an FC to contribute to the final decisions on spectrum occupancies. It is further noticed that some of the SUs experience deep fading or shadowing. They would send very low power values to the FC in a CSS network, which are labeled as the blocks with '+' in Fig. 5.1(a) and Fig. 5.1(b). The transmitted signal has a sparsity property in the frequency domain [8] and the nearby locations are assumed to share the similar spectrum occupancies [122], so the matrix constructed by the received signals at different

locations exhibits a low-rank property [18]. Fig. 5.1(b) illustrates the transformation of the sparsity property of transmitted signals into the low-rank property of the matrix at the FC, where the matrix is constructed by signals received at different locations. In such a CSS network, we propose to reconstruct the unsensed channels from the sensed channels by a low-rank MC technique.

In the case of a sensing malfunction, some of the active SUs in the CSS network, labelled as the blocks with 'X' in Fig. 5.1(a) and Fig. 5.1(b), send corrupted power values to the FC. Malicious users appear randomly in the considered CSS network. Malicious users that keep sending high power values or low power values are easily detected. However, malicious users that send random but very close to the true values are much more difficult to detect. This is the case we consider in this work. We propose to remove these malicious users during the MC at the FC, so that recovery performance is not degraded significantly as the corrupted power values are used for the MC process.

5.2.2 Signal Processing Model

Let us define $s\left(t\right) \in \mathcal{C}^{N\times 1}$ as the transmitted signals from unknown PUs, where N refers to the number of samples. All active SUs in CSS networks are assumed to keep silent. Additionally, $r_{ij}\left(t\right)$ refers to the signals of the ith channel received at the jth SU (SU_{ij}), which can be given by

$$r_{ij}\left(t\right) = d_{ij}^{-\chi/2} h_{ij}\left(t\right) s\left(t\right), \tag{5.1}$$

where d_{ij} refers to the distance from PUs to SU_{ij} when the ith channel with response $h_{ij}\left(t\right)$ is used for transmission, and χ is the propagation loss factor.

Once signals of the ith channel are received at SU_{ij}, the power value of the sensed channel p_{ij} can be calculated as

$$p_{ij} = \frac{1}{N} \int_{f_i - \mathcal{D}/2\mathcal{I}}^{f_i + \mathcal{D}/2\mathcal{I}} \boldsymbol{\mathcal{F}} r_{ij}\left(t\right) df, \tag{5.2}$$

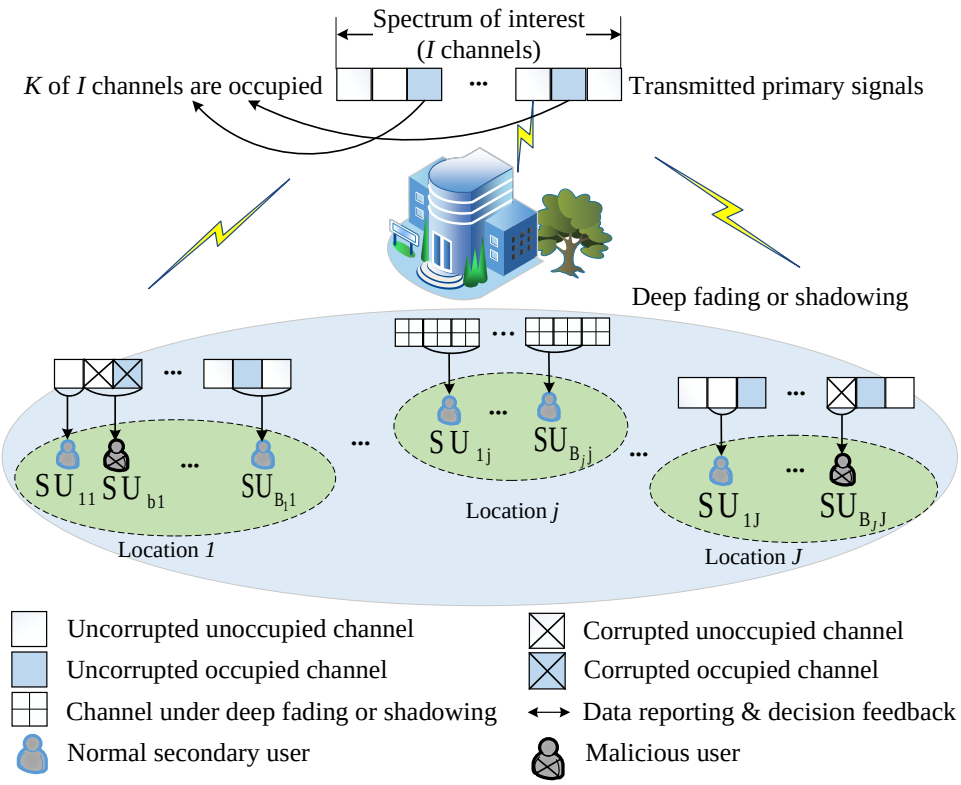

(a) Network model of cooperative spectrum sensing network with malicious users.

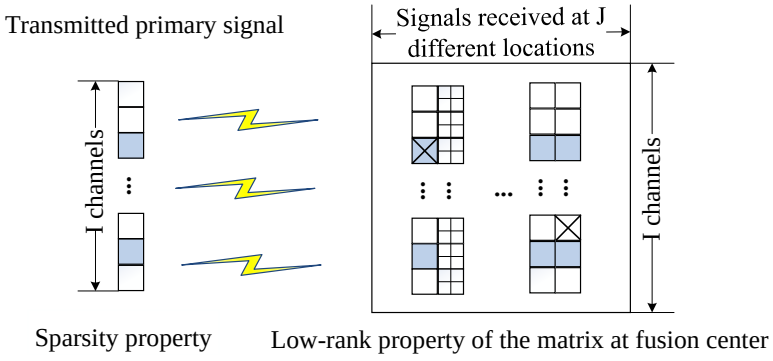

(b) Transformation of sparsity property into low-rank property.

Figure 5.1: Network model

where $\boldsymbol{\mathcal{F}}$ denotes the DFT matrix. Defining $\boldsymbol{\Omega}$ as the index set for complete matrix at

the FC, then the complete matrix $\mathbf{P^{\Omega}}$ can be illustrated as

$$\mathbf{P^{\Omega}} = \begin{bmatrix} p_{1,1} & \cdots & p_{1,j} & \cdots & p_{1,J} \\ \vdots & \vdots & \vdots & \vdots & \vdots \\ p_{i,1} & \cdots & p_{i,j} & \cdots & p_{i,J} \\ \vdots & \vdots & \vdots & \vdots & \vdots \\ p_{I,1} & \cdots & p_{I,j} & \cdots & p_{I,J} \end{bmatrix}_{\mathcal{I} \mathrm{x} J}, \tag{5.3}$$

where the ith row of $\mathbf{P^{\Omega}}$ represents the power values of the ith channel sensed by J SUs located spatially. The jth column of $\mathbf{P^{\Omega}}$ refers to the power values of different channels sensed by SUs at the jth location.

As each SU senses only one or a few channels among the whole spectrum of interest, power values collected at the FC $\mathbf{P^{E}}$ is incomplete, where $\mathbf{E}$ is defined as an index set of the sensed channels at the FC. Therefore, power values of sensed channels in the incomplete matrix $\mathbf{P^{E}}$ can be expressed as

$$p_{ij}^{\mathbf{E}} = \begin{cases} p_{ij}, & (i,j) \in \mathbf{E}, \\ 0, & \text{otherwise.} \end{cases} \tag{5.4}$$

If malicious users appear in CSS networks, part of the power values of the sensed channels would be corrupted during the data transmission from SUs to the FC. Let us define $\mathbf{O}$ as a subset of $\mathbf{E}$, which donates the sensed channels without corruption from malicious user. $\tilde{p}_{ij}$ is defined as the power value of corrupted channels. The value of $\tilde{p}_{ij}$ falls in the range of $[p_{min}^{\mathbf{EC}}, p_{max}^{\mathbf{EC}}]$, where $p_{min}^{\mathbf{EC}}$ and $p_{max}^{\mathbf{EC}}$ refer to the minimal and maximal values of the power values collected at the FC, respectively. Consequently, the partly

corrupted matrix $\mathbf{P^{EC}}$ generated at the FC can be expressed as

$$p_{ij}^{\mathbf{EC}} = \begin{cases} p_{ij}, & (i,j) \in \mathbf{O}, \\ \tilde{p}_{ij}, & (i,j) \in \mathbf{E}/\mathbf{O}, \\ 0, & \text{otherwise}, \end{cases} \tag{5.5}$$

5.3 Malicious User Detection Framework

In order to enhance the security of the CSS network, a malicious user detection framework based on low-rank MC is proposed in this section. Based on the network model described in Section 5.2.1, each SU is proposed to sense only a segment of the spectrum rather than the whole spectrum, in order to reduce the number of active SUs in the CSS network and the costs of data acquisition at each active SU. We propose to remove corrupted channels at the FC by invoking the AOP algorithm [123]. It is further noted that the rank of the matrix at the FC and the number of channels corrupted by the malicious users is normally unknown in reality, but are required by the proposed malicious user detection algorithm with AOP. To make the proposed malicious user detection framework completely blind, a rank estimation algorithm and an estimation strategy on the number of malicious users are proposed in this section. As a result, the malicious user detection process in the CSS network does not require any prior information. Once the exact matrix is obtained by the proposed framework, spectrum occupancies can be determined by a conventional energy detection method. The whole procedure of the proposed low-rank MC based malicious user detection framework in the CSS network is illustrated in Fig. 5.2.

5.3.1 Malicious User Detection Based on Adaptive Outlier Pursuit

As the spectrum is normally underutilized in reality, power values of all the channels received at SU_{ij} exploits a sparse property. This sparse property can be transformed

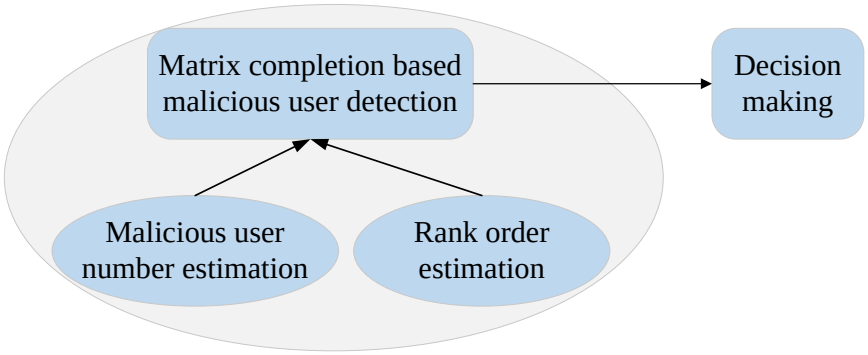

Figure 5.2: Flowchart of the proposed malicious user detection framework with low-rank matrix completion.

into a low-rank property of the complete matrix $\mathbf{P}^{\mathbf{\Omega}}$ at the FC. Therefore, the rank order of $\mathbf{P}^{\mathbf{\Omega}}$ is equal to the number of active PUs in the spectrum of interest. Here, it is assumed that there is at least one active PU in the spectrum of interest, which guarantees the rank order is not equal to zero. Therefore, this low-rank property makes it possible to recover the unsensed channels at the FC by invoking MC technique.

As aforementioned, the sensed channels are partly corrupted by malicious users, which affects the recovery accuracy of sensed channels at the FC. It is assumed that the corrupted channels are distributed sparsely and randomly in the incomplete matrix at the FC. The indices of corrupted channels are unknown at the FC. Additionally, in order to make attacks more difficult to be detected, fake data corrupted by malicious users are assumed to be in a bounded range as aforementioned, which are close to their true values. These fake data can be removed during the process of MC by invoking the AOP algorithm. In such a case, the malicious user detection problem can be formulated as follows:

$$\begin{aligned} &\min_{\mathbf{U},\mathbf{V},\mathbf{\Lambda}} \ \tfrac{1}{2} \sum_{(i,j)\in\mathbf{\Omega}} \Lambda_{ij} \Big((\mathbf{UV})_{ij} - p_{ij}^{\mathbf{EC}} \Big)^2, \\ &\text{subject to} \sum_{(i,j)\in\mathbf{\Omega}} (1-\Lambda_{ij}) \le L_c, \quad \Lambda_{ij} \in \{0,1\}, \end{aligned} \tag{5.6}$$

where $\mathbf{U} \in \mathcal{C}^{\mathcal{I}\times K}$ and $\mathbf{V} \in \mathcal{C}^{K\times J}$. The number of corrupted channels collected at the FC is L_c, and $\mathbf{\Lambda}$ is a binary matrix denoting the uncorrupted channels by one and the others are set be to zeros. An illustration for the structure of $\mathbf{\Lambda}$ is given in Fig. 5.3.

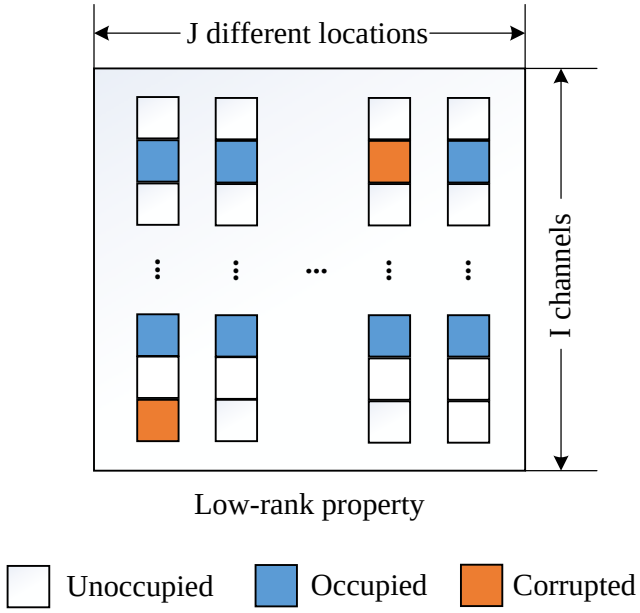

Figure 5.3: Relationship illustration between the complete matrix $\mathbf{P}^{\mathbf{\Omega}}$ and the corruption index matrix $\mathbf{\Lambda}$.

More particularly, an arbitrary element Λ_{ij} in $\mathbf{\Lambda}$ is defined as

$$\Lambda_{ij} = \begin{cases} 1, & (i,j) \in \mathbf{O}, \\ 0, & \text{otherwise}. \end{cases} \tag{5.7}$$

Here, $\mathbf{O}$ is updated in each iteration of solving problem (5.6). The details about how to update $\mathbf{O}$ will be given in **Algorithm 3** in the following.

It is noted that the problem (5.6) is non-convex, since it has both continuous and discrete variables. The following two steps can be performed to find a local optimal solution to (5.6).

1. Fix $\mathbf{\Lambda}$ and update $\mathbf{U}$, $\mathbf{V}$. If $(i,j) \notin \mathbf{O}$, the objective function of (5.6) would become zero. Therefore, $\mathbf{U}$ and $\mathbf{V}$ can be obtained by solving the simplified problem as follows:

$$\min_{\mathbf{U},\mathbf{V}} \sum_{(i,j)\in\mathbf{O}} \left((\mathbf{UV})_{ij} - p_{ij}^{\mathbf{EC}} \right)^2. \tag{5.8}$$

This problem can be easily solved by Riemannian trust-region for MC (RTRMC) [63].

2. With fixed $\mathbf{U}$ and $\mathbf{V}$, $\mathbf{\Lambda}$ can be updated by solving

$$\begin{aligned} &\min_{\mathbf{\Lambda}} \tfrac{1}{2} \sum_{(i,j)\in\mathbf{\Omega}} \Lambda_{ij}\left((\mathbf{UV})_{ij} - p_{ij}^{\mathbf{EC}}\right)^2, \\ &\text{subject to } \sum_{(i,j)\in\mathbf{\Omega}} (1-\Lambda_{ij}) \le L_c,\ \Lambda_{ij} \in \{0,1\}. \end{aligned} \tag{5.9}$$

The problem is to choose $(\mathcal{I} \times J - L_c)$ elements with least sum from $\boldsymbol{S}_{\mathbf{\Omega}} = \left\{ \left((\mathbf{UV})_{ij} - p_{ij}^{\mathbf{EC}}\right)^2, (i,j) \in \mathbf{\Omega} \right\}$. Given τ as the L_cth largest element in $\boldsymbol{S}_{\mathbf{\Omega}}$, Λ_{ij} can be updated as

$$\Lambda_{ij} = \begin{cases} 1, & (i,j) \in \mathbf{\Omega}, \left((\mathbf{UV})_{ij} - p_{ij}^{\mathbf{EC}}\right)^2 < \tau, \\ 0, & \text{otherwise.} \end{cases} \tag{5.10}$$

If the L_cth and (L_c+1)th largest elements in $\mathbf{S}_{\mathbf{\Omega}}$ are equal, we can choose any $\mathbf{\Lambda}$ such that $\sum_{(i,j)\in\mathbf{\Omega}} (1-\Lambda_{ij}) = L_c$. Meanwhile, $\mathbf{S}_{\mathbf{\Omega/O}} \ge \mathbf{S}_{\mathbf{O}}$ should be satisfied, where $\mathbf{S}_{\mathbf{\Omega/O}} = \min_{(i,j)\notin\mathbf{O}} \left((\mathbf{UV})_{ij} - p_{ij}^{\mathbf{EC}}\right)^2$ and $\mathbf{S}_{\mathbf{O}} = \min_{(i,j)\in\mathbf{O}} \left((\mathbf{UV})_{ij} - p_{ij}^{\mathbf{EC}}\right)^2$, respectively.

During the process of solving problem (5.6), corrupted channels are removed from the observed ones at the FC to alleviate the influences of malicious users. Once the complete matrix $\hat{\boldsymbol{P}}^{\mathbf{\Omega}}$ is recovered at the FC, final decision on spectrum occupancies can be determined by invoking the conventional energy detection. The ith channel is determined as occupied if the average energy of it is higher than the empirical threshold $\lambda_d = (\mu/2)^2$, where $\mu = \left\|\mathrm{vec}\left(\hat{\boldsymbol{P}}^{\mathbf{\Omega}}\right)\right\|_1 \Big/ \left\|\mathrm{vec}\left(\hat{\boldsymbol{P}}^{\mathbf{\Omega}}\right)\right\|_0$ is the average absolute value of all the $J \times K$ nonzero elements in $\mathrm{vec}\left(\hat{\boldsymbol{P}}^{\mathbf{\Omega}}\right)$ [18]. Here, $\mathrm{vec}\,(\cdot)$ stacks all columns of matrix $\hat{\boldsymbol{P}}^{\mathbf{\Omega}}$ into a long vector. The final binary decisions $\boldsymbol{d} = \{d_i, \forall i = 1, \ldots, \mathcal{I}\}$ on spectrum occupancies can be determined as

$$d_i = \left(\frac{1}{J} \sum_{j=1}^{J} |\hat{p}_{ij}| \ge \lambda_d \right),\ \forall i, \tag{5.11}$$

where $\hat{p}_{ij}$ is recovered power value of the ith channels sensed by SU_{ij}.

The proposed AOP based malicious user detection is summarized in **Algorithm 3**.

Algorithm 3 Proposed Malicious User Detection by Adaptive Outlier Pursuit

Initialization: $\mathbf{\Omega}$, P, $I_{\max}$, L, K, and λ_d.

Input: $l = 0$, $\Lambda_{ij} = 1$ for $(i,j) \in \mathbf{\Omega}$, $\mathbf{O} = \mathbf{\Omega}$.

1: **while** $l \leq I_{max}$ **do**
2: Update $\mathbf{U}^{(l)}$ and $\mathbf{V}^{(l)}$ with RTRMC as in (5.8);
3: Update $\mathbf{\Lambda}^{(l)}$ with (5.10);
4: Update $\mathbf{O}^{(l)}$ to be indices in $\mathbf{\Omega}$ where $\Lambda_{ij}^{l} = 1$;
5: **if** $\mathbf{O}^{(l)} = \mathbf{O}^{(l-1)}$ **then**
6: break;
7: **end if**
8: $l = l + 1$.
9: **end while**
10: $\hat{p}_{ij} = \left(\mathbf{U}^{(l)}\mathbf{V}^{(l)}\right)_{ij}$.
11: Making final decisions $\boldsymbol{d}$ on spectrum occupancy by (5.11).
12: **return** $\boldsymbol{d}$.

In the considered model, if the whole spectrum of interest are all sensed by SUs at different locations, the number of sensed channels at the FC is $P = \mathcal{I} \times J$. In such as case, a complete matrix is available at the FC. Otherwise, only an incomplete matrix can be constructed at the FC with $P < \mathcal{I} \times J$. Herein, the compression ratio $\gamma = \frac{P}{\mathcal{I} \times J}$ is defined as the ratio of number of the sensed channels P in the corrupted matrix $\mathbf{P}^{\mathbf{EC}}$ to the total number of channels $\mathcal{I} \times J$ in the complete matrix $\mathbf{P}^{\mathbf{\Omega}}$ at the FC. Additionally, the maximal number of iterations for solving (5.6) is predefined as $I_{\max}$, which means the iterative process for solving (5.6) will be terminated when iteration number reaches $I_{\max}$, even though the break condition of **Algorithm 3** is not satisfied. In the lth iteration, $\mathbf{\Lambda}^{(l)}$ is used to identify the locations of corrupted channels based on the newly constructed $\left(\hat{\boldsymbol{P}}^{\mathbf{\Omega}}\right)^{(l)} = \mathbf{U}^{(l)}\mathbf{V}^{(l)}$. After the complete matrix is recovered, final decisions $\boldsymbol{d}$ on spectrum occupancies are made according to (5.11).

As demonstrated in **Algorithm 3**, the rank order of the matrix K and the number of corrupted channels L_c are required as the inputs at the FC. Therefore, a rank order estimation algorithm and an estimation strategy on the number of malicious users are proposed, as introduced in the following, to enable the proposed malicious user detection framework.

5.3.2 Rank Order Estimation Algorithm

It is pointed out that the rank order estimation can be converted into a sparsity order estimation problem [18]. With the sensed channels at the FC, the rank order of a matrix can be estimated by the following two steps:

1. Recover the complete matrix by solving

$$\begin{aligned} &\min \left\| \text{vec}\left(\hat{\mathbf{P}}^{\mathbf{\Omega}}\right)\right\|_1, \\ &\text{subject to } \mathcal{A}\left(\hat{\mathbf{P}}^{\mathbf{\Omega}}\right) = \mathbf{P}^{\mathbf{EC}}, \end{aligned} \tag{5.12}$$

   where $\mathcal{A}$ is a operator from $\mathbf{\Omega}$ to $\mathbf{\Omega}/\mathbf{E}$. Here, the sparsity level of vec $\left(\hat{\boldsymbol{P}}^{\mathbf{\Omega}}\right)$ is equal to $J \times K$.

2. The estimated rank order $\hat{K}$ is given by

$$\hat{K} = \sum_{i=1}^{\mathcal{I}} \left(\left| \frac{1}{J} \sum_{j=1}^{J} \hat{p}_{ij} \right| \geq \lambda_r \right), \tag{5.13}$$

   where λ_r is a threshold for rank order estimation. By applying data fusion at the FC, the power value of each channel is calculated by averaging power values of the same channel sensed by spatially distributed SUs. During the rank order estimation process, it is assumed that the existence of malicious users in CSS networks would not influence the rank order, as they are distributed randomly. This assumption can be guaranteed by the AOP algorithm [123].

It is proved that exact signal recovery can be guaranteed when the number of sensed channels satisfies $P = c\,(K \times J) \log\left(\mathcal{I}/K\right) + d$ [14]. However, the number of sensed channels guaranteing exact rank order estimation and exact MC are different. When Monte Carlo simulations and curve fitting techniques are adopted to find the values of the constants c and d, the following two results can be obtained with given $\mathcal{I}$, J and K:

Result 1 [78]: A successful rank order estimation can be guaranteed when the number of sensed channels is not less than P_1 where

$$P_1 = c^1(K_{\max} \times J) \log\left(\mathcal{I}/K_{\max} + d^1\right), \tag{5.14}$$

where K_{max} is the statistical upper bound of the rank order K.

Result 2 [78]: A successful MC can be guaranteed when the number of sensed channels is not less than P, which is defined as follows:

$$P = c^2 \left(K \times J\right) \log\left(\mathcal{I}/K + d^2\right). \tag{5.15}$$

According to the results presented in [78], it always holds that $P > P_1$ with given $\mathcal{I}$, J and K. Therefore, $c^1 < c^2$ and $d^1 < d^2$.

Normally, the maximal rank order $K_{\max}$ is adapted as a statistical upper bound of the real rank order K. In practice, spectrum occupancies are normally dynamic. Therefore, $K_{\max}$ would not be a suitable upper bound in a dynamic spectrum environment. In order to obtain the exact rank order of the matrix at the FC, a novel dynamic rank order upper bound adjustment scheme is proposed to adjust $K_{\max}$ adaptively. One possible scenario is that $K_{\max}$ is much larger than K, which leads to that the number of data collected for rank order estimation is more than that for MC. Here, it is a waste on the costs of data acquisition at SUs or the number of active SUs implemented for sensing. As shown in **Algorithm 4**, the rank order upper bound adjustment can be achieved by the proposed shrink algorithm. $J_{\max}$ is defined the maximal iteration number which is adopted in **Algorithm 4** to update $K_{\max}$. It is assumed that the sensed channels $\mathbf{P^{EC}}$, step size Δ_1, threshold λ_r, $J_{\max}$ and the initial rank order upper bound $K_{\max}$ are known as the inputs at the FC. Then the value of P_1 by (5.14) can be calculated. Additionally, the complete matrix can be obtained with the P_1 sensed channels by (5.12), and $\hat{K}$ can be determined by (5.13). Furthermore, the number of sensed channels required for exact recovery is obtained by (5.15). Subsequently, P_2 is updated as $P_2 = P - P_1$. In the next

Algorithm 4 Proposed Shrink Algorithm

Input: $\mathbf{P^{EC}}$, Δ_1, $K_{\max}$, λ_r, and $J_{\max}$.
Initialization: $j = 1$, $P_2^{(1)} < 0$, $K_{\max}^{(1)} = K_{\max}$.
1: **while** $P_2^{(j)} < 0$ or $j \leq J_{\max}$ **do**
2: Calculate $P_1^{(j)}$ by (5.14);
3: Calculate $\hat{K}^{(j)}$ by (5.12) and (5.13) with $P_1^{(j)}$ channels;
4: Calculate $P^{(j)}$ with $\hat{K}^{(j)}$ by (5.15);
5: Calculate $P_2^{(j)}$=$P^{(j)}$−$P_1^{(j)}$;
6: Update $K_{\max}^{(j)} = K_{\max}^{(j)} - \Delta_1$ and $j = j + 1$.
7: **end while**
8: **return** Updated $K_{\max}$.

Algorithm 5 Proposed Enlargement Algorithm

Input: $\mathbf{P^{EC}}$, Δ_2, $K_{\max}$, λ_r, ε and $J_{\max}$.
Initialization: $j = 1$, $\hat{K}^{(1)} = 0$, $\hat{K}_{\max}^{(1)} = K_{\max}$.
1: **while** $\left(K_{\max}^{(j)} - \hat{K}^{(j)}\right) > \varepsilon$ or $j \leq J_{\max}$ **do**
2: Update $K_{\max}^{(j)} = K_{\max}^{(j)} + \Delta_2$ and $j = j + 1$;
3: Calculate $P_1^{(j)}$ by (5.14);
4: Calculate $\hat{K}^{(j)}$ by (5.12) and (5.13) with $P_1^{(j)}$ channels.
5: **end while**
6: **return** Updated $K_{\max}$.

loop, $K_{\max}$ is reduced by step size Δ_1 and this process is repeated until $P_2 > 0$ or the maximal iteration $J_{\max}$ is researched.

Another scenario is that the rank order upper bound $K_{\max}$ is much smaller than the real rank order K, which is caused by the over-utilizing of shrink algorithm or the dynamic spectrum occupancies. It leads to the result that P_1 is not enough for the exact rank order estimation $\hat{K}$. As shown in **Algorithm 5**, the enlargement algorithm is proposed to enlarge $K_{\max}$ until that the exact rank order estimation can be achieved. In the proposed enlargement algorithm, sensed channels $\mathbf{P^{EC}}$, step size Δ_1, threshold λ_r, tolerance ε and the initial rank order upper bound $K_{\max}$ are known as inputs at the FC. Subsequently, P_1 is determined by (5.14) to achieve exact rank order estimation. Additionally, $\hat{K}$ is determined by (5.12) and (5.13). In the following loop, $K_{\max}$ is increased by step size Δ_2 to get the updated $\hat{K}$ until the difference between $K_{\max}$ and $\hat{K}$ becomes less the error tolerance ε or the maximal iteration $J_{\max}$ is researched.

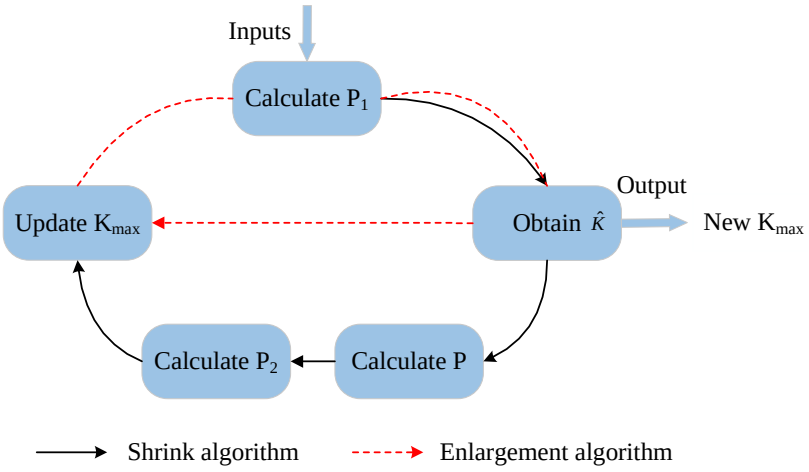

Figure 5.4: Flowchart of the proposed dynamic rank order upper bound adjustment scheme.

The whole process of the proposed dynamic rank order upper bound adjustment scheme is summarized as follows. As shown in Fig. 5.4, sensed channels $\mathbf{P}^{\mathbf{EC}}$, step size Δ_1, threshold λ_r, tolerance ε, $J_{\max}$, and the initial rank order upper bound $K_{\max}$ are the inputs of the proposed scheme. The updated $K_{\max}$ is as the output. Once the inputs are available, the proposed shrink algorithm starts working. The output of **Algorithm 4** $K_{\max}$ is adopted as one of the input for **Algorithm 5**. During this process, exact recovery cannot be achieved if the number of sensed channels P is smaller than P_1. As such, the FC should coordinate the number of active SUs in CSS networks to sense more channels. After the enlargement algorithm is performed, the updated $K_{\max}$ can be obtained and used as the rank order input K for **Algorithm 3**. According to the logic flow shown in Fig. 5.4, the step size should be carefully designed. If the step size is too small, more iterations are required before the algorithm converges, which results in high computational complexity. If the step size is too big, $K_{\max}$ might keep updating by **Algorithm 4** and **Algorithm 5** until the maximal iteration $J_{\max}$ is reached.

5.3.3 Malicious User Number Estimation

As aforementioned, the number of corrupted channels L_c is one of the inputs for **Algorithm 3**. However, it is usually unknown and needs to be estimated in practice. In the rest of this section, each SU is assumed to sense one channel to simplify the description. The number malicious user is equal to the number of corrupted channels. Therefore, the malicious user number estimation refers to estimate the number of corrupted channels in the following of this chapter.

If the estimated malicious user number $\hat{L}_c$ is smaller or greater than its real value L_c, the performance of **Algorithm 3** would be degraded significantly. More specifically, if $\hat{L}_c$ is underestimated, part of the corrupted channels will still be used to perform MC at the FC, which results in recovery errors in the reconstructed matrix. If $\hat{L}_c$ is overestimated, some of the uncorrupted channels would be removed during the MC process. The MC process would result in more than one solution. Consequently, exact MC is difficult to achieve as the number of available uncorrupted channels may not be enough. As proved in [123], a sufficient condition for the non-uniqueness of a matrix $\mathbf{P}^{\mathbf{\Omega}}$ is given as follows: suppose the number of sensed channels is P, and they are randomly distributed among the complete matrix $\mathbf{P}^{\mathbf{\Omega}} \in \mathcal{C}^{\mathcal{I}\times J}$. Let us define ΔL_c as the difference between the overestimated number of corrupted channels $\hat{L}_c$ and the real number of corrupted channels L_c. If $\Delta L_c > (P - L_c)/\max(\mathcal{I}, J) - K > 0$, then the reconstructed matrix is non-unique.

In the proposed framework, after the rank order estimation is performed, an initial guess for malicious user number is used as one input for the AOP algorithm illustrated as **Algorithm 3**. It is an iterative process to update the number of malicious users in combining with the AOP algorithm. In each iteration, after the AOP algorithm is performed, the value of the $\hat{L}_c$th largest term in set S_Ω should be checked. If it is less than the tolerance l_{tol}, $\hat{L}_c$ is determined as overestimated, and some of the removed channels are uncorrupted. The numerical analyses in [123] has proven that ΔL_c can

be bounded by $(l_{\min} - K)$, where $l_{\min}$ is defined as the minimum number of sensed channels in one row or one column of the incomplete matrix with $(P - L_c)$ elements at the FC. More specifically, let us define $\hat{l}_{\min}$ as the minimal number of sensed channels in one row or one column of the incomplete matrix with $\left(P - \hat{L}_c\right)$ elements. If $\hat{l}_{\min}$ is less than the rank order K, the estimated number of corrupted channels $\hat{L}_c$ is updated as $\hat{L}_c = \hat{L}_c + \hat{l}_{\min} - K$. If $\hat{l}_{\min}$ is no less than K and $\left(\left(\mathbf{P}^{\mathbf{\Omega}}\right)_{ij} - p_{ij}^{\mathbf{EC}}\right)^2$ is less than τ, the exact matrix is reconstructed. Consequently, the iterative process for MC is terminated. Otherwise, if $\hat{l}_{\min}$ is greater than K and $\left(\left(\mathbf{P}^{\mathbf{\Omega}}\right)_{ij} - p_{ij}^{\mathbf{EC}}\right)^2$ is greater than τ, $\hat{L}_c$ is considered to be underestimated. As a result, the value of $\hat{L}_c$ should be updated to be $\rho_1 \hat{L}_c$, where $\rho_1 > 1$ is a properly selected constant. Following this, the updated $\hat{L}_c$ is taken as the input for AOP algorithm in the next iteration until the exact matrix is obtained or the iteration number reaches its upper bound $I_{\max}$.

5.3.4 Analyses on Minimal Number of Active Secondary Users

As aforementioned, each SU can sense one or multiple channels depending on its sensing capability. To simplify the comparison, it is assumed that each SU only senses one of the $\mathcal{I}$ channels. Without the invoking of MC technique, regardless of malicious users, the total number of SUs to be implemented in the CSS networks is $C_1 = \mathcal{I} \times J$. Additionally, with the invoking of MC at the FC, a CSS network without malicious users is considered. Without loss of any cooperative gain, the minimal number of SUs to be implemented in the CSS networks is given by

$$C_2 = \gamma_{\min} \times \mathcal{I} \times J, \tag{5.16}$$

where $\gamma_{\min} \in (0, 1]$ is the lower bound of compression ratio for exact MC, which is dependent on the specific MC algorithm. Furthermore, based on the CSS networks considered in this chapter, in which malicious users exist and the AOP algorithm is invoked for MC, the minimal number of SUs required to be implemented in the CSS networks can be given by

$$C_3 = P = \hat{\gamma}_{\min} \times \mathcal{I} \times J, \tag{5.17}$$

where $\hat{\gamma}_{\min} \in [\gamma_{\min}, 1]$ is the minimal compression ratio that can be achieved by the AOP algorithm. The exact value of $\hat{\gamma}_{\min}$ is dependent on the malicious user ratio κ. When the malicious user ratio $\kappa = 0$, $C_3 = C_2 < C_1$. If $\kappa > 0$, $C_2 < C_3 < C_1$. No matter whether the malicious users exist in CSS networks, with MC invoked at the FC, the number of active SUs required to send data to the FC is less the case that MC is not invoked.

Besides reducing the number of active SUs in the considered CSS networks, the costs of data acquisition can be reduced significantly from another perspective. Here, it is assumed that each SU senses multiple channels. With the proposed malicious user detection framework, if the number of active SUs is fixed, each SU can sense less number of channels as the MC technique is invoked to recover the complete matrix with less number of sensed channels. By sensing less number of channels, the costs of data acquisition at each SUs can be lowered significantly.

5.4 Numerical Analyses

In this section, numerical analyses on the proposed malicious user detection framework are presented. Particularly, the proposed framework is tested on the real-world signals after being verified by the simulated signals over TVWS.

In simulations, the total number of channels in the spectrum of interest is assumed to be $\mathcal{I} = 40$, which is the number of TVWS channels in the UK. The size of CSS networks changes from small scale ($J = 40$) to large scale ($J = 400$). Here, the size of CSS networks is equal to the number of active SUs implemented to sense the same channel at different spatial locations. Additionally, the malicious user ratio $\kappa = \frac{L_c}{\mathcal{I} \times J}$ is defined as the ratio of the number of corrupted channels L_c to the total number of channels ($\mathcal{I} \times J$) to be sensed by different SUs in the considered CSS networks. $I_{\max} = 500$ and $I_{\max} = 10$.

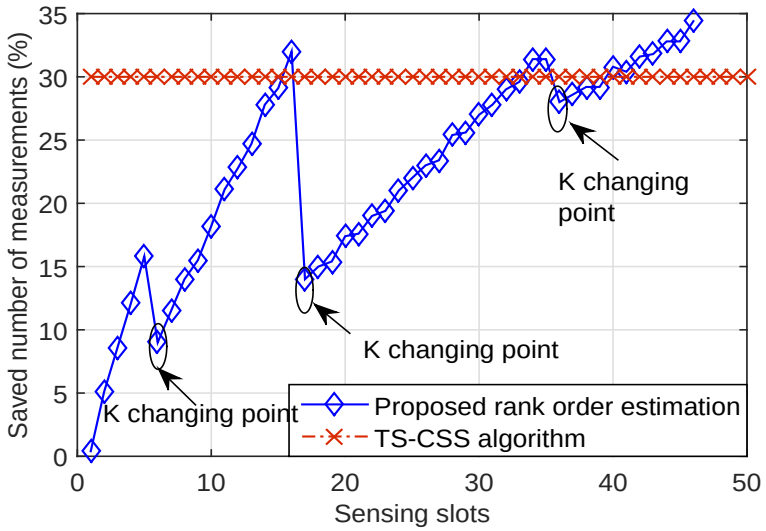

Figure 5.5: Saved measurements for exact MC with dynamic spectrum occupancies at the fusion center.

5.4.1 Numerical Results Using Simulated Signals

5.4.1.1 Results of the Proposed Rank Order Estimation

The simulation results of the proposed rank order estimation algorithm is presented in Fig. 5.5, with varying spectrum occupancies. In this scenario, dynamic spectrum occupancies result in changing rank order of the matrix at the FC. As shown in Fig. 5.5, when the rank order K changes, it can be observed that the saved number of channels to be sensed for exact MC is degraded at the changing point. However, performance of the proposed rank order estimation algorithm would be improved after the sensing slot during which rank order K changes. In practice, spectrum occupancies are assumed to be the same within a limited periods. Therefore, the proposed rank order estimation algorithm is reliable for practical scenario. As shown in Fig. 5.5, with longer sensing period, the proposed rank order estimation algorithm outperforms the traditional two-step compressive spectrum sensing algorithm (TS-CSS) [78] in terms of the saved number of channels to be sensed for exact MC.

5.4.1.2 Results of the Case with Unknown Number of Malicious Users

In Fig. 5.6, the influences of incorrect estimation on the number of malicious users $\hat{L}_c$ are analyzed. Therefore, the proposed estimation strategy on the number of malicious users is not invoked here. In this case, we choose $J = 40$ and $K = 1$ to simplify the simulation process. Additionally, the estimated number of corrupted channels $\hat{L}_c = \rho L_c$ varies from $0.7L_c$ to $1.3L_c$. Here, ρ, named as estimation accuracy ratio, is defined as the ratio of estimated number of corrupted channels to the actual number of corrupted channels. Here, the compression ratio is set to be 100%, which refers to the case that no MC is adopted. This kind of setting is to eliminate any possible performance degradation caused by recovery error. As a result, the performance difference shown in Fig. 5.6 is only caused by the incorrect estimation on the number of malicious users. Particularly, in Fig. 5.6, it is shown that the detection probability of the proposed malicious user detection framework gets degraded significantly if the estimated number of corrupted channels $\hat{L}_c$ is overestimated, especially in the case with high level of malicious user ratio. It is further noted that the detection performance would only be degraded slightly if the number of corrupted channels $\hat{L}_c$ is underestimated. In the following simulations, by invoking the proposed an estimation strategy on the number of malicious users, the correct estimation of the corrupted channels $\hat{L}_c$ is taken as the input of the AOP algorithm.

5.4.1.3 Results of the Proposed Malicious User Detection

Fig. 5.7 shows the detection performance of the proposed malicious user detection framework versus different compression ratios γ. Additionally, the detection performance of a traditional CSS network is also shown as a benchmark,in which malicious users do not exist and no MC technique is invoked at the FC. Therefore, for the case of the traditional CSS networks, matrix observed at the FC is complete. In this scenario, the number of active PUs in the spectrum of interest is one, which results in the rank order

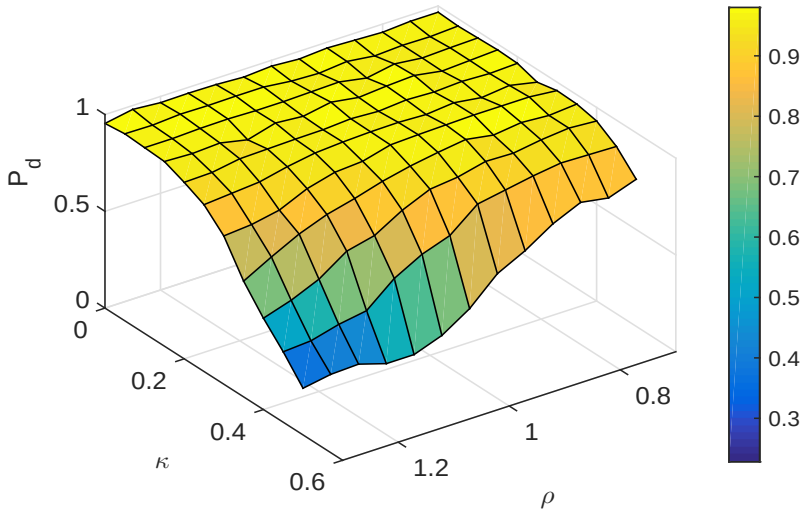

Figure 5.6: Detection performance of the proposed malicious user detection framework versus different estimation accuracy ratio ρ and malicious user ratios κ, compression ratio $\gamma = 100\%$, and $J = 40$.

as $K = 1$. The number of active SUs implemented to sense each channel is assumed to be $J = 40$. As shown in Fig. 5.7, with 10% of sensed channels corrupted by malicious user, the detection probability and false alarm probability of the proposed framework can almost match with the benchmark, when the compression ratio γ is increased to 30%. This means the detection performance of the CSS networks would not be degraded if the number of sensed channels are no less than 30% of the total number of channels $\mathcal{I} \times J$, even though 10% of them are corrupted by malicious users.

Fig. 5.8 shows the detection performance of the proposed malicious user detection framework versus varying malicious user ratios κ. In this case, the number of active PUs is set to be $K = 1$. The total number of active SUs implemented to sense each channel is $J = 40$. It is noted that detection probability of the proposed malicious user detection algorithm decreases with increasing number of channels corrupted by malicious users. More specifically, when malicious user ratio is increased to 60%, detection probability of the proposed framework is heavily degraded regardless of the compression ratio. It is reasonable because that the number of uncorrupted channels is not enough to guarantee the exact MC at the FC.

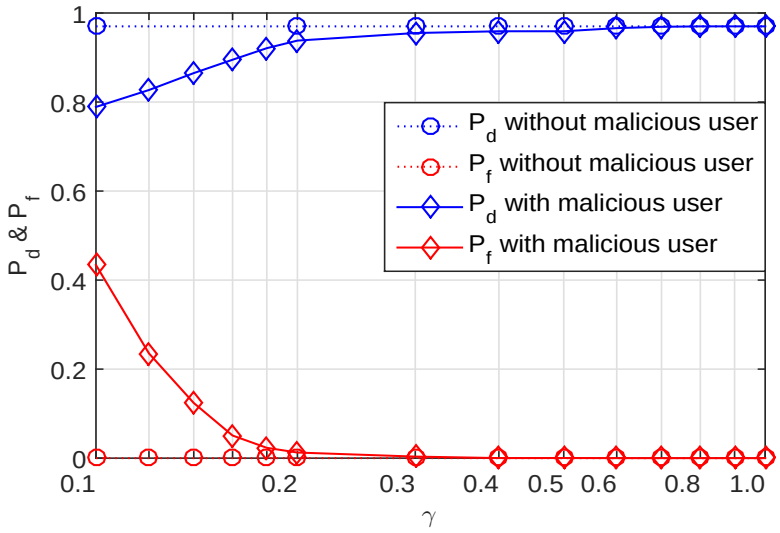

Figure 5.7: Detection performance of the proposed malicious user detection framework versus different compression ratios γ, malicious user ratio $\kappa = 10\%$, and $J = 40$.

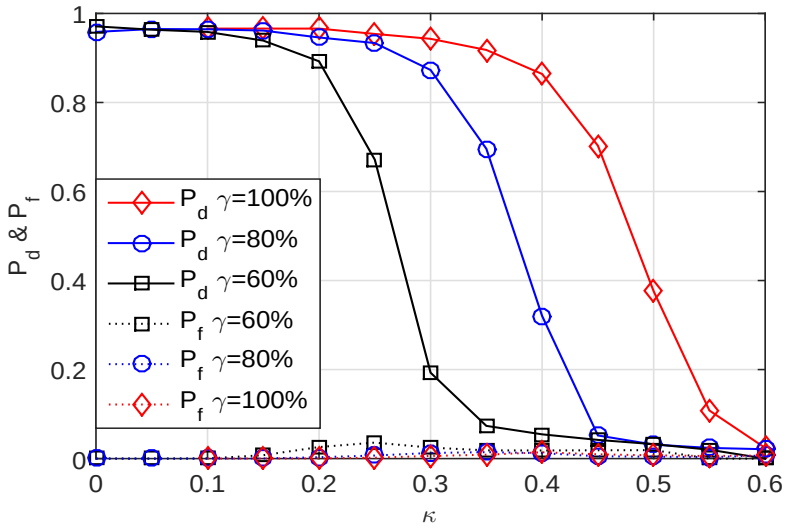

Figure 5.8: Detection performance of the proposed malicious user detection framework versus different compression ratios γ, malicious user ratio κ varies from 0 to 60%, and $J = 40$.

Fig. 5.9 shows the detection performance of the proposed malicious user detection framework versus different number of active SUs J for sensing the same channel. Here, different number of active SUs for sensing the same channel leads to different sizes of CSS networks. In this scenario, the active of active PUs is set to be $K = 4$ with random

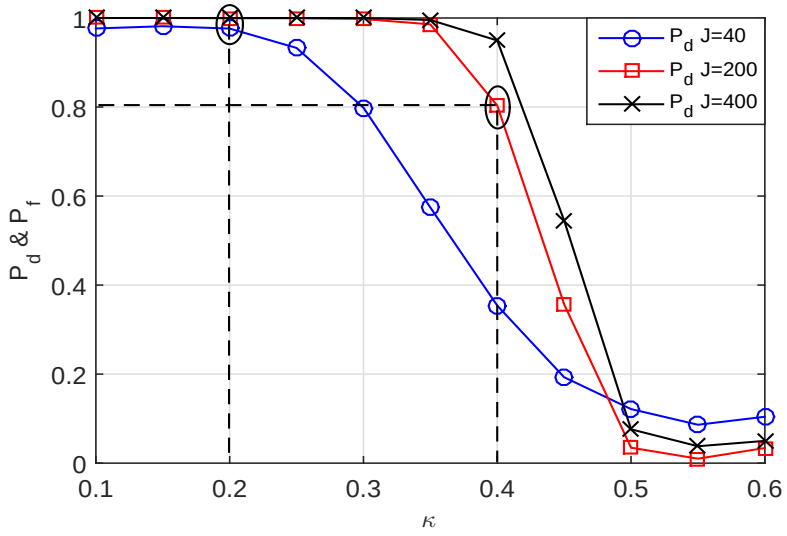

Figure 5.9: Detection performance of the proposed malicious user detection framework versus different sizes of CSS networks J, malicious user ratio κ changes from 10% to 60%, and compression ratio $\gamma = 100\%$.

positions. The size of CSS networks J varies from 40 to 400. The malicious user ratio varies from 10% to 60%. If the malicious user ratio is fixed, the number of corrupted channels would increase accordingly with the increasing size of CSS networks. Therefore, as illustrated in Fig. 5.9, with the same malicious user ratio, the case with larger CSS network size may have worse detection performance than the case with smaller CSS networks. Additionally, as circled in Fig. 5.9, for the scenarios of $J = 200$ and $J = 400$, the number of corrupted channels becomes the same if the malicious user ratio is set to be 0.4 and 0.2, respectively. In such a case, it can be also noticed that detection performance of CSS networks with $J = 400$ is much higher than that with $J = 200$. Therefore, it can be concluded that the more number of active SUs in CSS networks (larger size of CSS networks), the better defense to the same number of malicious users.

In Fig. 5.10, detection performance of the proposed malicious user detection framework is presented versus different malicious user ratios κ and different rank orders K. As aforementioned, the rank order of the matrix at the FC is determined by the number of active PUs in the spectrum of interest. Positions of the active PUs are randomly

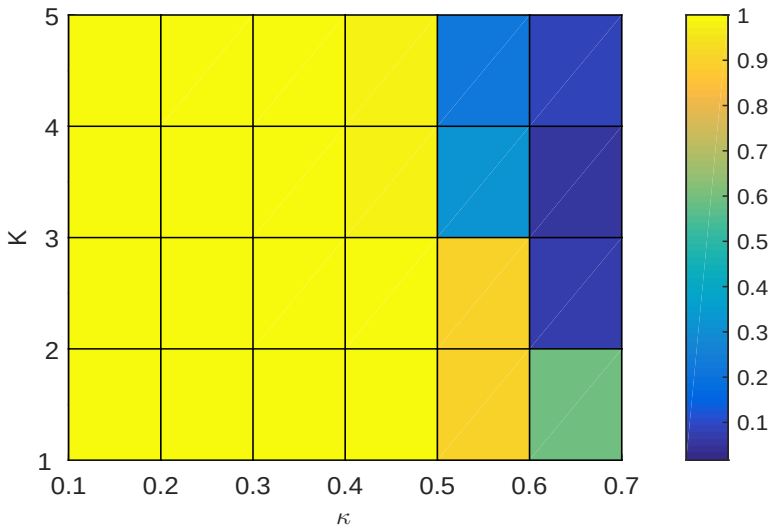

Figure 5.10: Detection performance of the proposed malicious user detection framework versus different rank orders K and different malicious user ratios κ, compression ratio $\gamma = 100\%$, $J = 400$.

generated in the spectrum of interest. In this case, compression ratio is set to be 100% to avoid any possible performance degradation caused by not enough number of sensed channels at the FC. The number of active SUs to sense each channel is set to be $J = 400$. It shows that the detection performance can be improved accordingly with decreasing rank order as well as decreasing malicious user ratio. This observation is reasonable, as increasing rank order and malicious user ratio would make the exact MC more difficult or even impossible at the FC.

5.4.2 Numerical Results Using Real-World Signals

As aforementioned, Ofcom has conducted serial trials on the TVWS pilots. One of the trials is conducted in our campus. In this trial, the DVB-T signal is allowed to be transmitted over TVWS channel 27 (518 MHz to 526 MHz), which is used to be vacant. During this trial, the real-world signals over TVWS are collected by a portable CRFS RFeye node [92] as shown in Fig. 3.6. To simulate the CSS networks with malicious users, the signal transmitted in channel 27 is regarded as the malicious users over TVWS.

Signals collected at different time slots are recorded to formulate the CSS networks by utilizing the time diversity. Malicious users may show up in any time slot during the signals recording period. The proposed low-rank MC based malicious user detection framework is tested on the collected real signals.

In this case, the number of active PUs is $K = 9$. The total number of channels is $\mathcal{I} = 40$ over TVWS. The number of active SUs implemented to sense the same channel is $J = 50$. Malicious users show up in channel 27 randomly because the trial signal is set to be discontinuously. With the real signals, Fig. 5.11 shows the detection performance of the proposed malicious user detection algorithm versus varying compression ratios γ. The detection performance comparison is demonstrated for the cases with and without malicious users in the CSS networks. When no malicious user shows up in the CSS networks, it shows that the perfect detection performance (P_d=100% and P_f=0%) can be achieved by choosing the suitable threshold for decision making. If malicious users show up in the CSS networks, false alarm probability becomes higher than the case without malicious users. This is because the false alarm happens if the corrupted value on TVWS channel 27 is not removed properly during the MC process. With the increasing compression ratio, the false alarm probability gets closer to the case without malicious users, as the exact MC can be guaranteed with more sensed channels at the FC.

5.5 Summary

In this chapter, a low-rank MC based malicious user detection framework was proposed for secure CSS networks, with the purpose of alleviating the costs of data acquisition at SUs and improving the malicious user detection accuracy. Each SU only sensed a segment of the spectrum of interest. The number of active SUs in CSS networks was less than the case that MC technique is not invoked at the FC. More particularly, a low-rank MC based malicious user detection algorithm was proposed by adopting the AOP algorithm, in which the channels corrupted by malicious users were removed during

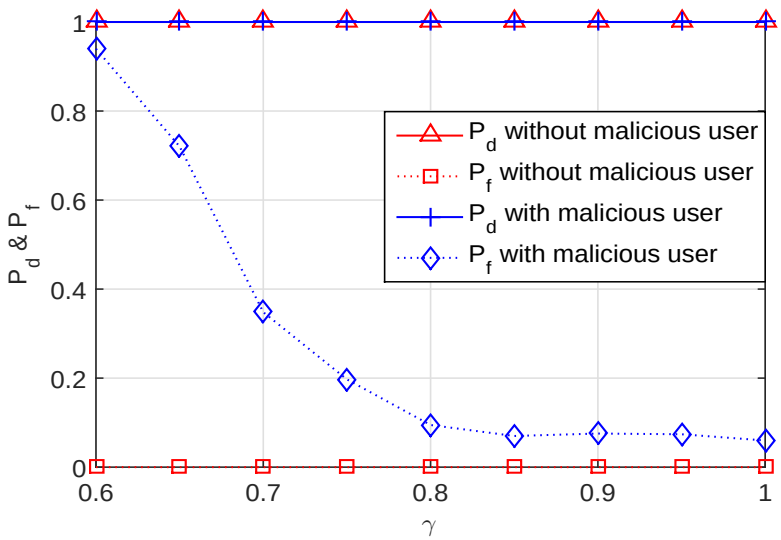

Figure 5.11: Detection performance of the proposed malicious user detection algorithm with real signals under different compression ratio γ, rank order $K = 9$.

the MC process. In order to make the malicious user detection process blind, a rank order estimation algorithm and an estimation strategy on the number of malicious users were proposed to provide the required inputs for the AOP algorithm. Furthermore, the proposed malicious users detection framework was tested on both the simulated signals and the real-world signals over TVWS. Numerical analyses showed that the proposed framework achieved good detection performance with limited number of active SUs or lower costs of data acquisition at each participating SU. It can be concluded that the proposed malicious user detection framework is a good candidate for the secure CSS networks.

Chapter 6

Throughput Analyses of Wireless Powered Cognitive Radio

In this chapter, the throughput of wireless powered CRNs is analyzed, in which the SUs are powered by harvesting energy from the RF. Section 6.1 introduces the related work and main contributions of the work in this chapter. Section 6.2 describes the considered WPT model and spectrum sensing model with a new proposed frame structure. Section 6.3 presents the throughput analyses of single SU scenario with the CS technique invoked. Section 6.4 provides the throughput analyses of multiple SUs with the MC technique invoked. Furthermore, Section 6.5 shows the numerical analyses of the considered network model with the optimized throughput of single SU and multiple SUs, respectively. Section 6.6 concludes this chapter.

6.1 Introduction

Energy efficiency and spectrum efficiency are two critical issues in designing wireless networks. Recent developments in energy harvesting provides a promising technique to improve the energy efficiency in wireless networks. Different from harvesting energy from

traditional energy sources (e.g., solar, wind, water, and other physical phenomena) [19], the emerging WPT further underpins the trend of green communications by harvesting energy from RF signals [20]. Inspiring by the great convenience offering by WPT, several pieces of work have been studied to investigate the performance of different kinds of energy constraint networks [12, 124–127]. Two practical receiver architectures, namely a time switching receiver and a power splitting receiver, were proposed in a multi-input and multi-output (MIMO) system in [12], which laid a foundation in the recent research of WPT. In [124], a new hybrid network architecture is designed to enable charging mobiles wirelessly in cellular networks. For cooperative systems, new power allocation strategies are proposed in a cooperative networks where multiple sources and destinations are communicated by an energy harvesting relay [125]. For non-orthogonal multiple access (NOMA) networks, in [127], a new cooperative simultaneously wireless information and power transfer NOMA protocol is proposed with considering the scenario where all users are randomly deployed.

Along with improving energy efficiency through energy harvesting, CR techniques can improve the spectrum efficiency and capacity of wireless networks through DSA [128]. Therefore, in order to design networks which are both spectrum and energy efficient, SUs in CRNs can be equipped with the energy harvesting capability. For the SUs powered by energy harvested from wireless RF, high sampling rate is difficult to be achieved. To overcome this issue, CS, which was initially proposed in [14], is introduced to wideband spectrum sensing in [8] to reduce the power consumption at SUs. Additionally, when dealing with matrices containing limited sensed channels, low-rank MC [96] was proposed to recover the unsensed channels.

6.1.1 Related Work

Some throughput optimization work has been recently developed in wireless powered communication networks. Che *et al.* [129] considered the throughput maximization problem for both battery-free and battery-deployed cases by optimizing the time slots

for energy harvesting and data transmission. Additionally, recent work [130–132] on the CRNs powered by energy harvesting mainly focuses on the spatial throughput optimization under various constraints. Park *et al.* [130] considered CRNs with an energy-harvesting SU with infinite battery capacity. The goal is to determine an optimal spectrum sensing policy that maximizes the expected total throughput subject to an energy causality constraint and a collision constraint. In order to improve both energy efficiency and spectral efficiency, Park *et al.* [131] considered a similar network model and the stochastic optimization problem is formulated into a constrained partially observable Markov decision process. At the beginning of each time slot, a SU needs to determine whether to remain idle so as to conserve energy, or to execute spectrum sensing to acquire knowledge of the current spectrum occupancy state. The throughput is maximized by the design of a spectrum sensing policy and a detection threshold. Chung *et al.* [132] considered an energy constraint RF-powered CRN by optimizing the pair of the sensing duration and the sensing threshold to maximize the average throughput of the secondary network.

6.1.2 Motivations and Contributions

The aforementioned work has played a vital role and laid solid foundation for developing new strategies for frame structure design. However, spectrum sensing is not considered in the frame structure designin [129]. Additionally, in [130–132], the proposed frame structure designs mainly aim to maximize the throughput by optimizing the threshold and time slots. When considering the energy efficiency and spectrum efficiency, it is meaningful to introduce sub-Nyquist sampling to reduce the energy consumption at SUs in wireless powered CRNs. In this chapter, a new frame structure design is proposed for wireless powered CRNs with implementing sub-Nyquist sampling at SUs. The CS and MC techniques are adopted to perform the signal recovery at a remote FC for making decision on spectrum occupancy. To the best of my knowledge, this is the first piece of work on the frame structure design employing the sub-Nyquist sampling rates based

spectrum sensing in wireless powered CRNs.

The summarized contributions of this chapter are illustrated as follows:

- A new frame structure is proposed for wireless powered CRNs, which includes four time slots: energy harvesting, spectrum sensing, energy harvesting and data transmission. A WPT model and a spectrum sensing model with sub-Nyquist sampling are introduced for the considered networks.

- In the WPT model, a new bounded WPT scheme is proposed where each SU selects a PB nearby with the strongest channel to harvest energy. The closed-form expressions is detrived for the power outage probability.

- In the spectrum sensing model, sub-Nyquist sampling is performed at each SU to reduce the energy consumption during spectrum sensing period. Two scenarios are considered: single SU scenario and multiple SUs scenario. In the single SU scenario, CS technique is invoked to obtain the original signals. In the multiple SUs scenario, low-rank MC technique is invoked to obtain the complete matrix at the FC. When the signal recovery process is performed at the remote FC, energy harvesting can be performed again at the SUs locally in the third time slot.

- Throughput optimizations of the proposed frame structure are formulated into two linear constrained problems with the purpose of maximizing the throughput of a single SU and the whole cooperative networks, respectively. The formulated problems are solved by using three different methods to obtain the maximal achievable throughput respectively.

- Simulation results show that the proposed frame structure design outperforms the traditional one in terms of throughput. It is noted that the multiple SUs scenario can achieve better outage performance than the single SU scenario.

6.2 Network Model

6.2.1 Network description

A CRN with energy-constrained SUs is considered. The whole spectrum of interest can be divided into I channels. A channel is either occupied by a PU or unoccupied. Meanwhile, there is no overlap between different channels. The number of occupied channels is assumed to be K, where $K \leq I$. Each SU is supposed to perform sensing on the whole spectrum. It is assumed that all SUs keep quiet as forced by protocols, e.g., at the media access control layer during spectrum sensing period. Thus the received signals only contain the signals of active PUs and channel noise. As shown in Fig. 6.1, for each SU, it is assumed that the sensing and transmission can only be scheduled by utilizing energy harvested from power beacons (PBs). The spatial topology of all PBs are modeled using homogeneous poisson point process (PPP) Φ_p with density λ_p. Without loss of generality, a typical SU is considered to be located at the origin in a two-dimensional plane. Each SU is equipped with a single antenna and has a corresponding receiver with fixed distance. Each PB is furnished with M antennas and maximal ratio transmission is employed at PBs to perform WPT to the energy constrained SU. The energy harvesting channels are assumed to be quasi-static fading channels where the channel coefficients are constant for each transmission block but vary independently between different blocks. The spectrum of interest is wideband and each SU performs wideband spectrum sensing to discover spectrum holes for data transmission. Once the spectrum holes are identified, SUs can start data transmission. It is assumed that the time of each frame is T. In the considered networks, single SU and multiple SUs scenarios are analyzed to achieve different throughput targets.

1. Single SU scenario: in the considered spectrum sensing network with single SU, a frame period at a single SU includes four time slots as outlined in the blue oval in Fig. 6.1: 1) energy harvesting time slot, in which each SU harvests the energy from PBs during the $\alpha_1 T$ period, with α_1 being the fraction of energy harvesting

in one frame period; 2) spectrum sensing time slot, in which each SU performs sub-Nyquist sampling by applying the CS technique. The compressed measurements are then sent to a remote powerful FC during the βT period by using the harvested energy during the $\alpha_1 T$ period; 3) energy harvesting time slot for data transmission, in which each SU harvests the energy from PBs during the $\alpha_2 T$ period, with α_2 being the fraction of energy harvesting in one frame period. As the spectrum is typically underutilized in practice, signals received at each SU exhibits a sparse property. In this time slot, the original signals can be recovered based on the collected measurements. The sensing decisions are sent back to the corresponding SU at the end of the third time slot; and 4) data transmission slot, in which each SU performs data transmission during the $(1 - \alpha_1 - \beta - \alpha_2) T$ period.

2. Multiple SUs scenario: as shown in Fig. 6.1, in the considered networks with multiple SUs, named as CSS, SUs are spatially randomly distributed. The total number of participating SUs is J ($J \geq 1$) in the CSS networks. Before performing spectrum sensing, each participating SU compare the energy E_{H_1} harvested during the first time slot with the energy consumption for spectrum sensing $E_S = P_{H_1} \beta T$ at the first time slot. If E_{H_1} is greater than E_S, the SU would continue performing spectrum sensing. This kind of SUs are named as active SUs. The frame structure of active SUs is same as that of single SU as described above. If E_{H_1} is less than E_S, the SU would switch to energy harvesting model again and wait for the decision on spectrum occupancies from the FC before starting data transmission. Therefore, the framework structure of inactive SUs would only includes two time slots: $(\alpha_1 + \beta + \alpha_2) T$ for energy harvesting and the rest for data transmission. In the case of CSS, only measurements from active SUs are collected at the FC. The signals received at SUs exhibit a sparsity property that yields a low-rank matrix of compressed measurements at the FC. Therefore, the full information of spectrum occupancies can be obtained by adopting low-rank MC methods.

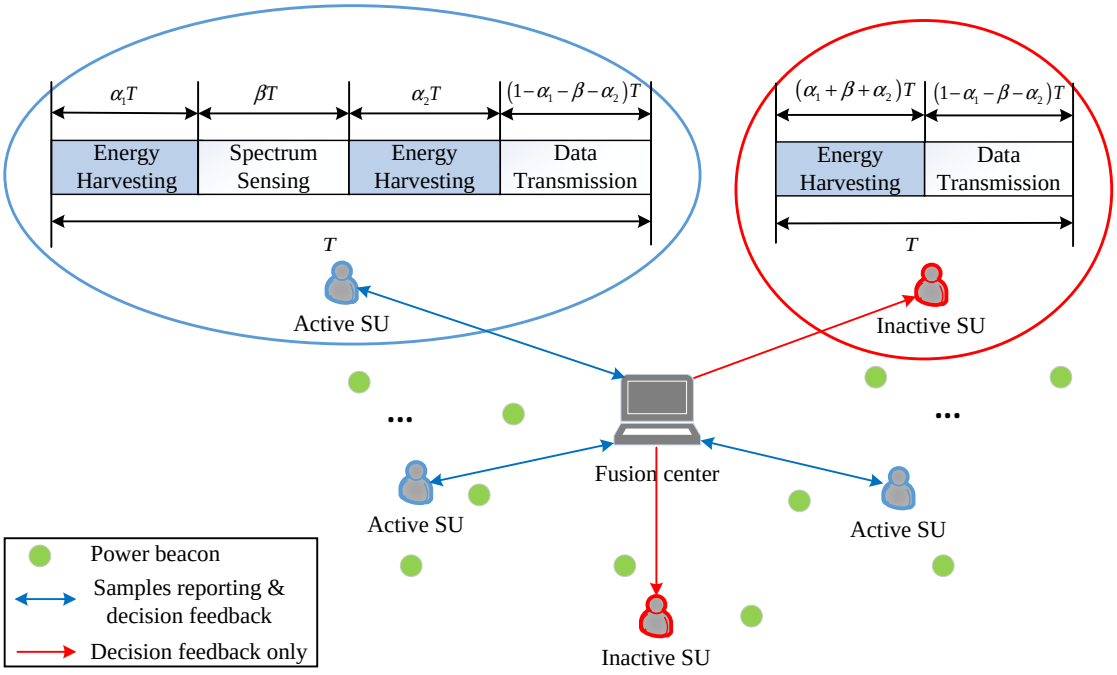

Figure 6.1: Proposed frame structure design with energy harvesting, spectrum sensing and data transmission.

6.2.2 Wireless Power Transfer Model

A bounded power transfer model with a protection zone with a radius d_0 is considered, which means that no PB is allowed to exist in this zone. If PBs are really close to the SU, the harvested energy would mathematically go to infinity [133]. It is assumed that the SU is battery-free [127, 134], which means that there is no battery storage energy for future use and all the harvested energy during energy harvesting time slots is used to perform spectrum sensing and data transmission in the current frame period. From the implementation point of view, this rechargeable storage unit can be a supercapacitor or a short-term/high-efficiency battery to support the switching between energy harvesting and information transmission [135]. It is worth pointing out that "Power from the Air" has been listed as one of the ten breakthrough technique by the MIT technology review. The idea is to enable battery-free devices connect with conventional devices by backscattering Wi-Fi signals.

A power transfer scheme is adopted, where the SU selects the PB with the strongest channel to harvest energy. At each SU, the energy harvested from the selected PB in the first and the third time slots can be obtained as follows:

$$E_H = \max_{p\in\Phi_p, \|d_p\|\geq d_0} \left\{ \|\mathbf{h}_p\|^2 L\left(d_p\right) \right\} \eta P_p \gamma_p T, \tag{6.1}$$

where γ_p is the ratio of the time used for energy harvesting to the total time of a frame, η is the power conversion efficiency at the SU, P_p is the transmission power of PBs. Here, $\mathbf{h}_p$ is a $\mathcal{C}^{M\times 1}$ vector, whose entries are independent complex Gaussian distributed with zero mean and unit variance employed to capture the effects of small-scale fading between PBs and the SU. $L\left(d_p\right) = Ad_p^{-\xi}$ is the power-law path-loss exponent. The path-loss function depends on the distance d_p, a frequency dependent constant A, and an environment/terrain dependent path-loss exponent $\xi \geq 2$. All the channel gains are assumed to be i.i.d.

For the active SUs, based on (6.1), defining E_{H_1} as the energy harvested during the first time slot of the frame, the maximum sensing power at the SU is given by

$$P_{H_1} = \frac{E_{H_1}}{\beta T} = \max_{p\in\Phi_p, \|d_p\|\geq d_0} \left\{ \|\mathbf{h}_p\|^2 L\left(d_p\right) \right\} \frac{\eta P_p \alpha_1}{\beta}. \tag{6.2}$$

As energy can only be stored in the current frame, the total energy for data transmission is the sum of the remaining energy in the second slot and the energy harvested in the third time slot, which is given by

$$E_{T_2} = \left(E_{H_1} - E_S\right) + E_{H_2}, \tag{6.3}$$

where E_s is the energy consumed for spectrum sensing at an SU.

Based on (6.1) and (6.3), the corresponding power for data transmission is given by

$$P_{T_2} = \frac{\max\limits_{p\in\Phi_p,\|d_p\|\geq d_0} \left\{\|\mathbf{h}_p\|^2 L\left(d_p\right)\right\} \eta P_p\left(\alpha_1+\alpha_2\right) - P_s\beta}{1-\alpha_1-\beta-\alpha_2}. \tag{6.4}$$

For those inactive SUs, the harvested energy before data transmission is given by

$$E_{H_3} = \max_{p\in\Phi_p,\|d_p\|\geq d_0} \left\{\|\mathbf{h}_p\|^2 L\left(d_p\right)\right\} \eta P_p(\alpha_1+\beta+\alpha_2)T. \tag{6.5}$$

Based on (6.5), the maximum sensing power at the SU can be expressed as

$$P_{H_3} = \frac{E_{H_3}}{\left(1-\alpha_1-\beta-\alpha_2\right)T}. \tag{6.6}$$

6.2.3 Compressive Spectrum Sensing Model

The considered compressive spectrum sensing model is similar as that introduced in Section 2.3.4 of Chapter 2. To avoid any confusion, a brief introduction for specific model used in this chapter is given. In the considered spectrum sensing model, when $J = 1$, the considered network becomes a single node scenario. At the jth SU (SU_j) in the considered network, the received signals can be expressed as

$$r_j\left(t\right) = h_j\left(t\right) * s\left(t\right) + w_j\left(t\right), \tag{6.7}$$

where $s\left(t\right) \in C^{n\times 1}$ refers to the transmitted primary signals in time domain with power σ_s^2, and $h_j\left(t\right)$ is the channel gain between the transmitter and receiver, and $w_j\left(t\right) \sim \mathcal{CN}(0, \sigma_n^2\mathbf{I}_n)$ refers to AWGN with zero mean and variance σ_n^2.

With CS technique invoked, the compressed measurements collected at SU_j can be

expressed as

$$\mathbf{x_j} = \mathbf{\Phi_j}\mathcal{F}^{-1}\mathbf{r_{fj}} = \mathbf{\Theta_j}\left(\mathbf{h_{fj}}\mathbf{s_f} + \mathbf{w_{fj}}\right), \tag{6.8}$$

where $\mathbf{\Phi_j} \in \mathcal{C}^{p\times n}$ $(p < n)$ is the measurement matrix utilized to collect the compressed measurements $\mathbf{x_j} \in \mathcal{C}^{p\times 1}$, and $\mathbf{s_f}$ and $\mathbf{n_{fj}}$ refer to the transmitted signals and the AWGN received in frequency domain. The compression ratio at SUs is defined as $\gamma = \frac{p}{n}, (0 \leq \gamma \leq 1)$. Additionally, $\mathbf{\Theta_j} = \mathbf{\Phi_j}\mathcal{F}^{-1}$, where $\mathcal{F}^{-1}$ is IDFT matrix.

After the compressed measurements are collected, SUs will send them to a remote FC by a error-free reporting channel. In both the single node and multiple nodes scenarios, FC is proposed to perform signal recovery efficiently. By adopting such a powerful FC, energy constrained SUs can get rid of signal recovery process and continue harvesting energy from PSs. At the FC, the compressed measurements $\mathbf{X}$ can be expressed as

$$\mathbf{X} = \mathbf{\Theta}\mathbf{R_f} = \mathbf{\Theta}\left(\mathbf{H}\mathbf{S_f} + \mathbf{W_f}\right), \tag{6.9}$$

where $\mathbf{R_f} = [\mathbf{r_{f1}}, \mathbf{r_{f2}}, \ldots, \mathbf{r_{fJ}}]$ which is in size of $n \times J$, $\mathbf{H} = diag\left(\mathbf{h_{f1}}, \mathbf{h_{f2}}, \ldots, \mathbf{h_{fJ}}\right)$ and $\mathbf{S_f}$, and $\mathbf{W_f}$ refer to the matrix constructed by transmitted signals and AWGN. Additionally, the measurement matrix is a diagonal matrix $\mathbf{\Theta} = diag\left(\mathbf{\Theta_1}, \mathbf{\Theta_2}, \ldots, \mathbf{\Theta_J}\right)$ in size of $P \times N$, with $P = p \times J$ and $N = n \times J$. After the compressed measurements are collected at the FC, signal recovery can be formulated as a convex optimization problem. As aforementioned, the considered network becomes a single node case when $J = 1$. Then the existing algorithm for CS can be utilized to recover the original signals. In the cooperative networks $(J > 1)$, existing algorithms for low-rank MC can be implemented to complete the matrix. It has been proved that the exact signal or matrix can be recovered if the number of available measurements are no less than the minimum bound. With enough number of measurements, exact transmitted signals can be obtained at the FC. Then energy detection is adopted to determine the spectrum occupancies, in which the decision is made by comparing the energy of recovered signal

with a threshold defined as (2.17) [136]. Once the sensing decisions are determined at the FC, they would be sent back to the participating SUs in the CSS network by the reporting channel to start the data transmission period.

6.3 Throughput Analyses of Single User

In this section, the closed form expressions are derived for the power outage probability of spectrum sensing and data transmission, respectively. With CS technique implemented, the analyses with the target of maximizing throughput of each SU locally is provided in this section.

6.3.1 Power Outage Probability Analyses

It is assumed that there exists a threshold transmission power, below which the spectrum sensing in the second slot or the data transmission in the fourth slot cannot be scheduled. We introduce power outage probability, i.e., probability that the harvested energy is not sufficient to perform spectrum sensing or carry out the data transmission at a certain desired quality-of-service level. In practical scenarios, a constant power for the data transmission is expected. Therefore, the power threshold P_s can be denoted as the sensing power in the second slot and P_t as the transmission power of the SU, respectively. The following theorem provides the exact analyses for the power outage probability at the single SU scenario.

Theorem 2. *The power outage probability of spectrum sensing P_s^{out} in the second time slot and the power outage probability of data transmission P_t^{out} in the fourth time slot can be expressed in closed-form as follows:*

$$P_{\zeta}^{out} = \exp\left[-\frac{\pi\lambda_p\delta}{\mu_{\zeta}^{\delta}}\sum_{m=0}^{M-1}\frac{\Gamma\left(m+\delta,\mu_{\zeta}d_0^{\xi}\right)}{m!}\right], \tag{6.10}$$

where $\zeta \in (s,t)$, $\mu_s = \frac{\beta P_s}{\eta P_p A \alpha_1}$, $\mu_t = \frac{P_t(1-\alpha_1-\beta-\alpha_2)+P_s\beta}{\eta P_p A(\alpha_1+\alpha_2)}$, $\delta = 2/\xi$, *and* $\Gamma(\cdot,\cdot)$ *is the upper incomplete Gamma function.*

Proof. Based on (6.2), the power outage probability of spectrum sensing can be expressed as

$$\begin{aligned} P_s^{out} &= \Pr\left\{P_{H_1} \le P_s\right\} \\ &= E_{\Phi_p}\left\{\prod_{p\in\Phi_p, \|d_p\|\ge d_0} \Pr\left\{\|\mathbf{h}_p\|^2 \le d_p^{\xi}\mu_s\right\}\right\} \\ &= E_{\Phi_p}\left\{\prod_{p\in\Phi_p, \|d_p\|\ge d_0} F_{\|\mathbf{h}_p\|^2}\left(d_p^{\xi}\mu_s\right)\right\}, \end{aligned} \tag{6.11}$$

where $F_{\|\mathbf{h}_p\|^2}$ is the cumulative density function (CDF) of $\|\mathbf{h}_p\|^2$ and is given by

$$F_{\|\mathbf{h}_p\|^2}(x) = 1 - e^{-x}\left(\sum_{m=0}^{M-1}\frac{x^m}{m!}\right). \tag{6.12}$$

Applying the moment generating function, (6.11) can be rewritten as

$$P_s^{out} = \exp\left[-\lambda_p \int\limits_{R^2}\left(1 - F_{\|\mathbf{h}_p\|^2}\left(d_p^{\xi}\mu_s\right)\right)dd_p\right]. \tag{6.13}$$

Then changing to polar coordinates and substituting (6.12) into (6.13), we obtain

$$P_s^{out} = \exp\left[-2\pi\lambda_p \sum_{m=0}^{M-1}\frac{\mu_s^m \int_{d_0}^{\infty} {d_p}^{m\xi+1} e^{-\mu_s d_p^{\xi}} dd_p}{m!}\right]. \tag{6.14}$$

Applying [137, Eq. (3.381.9)] to calculate the integral, (6.10) can be obtained.

Similarly, based on (6.4), the power outage probability of data transmission P_t^{out} can be expressed as follows:

$$P_t^{out} = \Pr\left\{P_{T_2} \le P_t\right\} = \Pr\left\{\max_{p\in\Phi_p, \|d_p\|\ge d_0}\left\{\|\mathbf{h}_p\|^2 {d_p}^{-\xi}\right\} \le \mu_t\right\}. \tag{6.15}$$

Following the similar procedure as (6.14) and applying $\mu_t \rightarrow \mu_s$, P_t^{out} in (6.10) is obtained.

The proof is completed. □

6.3.2 Compressive Spectrum Sensing Analyses

In the scenario of CS based single SU with WPT, the original signals can be obtained by solving the l_1 norm optimization problem as follows:

$$\begin{aligned} &\min \|\hat{\mathbf{s}}_{\mathbf{fj}}\|_1, \\ &\text{subject to } \ \|\boldsymbol{\Theta}_{\mathbf{j}} \cdot \mathbf{h}_{\mathbf{fj}} \hat{\mathbf{s}}_{\mathbf{fj}} - \mathbf{x}_{\mathbf{j}}\|_2^2 \leq \varepsilon, \end{aligned} \tag{6.16}$$

where $\hat{\mathbf{s}}_{\mathbf{fj}}$ refers to the reconstructed signal, and ε is the error bound related to the noise level. This optimization problem can be solved by many existing algorithms for CS, such as by adopting many existing algorithms such as CoSaMP [43], etc.

The performance metric of spectrum sensing at single SU can be measured by P_d and P_f. For a target probability of detection, $\bar{P}_d$, with which the PUs are sufficiently protected, the threshold can be determined by (2.17) accordingly, with the number of samples is n. As a result, P_f at a single SU can be derived as follows:

$$P_f = Q\left(Q^{-1}\left(\bar{P}_d\right)\sqrt{\frac{\sigma_s^2+\sigma_n^2}{\sigma_n^2}} + \sqrt{\frac{n}{2}}\frac{\sigma_s^2}{\sigma_n^2}\right). \tag{6.17}$$

Assuming the energy cost per sample e_s in spectrum sensing is fixed, the energy consumption of spectrum sensing is proportional to the number of collected samples as given by

$$n = \frac{\beta T P_s}{e_s}. \tag{6.18}$$

In fact, the number of collected samples n is determined by the sensing time slot. In this

case, the energy consumed by reporting collected measurements and receiving decision results between SUs to the FC is ignored. Substituting (6.18) into (6.17), we obtain

$$P_f = \left(1 - Q\left(Q^{-1}\left(\bar{P}_d\right)\left(1 + \frac{\sigma_s^2}{\sigma_n^2}\right) + \sqrt{\frac{\beta T P_s}{2e_s}}\frac{\sigma_s^2}{\sigma_n^2}\right)\right). \tag{6.19}$$

6.3.3 Throughput Analyses

By considering the power outage probability, the throughput at the single SU in the CRNs can be expressed as

$$\tau = \left(1 - P_s^{out}\right) \times \left(1 - P_t^{out}\right) \times (1 - P_f) \times (1 - \alpha_1 - \beta - \alpha_2)\,\tau_t, \tag{6.20}$$

where $\tau_t = \log_2\left(1 + \frac{P_t}{N_0}\right)$ is the throughput for the data transmission slot, and N_0 refers to the AWGN level in the data transmission channel. Here, the data transmission process is simplified without consideration the fading, which means the throughput τ_t is only determined by the transmit SNR.

When implementing CS technique to achieve sub-Nyquist sampling rate at an SU, It has been proven that the exact signal recovery can be guaranteed if the number of collected measurements satisfies $p \geq c \cdot K \log(n/K)$, where c is some constant depending on each instance [138]. If the signal is recovered successfully by Λ samples, the achieved P_f would be the same as that no CS technique is implemented with n samples. Therefore, the necessary sensing time slot to achieve the same P_f can be reduced to $\gamma\beta$ with CS implemented. Replacing P_s^{out}, P_t^{out} and P_f in (6.20) by (6.10) and (6.19) respectively,

the full expression of the throughput with CS implemented can be expressed as follows:

$$\begin{aligned}\tau_{cs} = \prod_{\zeta=\{s,t\}} \left(1 - \exp\left(-\frac{\pi\lambda_p\delta}{\left(\mu_\zeta^{cs}\right)^\delta} \sum_{m=0}^{M-1} \frac{\Gamma\left(m+\delta, \mu_\zeta^{cs} d_0^\xi\right)}{m!}\right)\right) \\ \times \left(1 - Q\left(Q^{-1}\left(\bar{P}_d\right)\left(1+\frac{\sigma_s^2}{\sigma^2}\right) + \sqrt{\frac{\beta T P_s}{2e_s}}\frac{\sigma_s^2}{\sigma^2}\right)\right) \\ \times (1-\alpha_1-\gamma\beta-\alpha_2) \times \log_2\left(1+\frac{P_t}{N_0}\right). \end{aligned} \tag{6.21}$$

If there is no CS technique implemented at SUs, the time slot fraction for spectrum sensing follows the condition that $0 \leq \beta \leq 1$. When the CS technique is implemented at SUs, the time slot for spectrum sensing follows the condition that $cK\log(n/K) \leq \frac{\gamma\beta T P_s}{e_s} \leq n$. By combining these two conditions, the constraint for β becomes $\frac{e_s(cK\log(n/K))}{\gamma T P_s} \leq \beta \leq 1$. With the implementation of CS, the β in (6.10) is replaced by $\gamma\beta$.

Furthermore, the throughput can be maximized by solving the following problem:

$$\begin{aligned} (\text{P0}): \max_{\alpha_1,\beta,\alpha_2,P_t} \quad & \tau_{cs}, \\ \text{subject to} \quad & C_1: 0 \leq \alpha_1 \leq 1, \\ & C_2: \frac{e_s\left(cK\log\left(n/K\right)\right)}{\gamma T P_s} \leq \beta \leq 1, \\ & C_3: \alpha_{2,\min} \leq \alpha_2 \leq 1, \\ & C_4: 0 \leq 1-\alpha_1-\gamma\beta-\alpha_2 \leq 1, \\ & C_5: P_{t,\min} \leq P_t \leq P_{t,\max}, \end{aligned} \tag{6.22}$$

where $\alpha_{2,\min}$ refers to the minimum time slot fraction for signal recovery at the FC and data transmission between the SU and FC. $P_{t,\min}$ and $P_{t,\max}$ refer to the allowed minimum and maximum power levels for data transmission period. It is noticed that (6.22) is a constrained nonlinear optimization problem and the objective function is very complex. However, the constraints are linear, which motives us to solve the optimization problem by the following three methods:

Algorithm 6 Grid Search for Solving (6.22)

1: Initialization: Δ_1, Δ_2, Δ_3, Δ_4, and $\tau_{temp} = \emptyset$.
2: **for all** $\alpha_1 \in (0 : \Delta_1 : 1)$, $\beta \in \left(\frac{e_s(cK\log(n/K))}{\gamma T P_s} : \Delta_2 : 1\right)$, $\alpha_2 \in (\alpha_{2,\min} : \Delta_3 : 1)$, $P_t \in (P_{t,\min} : \Delta_4 : P_{t,\max})$ **do**
3: **while** $0 \leq 1 - \alpha_1 - \gamma\beta - \alpha_2 \leq 1$ **do**
4: $\tau_{temp} = [\tau_{temp}, \tau_{cs}]$ where τ_{cs} is expressed as (6.21).
5: **end while**
6: **end for**
7: **return** $\tau_{\max} = \tau_{temp}$.

1. *Grid search*: The grid search algorithm for solving (6.22) can be described in **Algorithm 6**. The grid search algorithm can find out the global optimal value if the step size $\Delta_i\,(i = 1, 2, 3, 4)$ for α_1, β, α_2, P_t are small enough. However, the computational complexity would greatly increase if the step is set to be small enough.

2. *fmincon*: *fmincon* is a toolbox in MATLAB which is efficient but it may return a local optimal value.

3. *Random sampling*: A set $\{v_1, v_2, \cdots, v_{\mathrm{Z}}\}$ that satisfies the conditions in (6.22) is generated randomly, where $v_i = (\alpha_1, \beta, \alpha_2, P_t)$ $(i \in \{1, 2, \cdots, \mathrm{Z}\})$ is a tuple of generated random samples, and Z is the number of generated tuples. The accuracy of this method depends on number of tuples Z generated for calculation. This method is efficient for solving (6.22) as it does not rely on advanced optimization techniques and the method of generating $(\alpha_1, \beta, \alpha_2, P_t)$ is efficient.

6.4 Throughput Analyses of Multiple Cooperative Users

In this section, the closed-form expressions for the power outage probability of data transmission are deprived for both the active and inactive SUs, respectively. After considering the throughput optimization of a single SU locally in Section III, we optimize the throughput of the CSS networks with multiple SUs including the active and inactive ones with implementing MC technique.

6.4.1 Power Outage Probability Analyses

In this subsection, we provide power outage probability analyses for spectrum sensing and data transmission for both active and inactive SUs. In the considered CSS networks, the number of active participating SUs is J_1 and the number of inactive SUs is J_2.

6.4.1.1 Power Outage Probability of Spectrum Sensing

Note that the power outage probability of sensing is always zero. This behavior can be explained as follows: 1) For active SUs, it is assumed that the harvested energy from the first time slot is enough for them to take measurements for spectrum sensing. Therefore, the power outage probability of spectrum sensing for active SUs are zero; and 2) For the inactive SUs, they will not perform spectrum sensing and only transmit data. As a consequence, there is no spectrum sensing outage.

6.4.1.2 Power Outage Probability of Data Transmission

For those active SUs, the power outage probability of data transmission is same that of the single SU scenario. For those inactive SUs, as all the time slots before data transmission are used for energy harvesting, the power outage probability is different as that of active SUs. The following theorem provides the exact analyses for the power outage probability of data transmission for both active and inactive SUs in CSS networks.

Theorem 3. *The power outage probability of data transmission at the active and inactive SUs in the fourth time slot can be expressed in closed-form as follows:*

$$P_{\psi}^{out} = \exp\left[-\frac{\pi\lambda_p\delta}{\mu_{\psi}^{\delta}}\sum_{m=0}^{M-1}\frac{\Gamma\left(m+\delta,\mu_{\psi}d_0^{\xi}\right)}{m!}\right] \tag{6.23}$$

where $\psi \in (a,i)$, $\mu_a = \frac{P_t(1-\alpha_1-\beta-\alpha_2)+P_s\beta}{\eta P_p A(\alpha_1+\alpha_2)}$, *and* $\mu_i = \frac{P_t(1-\alpha_1-\beta-\alpha_2)}{\eta P_p A(\alpha_1+\beta+\alpha_2)}$.

Proof. Based on (6.6), the power outage probability of data transmission at the active SUs is the same as P_t^{out} as given in (6.10) by replacing $\mu_a \to \mu_\zeta$.

Similarly, based on (6.6), the power outage probability of data transmission at the inactive SUs can be expressed as follows:

$$P_i^{out} = \Pr\left\{P_{H_3} < P_t\right\} = \Pr\left\{\max_{p\in\Phi_p, \|d_p\|\geq d_0}\left\{\|\mathbf{h}_p\|^2 {d_p}^{-\xi}\right\} < \mu_i\right\}. \tag{6.24}$$

Following the similar procedure as (6.14) and applying $\mu_i \to \mu_s$, P_i^{out} in (6.23) can be obtained.

The proof is completed. □

6.4.2 Matrix Completion Based Cooperative Spectrum Sensing Analyses

As the spectrum is normally underutilized in practice, the transmitted signals exhibit a sparse property in frequency domain, which can be transformed into a low-rank property of the matrix $\mathbf{X}$ at the FC. When only the J_1 active SUs send compressed samples to the FC, the matrix with collected samples is incomplete at the FC. The exact matrix can be obtained by solving the following problem:

$$\begin{aligned} &\min \ \left\|\hat{\mathbf{S}}_\mathbf{f}\right\|_*, \\ &\text{subject to } \left\|\mathbf{\Theta}\cdot\text{vec}\left(\mathbf{H}\hat{\mathbf{S}}_\mathbf{f}\right) - \text{vec}\left(\mathbf{X}\right)\right\|_2^2 \leq \boldsymbol{\varepsilon}. \end{aligned} \tag{6.25}$$

where $\hat{\mathbf{S}}_\mathbf{f}$ refers to the reconstructed matrix, and $\boldsymbol{\varepsilon} = [\varepsilon_1, \ldots, \varepsilon_J]$. This problem can be solved by amount of existing MC solvers.

Once the exact matrix is recovered, energy detection can be used to determine the spectrum occupancy. In the CSS networks, as all the participating SUs send the collected samples to the FC, the data fusion is considered. Suppose the channel coefficients from the PUs to each participating SUs are known. When the channel coefficients are

unknown, the weighting factor associated with the jth SU is set to be $g_j = \frac{1}{\sqrt{J}}$. By using the maximal ratio combining, probability of false alarm of the CSS networks Q_f becomes

$$Q_f = Q\left(Q^{-1}\left(\bar{P}_d\right)\sqrt{1+\frac{\sigma_s^2}{J\sigma_n^2}\mathbf{H_1}} + \sqrt{\frac{n}{2J}}\frac{\sigma_s^2}{\sigma_n^2}\mathbf{H_1}\right). \tag{6.26}$$

where $\mathbf{H_1} = \sum_{j=1}^{J} |\mathbf{h_{fj}}|^2$ refers to the channel coefficients for all the participating SUs in the considered CSS networks. In order to simplify the case, all coefficients in $\mathbf{h_{fj}}$ as set to be one. Consequently, Q_f can be expressed as

$$Q_f = Q\left(Q^{-1}\left(\bar{P}_d\right)\sqrt{1+\frac{\sigma_s^2}{\sigma^2}} + \sqrt{\frac{nJ}{2}}\frac{\sigma_s^2}{\sigma^2}\right). \tag{6.27}$$

6.4.3 Throughput Analyses

By applying the MC technique at the FC, β in (6.23) should be replaced by $\gamma\beta$. Additionally, the throughput of considered CSS networks with multiple SUs can be expressed as

$$\tau_{mc} = \prod_{j=1}^{J}\left(1 - P_{\psi}^{out}\left(j\right)\right) \times \left(1 - Q_f\right) \times \left(1 - \alpha_1 - \gamma\beta - \alpha_2\right)\tau_t, \tag{6.28}$$

where γ is defined as the compression ratio at active SUs. $\psi = a$ refers to the J_1 number of active SUs and $\psi = i$ refers to the rest of inactive SUs in the considered networks. If no MC technique is implemented at the FC and each SU is supposed to take samples at Nyquist rate, all the participating SUs will send samples to the FC. Then the throughput of the considered networks can be given by replacing $P_{\psi}^{out}\left(j\right)$ in (6.28) with $P_{a}^{out}\left(j\right)$ and $\gamma = 1$. The constraints for the multiple nodes case are the same as that for the single node case except the condition for β. In the multiple nodes case, the condition for β follows $c\mu^2\nu K\log^6\nu \leq \frac{\gamma\beta T P_s J_1}{e_s} \leq nJ$. Combining the condition for β in case of no MC implemented, β should satisfy $\frac{e_s\left(c\mu^2\nu K\log^6\nu\right)}{\gamma T P_s J_1} \leq \beta \leq 1$.

The throughput can be maximized by solving the following problem:

$$\begin{aligned} (\text{P1}): \max_{\alpha_1,\beta,\alpha_2,P_t} \quad & \tau_{mc} \ , \\ \text{subject to} \quad & C_1,\ C_3,\ C_4 \text{ and } C_5, \\ & C_6: \frac{e_s\left(c\mu^2\nu k\log^6\nu\right)}{\rho T P_s J_1} \leq \beta \leq 1, \end{aligned} \tag{6.29}$$

where $c\mu^2\nu k\log^6\nu$ is the lower bound of the number of observed measurements at the FC to guarantee the exact matrix recovery [139]. Here, $\nu = \max(n, J)$ and $\mu = \mathrm{O}\left(\sqrt{\log\nu}\right)$. It is noticed that the structure of (P1) is similar as (P0). Thus, the similar methods can be utilized to obtain the optimal throughput for the CSS network.

6.5 Numerical Results

In the simulation, the frame period is set to be $T = 1$ s, the transmission power of PBs to be $P_p = 43$ dBm, the number of antennas of PB to be $M = 32$, the carrier frequency for power transfer to be 900 MHz, and the energy conversion efficiency of WPT to be $\eta = 0.8$. Additionally, it is assumed that the target probability of detection $\bar{P}_d$ is 90%. In this chapter, $d_0 \geq 1$ m, in order to make sure the path loss of WPT is equal or greater than one.

6.5.1 Numerical Results on Optimizing Throughput of Single User

In this subsection, simulation results of the optimized throughput of single SU are demonstrated after the derived power outage probability in (6.10) and P_f in (6.19) are verified by Monte Carlo simulations.

Fig. 6.2 plots the power outage probability of spectrum sensing versus density of PBs with different power threshold P_s. The black solid and dash curves are used to represent the analytical results with $d_0 = 1$ m and $d_0 = 1.5$ m, respectively, which

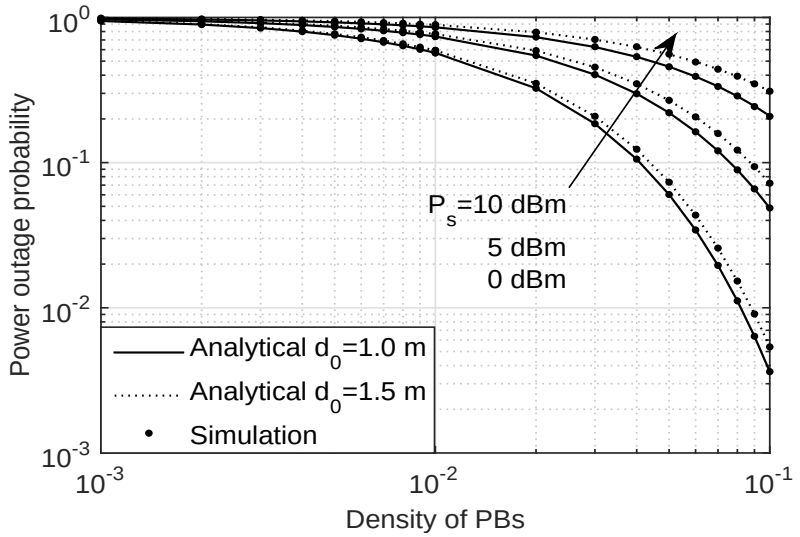

Figure 6.2: Power outage probability of spectrum sensing versus density of PBs with $M = 32$, $P_p = 43$ dBm, $\alpha_1 = 0.25$, $\alpha_2 = 0.2$, and $\beta = 0.25$.

are both obtained from (6.10). Monte Carlo simulations are marked as "•" to verify the derivation. The figure shows the precise agreement between the simulation and analytical curves. One can be observed is that as density of PBs increases, the power outage probability dramatically decreases. This is because the multiuser diversity gain is improved with increasing number of PBs when charging with WPT. The figure also demonstrates that the outage occurs more frequently as the power threshold P_s and the radius of protection zone d_0 increase.

Fig. 6.3 plots the probability of false alarm P_f versus SNR in sensing channels with different compression ratio γ. It is observed that P_f decreases with higher SNR, which would improve the throughput of secondary network. The black solid curve is used to represent the analytical result which is obtained from (6.19) with enough protection to PUs being provided. Monte Carlo simulations with compression ratio $\gamma = 100\%$ are marked as "○" to verify the derivation, which represents the scenario without CS technique implemented. The figure shows precise agreement between the simulation and analytical curves. When γ is reduced to 50%, it is noticed that P_f is still well matched with the analytical result, which means the performance of spectrum sensing would not

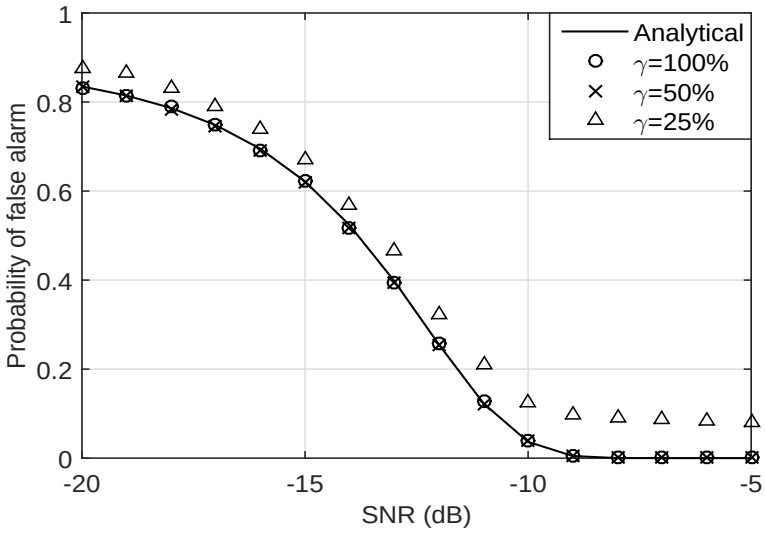

Figure 6.3: Probability of false alarm versus SNR in sensing channels with different compression ratio γ, $\bar{P}_d = 90\%$, and sparsity level = 12.5%.

be degraded when only 50% of the samples are collected at an SU. When γ is further reduced to 25%, P_f is increased, which means the signal recovery is not exact any more. As a result, throughput of the secondary network would be degraded correspondingly. Actually, the lowest compression ratio for successful signal recovery is dependent on the sparsity levels of received signals and the available prior information. This is out of the scope of this chapter and would not be discussed further.

Fig. 6.4 plots the achievable throughput τ_{cs} versus the lower bound of time allocated to the third slot α_2. Here α_2 is reserved for signal recovery at the FC and data transmission between the SU and the FC. In this figure, several observations are drawn as follows: 1) The maximal throughput achieved by grid search method is slight higher than that of *fmincon* method as *fmincon* relies on the initial input and may return a local optimal value. However, the accuracy of grid search method is dependent on the step sizes; 2) The random sampling method achieves lower throughput than grid search and *fmincon* methods, which demonstrates the benefits of the presented grid search and fmincon methods. When the generated sets increase for random sampling, the achieved maximal throughput get closer to the optimal but the computational complexity is much

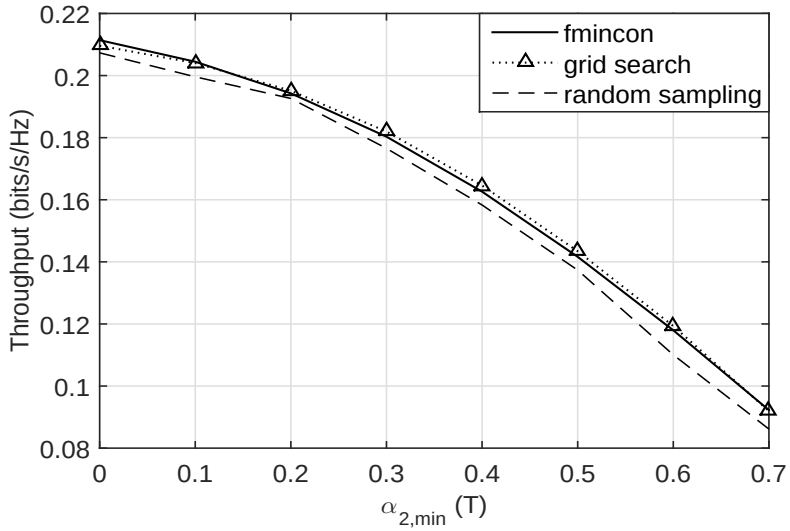

Figure 6.4: Throughput of single SU τ_{cs} versus lower bound of the third time slot $\alpha_{2,\min}$, $SNR = -10$ dB, and compression ratio $\gamma = 100\%$.

increase; 3) It is seen that the optimal value of time assigned to the third slot α_2 always equals to the lower bound $\alpha_{2,\min}$. This gives a sign that the throughput can be improved if the time slot for the signal recovery at the FC and data transmission between SUs and the FC is reduced. In other words, the energy harvesting should be done mainly in the first time slot α_1 to reduce the power outage probability in the following spectrum sensing slot if the signal recovery and data transmission between the SU and FC can be promised.

Fig. 6.5 plots the achieved optimal throughput τ_{cs} versus lower bound α_2 and compression ratio γ when solving the problem in (6.22). It shows that the achieved maximal throughput increases with decreasing γ and increasing $\alpha_{2,\min}$. This behavior can be explained as follows: as γ decreases, the number of samples to be collected for spectrum sensing at an SU is reduced as the signal in original size of $N \times 1$ can be recovered from less number of Λ measurements by utilizing CS technique. When the time slot assigned for spectrum sensing is reduced, the energy consumption for spectrum sensing is reduced. As a result, the time which can be assigned for data transmission is increased. Therefore, the throughput of the secondary network is improved. By optimizing the transmission

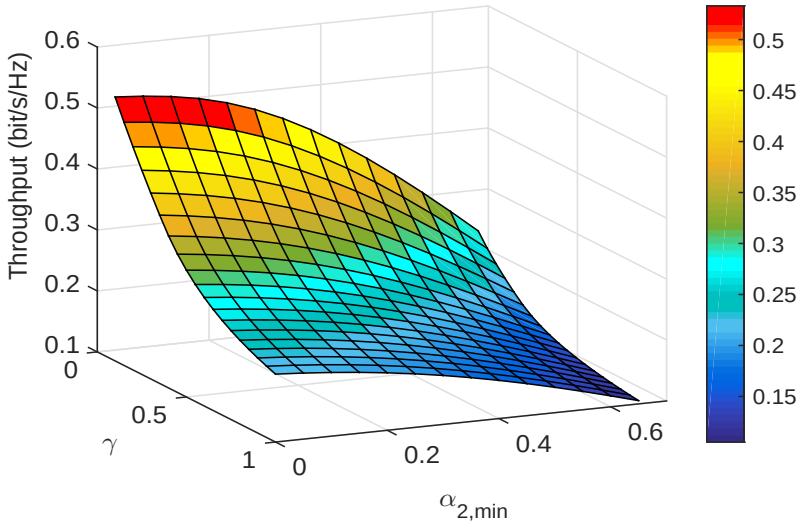

Figure 6.5: Optimized throughput of single SU τ_{cs} versus lower bound of the third time slot $\alpha_{2,\min}$ and compression ratio γ, and $SNR = -10$ dB in sensing channels.

power P_t, the energy harvested in the current frame period would be fully utilized and the maximal throughput can be achieved accordingly. It should be noted that when the compression ratio γ is set to 100% and the lower bound of the third time slot $\alpha_{2,min}$ is zero, the achieved throughput can be regarded as that of the traditional frame structure design without considering sub-Nyquist sampling. The case when γ is set to 100% can be regarded as a benchmark for the performance metric.

6.5.2 Numerical Results on Optimizing Throughput of Multiple Cooperative Users

In the case of optimizing the throughput of the CSS networks, the total number of participating SUs is set be to $J = 50$, including both the active and inactive SUs. Comparing the format of (P1) and (P0), it can be observed that both of them are linear constrained. Therefore, similar as (P0), the grid search method can be applied to obtain the optimal throughput but with non-negligible complexity, especially for the case of optimizing throughput of the whole cooperative network. The *fmincon* method can be

adopted to obtain the sub-optimal throughput efficiently. In the following simulations, the *fmincon* method is utilized to solve the optimization problem (P1). Additionally, as aforementioned, many algorithms have been proposed for the low-rank MC based CSS. With $\bar{P}_d = 90\%$, the detection performance with different compression ratios is presented in the work represented in Chapter 3 of this thesis, which would not be demonstrated here again to reduce redundancy. In the following simulations, how the achieved throughput is influenced by parameters, such as the number of active SUs J_1, compression ratio γ and the lower bound of the third time slot $\alpha_{2,\min}$, would be demonstrated.

Fig. 6.6 plots the power outage probability P_{out} versus density of PBs with different power threshold P_s. In this case, the power outage probability here is for the whole system, which can be calculated as $P_{out} = 1 - (1 - P_{out}^s) \times \left(1 - P_{out}^t\right)$. Both the single SU scenario and multiple SUs scenario are illustrated in the figure. It can be observed that as density of PBs increases, the power outage probability dramatically decreases, which is caused by that the multiuser diversity gain is improved with increasing number of PBs when charging with WPT. It can be also observed that the P_{out} of multiple SUs scenario is lower than that of single SU scenario. This is because the power outage probability of spectrum sensing is always zero in multiple SUs scenario, which in turn lower the power outage probability of the whole system. For the multiple SUs scenario, the P_{out} of the active SUs, inactive SUs and the average P_{out} of the CSS networks are all presented in the figure. It is noted the averaged P_{out} falls between the P_{out} of active SUs and inactive SUs, which is as expected.

Fig. 6.7 plots the throughput averaged on per SU τ_{mc} with different number of active SUs J_1 and different compression ratios γ. In this case, it is assumed that the exact MC can be guaranteed when the number of active SUs J_1 is in the range of 10 to 50 with compression ratio γ changes from 20% to 100%. It shows that the average throughput achieves the best performance when the number of active SUs J_1 is set to be the minimal number in comparison with that of case $J_1 = J$. This benefits from the non-active SUs, which can save energy for spectrum sensing and harvest more energy

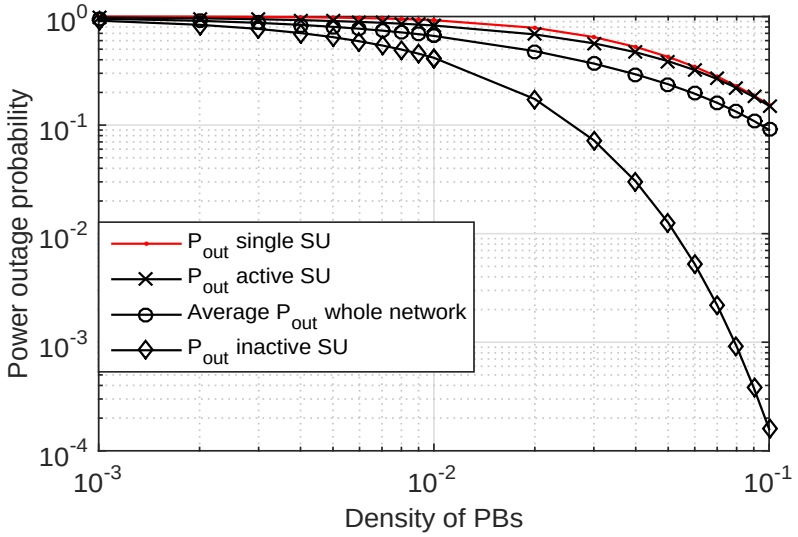

Figure 6.6: Power outage probability comparison for single SU and multiple SUs with versus density of PBs, $P_s = 0$ dBm, $\alpha_1 = 0.25$, $\alpha_2 = 0.20$, and $\beta = 0.25$.

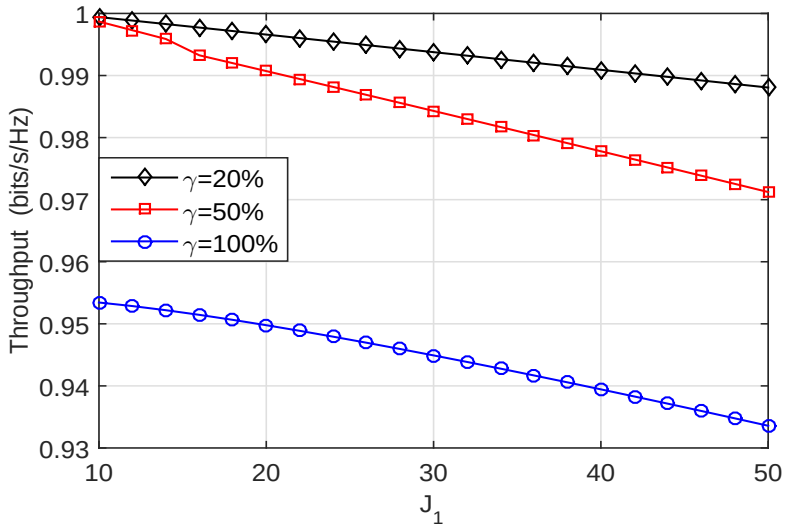

Figure 6.7: Optimized throughput averaged on per SU of multiple SUs τ_{mc} versus number of active SUs J_1 and compression ratio γ, $SNR = -10$ dB in sensing channels, and $\alpha_{2,\min} = 0.05$.

for data transmission. With compression ratio γ decreasing from 75% to 20%, the achieved optimal throughput is increased as the necessary time slot for spectrum sensing is reduced.

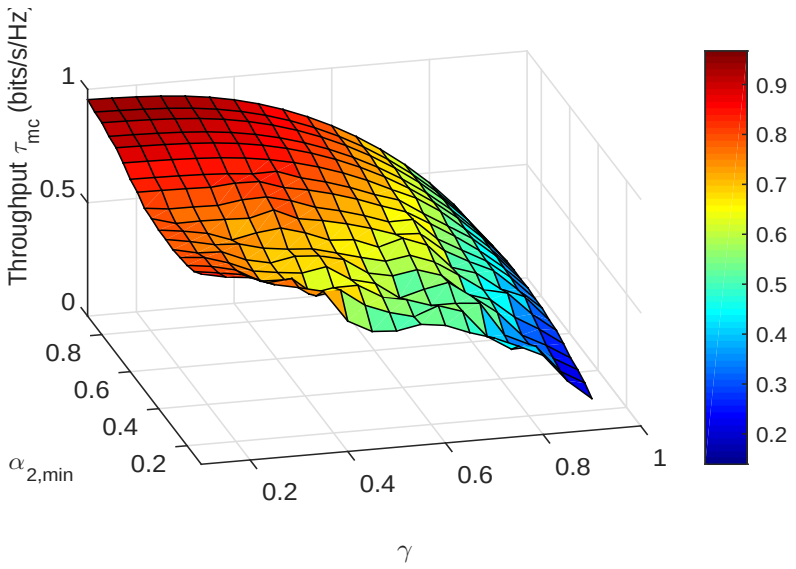

Figure 6.8: Optimized throughput averaged on per SU of multiple SUs τ_{mc} versus lower bound $\alpha_{2,\min}$ and compression ratio γ, and $SNR = -10$ dB in sensing channels.

Fig. 6.8 plots the achieved maximum throughput averaged on per SU versus different compression ratio γ and lower bound for the third time slot $\alpha_{2,min}$. In this case, the number of active SUs is $J_1 = 30$. The achieved throughput shown in Fig. 6.8 is based on the condition that the exact matrix recovery can be guaranteed with the given compression ratio. As shown in the figure, the maximum achieved throughput increases with decreasing γ and $\alpha_{2,\min}$. The minimal compression ratio guaranteing the exact matrix recovery is nondeterministic, which is dependent on the rank order of the matrix to be recovered. If the rank order J_1 is fixed, the larger network size J, the lower minimal compression ratio which can guarantee the exact matrix recovery.

6.6 Summary

In this chapter, a wireless powered CRNs has been considered. In the considered networks, while protecting the PUs, a new frame structure was proposed, which includes energy harvesting, spectrum sensing, energy harvesting and data transmission. In the proposed frame structure, closed-form expressions in terms of power outage probability

was derived for the proposed WPT scheme. Additionally, sub-Nyquist sampling was performed at wireless powered SUs in CRNs to reduce the energy consumption during spectrum sensing, by invoking CS and MC techniques. By optimizing the four time slots, throughput of a single SU and the whole cooperative networks were maximized, respectively. Simulation results showed that the throughput can be improved by the proposed new frame structure. It can be further concluded that by carefully tuning the parameters for different time slots and transmission power, WPT can be used along with CS and MC to provide a high quality of throughput performance for CRNs, with significantly energy computation reduction at energy-constrained SUs.

Chapter 7

Conclusions and Future Work

7.1 Conclusions

This thesis presented research work on the promising applications of compressive sensing (CS) technique in wideband spectrum sensing, which is regarded as one of the most challenging tasks in cognitive radio networks (CRNs). It has been demonstrated that CS is capable of enabling sub-Nyquist sampling at secondary users (SUs), by exploiting the natural sparsity of spectral signals. By invoking CS technique, the signal sampling costs at SUs are significantly reduced, which is of great significance in CRNs as the SUs are normally energy-constrained devices. During my Ph.D research, the fundamental research has been carried out on the design of novel compressive spectrum sensing algorithms, with particular efforts to improve energy efficiency, robustness and security of CRNs. Moreover, the performance of wireless powered CRNs with CS has been investigated with particular emphasis on throughput optimization.

In Chapter 3, through proposing new channel division schemes for single SU and multiple cooperative SUs scenarios, the amount of both data sensing at SUs and data transmission among the whole CRNs were significantly reduced. Additionally, a denoising algorithm was proposed to improve the robustness to channel noise. Inspired by

the TV white space (TVWS) pilots conducted in the UK, the proposed algorithms were tested on both the simulated and real-world signals over TVWS. Furthermore, numerical results demonstrated that: i) the computational complexity of signal recovery process was significantly reduced, and the robustness of the proposed algorithm to channel noise was dramatically improved.

In Chapter 4, a novel compressive spectrum sensing algorithm was proposed to improve the recovery performance, in which geolocation database was invoked for providing prior information over TVWS. By doing so, original signals were able to be recovered with requiring fewer measurements, which lowered the computational complexity of signal recovery compared to that without prior information. Simulations have been done on both the real-world and the simulated data for evaluating performance of the proposed algorithm. It is worth pointing out that SUs are capable of estimating the sparsity level efficiently by utilizing the geolocation database, which makes the proposed algorithm be more adaptive to dynamic spectrum variation. Consequently, the unnecessary energy consumption at SUs can be eliminated.

Aiming at enhancing the security in CRNs, a malicious user detection framework was proposed in Chapter 5, by invoking low-rank matrix completion (MC) technique. The channels corrupted by malicious users were removed during the process of MC. Additionally, in order to ensure the malicious user detection process be independent on the prior information of networks and spectrum diversity, a rank order estimation algorithm and a malicious user number estimation strategy were proposed. Furthermore, the proposed framework was tested on both the simulated and real-world signals over TVWS. It was demonstrated that the proposed framework was capable of achieving good detection performance, with limited number of active SUs or low costs of data acquisition at each individual SU.

Finally, in Chapter 6, the throughput of wireless powered CRNs was analyzed with invoking of CS and MC techniques. Besides invoking CS and MC techniques to reduce energy consumption, each SU is supposed to harvest energy through wireless power

transfer to further power itself. Additionally, the signal recovery process was proposed to be conducted at a powerful data fusion center to relax SUs. Both the throughput of a single SU and the whole network can be optimized by opportunistically scheduling the time slots assigned for energy harvesting, spectrum sensing and data transmission. Numerical results demonstrated that CS and MC techniques are capable of offering a higher throughput performance for wireless powered CRNs.

In a summary, in this thesis, novel compressive spectrum sensing designs were proposed with particular emphasis on the robustness, computational complexity, security and throughput optimization in CRNs. Amount of simulations have been done on the real-world signals over TVWS, which demonstrated that the effectiveness of applying CS in wideband spectrum sensing, for improving the spectrum efficiency and energy efficiency of CRNs.

7.2 Future Work

The following three research issues have been identified and are to be addressed in future work, for the applications and implementations of CS in CRNs.

7.2.1 Implementable Measurement Matrices Design

Before invoking CS technique to practical scenario, the implementable measurement matrices should be designed carefully. As mentioned in Section 2.1.2 of Chapter 2, the existing structured measurement matrices have their own drawbacks, which limit their applications in reality. Moreover, the current structured measurement matrices are designed for the implementation of CS in a general case. For the application of CS in CRNs, more specific measurement matrices should be designed, with particular considerations on the universality, recovery complexity, recovery speed, minimum number of measurements required exact recovery, and the implementation costs. Some available

information, such as geolocation database for TVWS, might be utilized to construct a structured measurement matrix for CRNs particularly, with affordable costs and acceptable performance.

7.2.2 Performance Limitations under Practical Constraints

To date, most of work on CS based CRNs were based on ideal operating conditions. However, in practice, there may occur various imperfections, such as noise uncertainty, channel uncertainty, dynamic spectrum occupancy, and transceiver hardware imperfections like analog-to-digital converter errors, synchronization errors, etc. Taking the centralized compressive collaborative approach as an example, it considers ideal reporting channels, which is not the case in practice. These imperfections may lead to significant performance degradation of a compressive spectrum sensing algorithm in the implementation of CRNs. Therefore, it is a big challenge to further investigate the compressive spectrum sensing in the presence of practical imperfections, and to develop a common framework to combat their aggregate effects in a CS based CRNs.

7.2.3 Generalized Hardware Platform for Compressive Spectrum Sensing

For the existing hardware implementation of CS, the theoretic algorithm is specifically designed based on available hardware devices. However, it is difficult or even impossible to extend current hardware architecture for implementing other algorithms on compressive spectrum sensing. Meanwhile, it has been noted that there is a bright future for the application of CS in networks with energy-constrained devices, such as CRNs. Thus, a generalized hardware platform or test-bed is quite desired for conducting the real implementations of CS. Therefore, a more generalized hardware platform for compressive spectrum sensing for CRNs is strongly desired, in which the different functional components of compressive spectrum sensing can be easily extended, in an effort to test

the various algorithms with different types of measurement matrices and signal recovery algorithms.

Appendix A

Wilkinson's Method

Assuming I_k $\left(k = 1, 2, \ldots, \tilde{K}\right)$ is a log-normal random variable, then $M_k = 10\log_{10} I_k$ can be modeled as a Gaussian random variable and $M = 10\log_{10}\left(\sum_{k=1}^{\tilde{K}} 10^{\frac{M_k}{10}}\right)$. It is assumed that $e^{\Lambda_1} + e^{\Lambda_2} + \cdots + e^{\Lambda_{\tilde{K}}} = e^Z = 10^M$, $Z = \rho M$, and $\rho = \frac{1}{10}\ln 10 = 0.2302$, the mean and standard deviation of parameter M could be calculated by introducing two parameters μ_1 and μ_2, which are given as follows:

$$\mu_1 = \mathrm{E}\left(m_Z + \frac{1}{2}\sigma_Z^2\right) = \sum_{i=1}^{\tilde{K}} \mathrm{E}\left(m_{\Lambda_i} + \frac{1}{2}\sigma_{\Lambda_i}^2\right), \tag{A.1}$$

$$\begin{aligned}\mu_2 = {} & \mathrm{E}\left(2m_Z + 2\sigma_Z^2\right) = \sum_{i=1}^{\tilde{K}} \mathrm{E}\left(2m_{\Lambda_i} + 2\sigma_{\Lambda_i}^2\right) \\ & + 2\sum_{i=1}^{\tilde{K}-1}\sum_{j=i+1}^{\tilde{K}} \mathrm{E}\left(m_{\Lambda_i} + m_{\Lambda_j}\right) \times \mathrm{E}\left[\frac{1}{2}\left(\sigma_{\Lambda_i}^2 + \sigma_{\Lambda_j}^2 + 2r_{ij}\sigma_{\Lambda_i}\sigma_{\Lambda_j}\right)\right],\end{aligned} \tag{A.2}$$

where m_{Λ_i} and σ_{Λ_i} are the mean and standard deviation of Λ_i, and r_{ij} are the correlation coefficients of Λ_i and Λ_j. Consequently, the mean and standard deviation of M can be calculated as

$$\sigma_M = \frac{1}{\rho}\left(2\ln\mu_1 - \frac{1}{2}\ln\mu_2\right), \tag{A.3}$$

$$\sigma_M = \frac{1}{\rho}(\ln \mu_2 - 2 \ln \mu_1)^{\frac{1}{2}}. \tag{A.4}$$

References

[1] P. Kolodzy, "Spectrum policy task force," *Federal Commun. Comm., Washington, DC, Rep. ET Docket*, no. 02-135, Jun. 2002.

[2] UK Office of Communications (Ofcom), *"Staement on Cognitive Access to Interleaved Spectrum,"* Jul. 2009.

[3] J. Mitola and G. Q. Maguire, "Cognitive radio: making software radios more personal," *IEEE Pers. Commun.*, vol. 6, no. 4, pp. 13 –18, Aug. 1999.

[4] Federal Communications Commission (FCC), *"Second Report and Order and Memorandum Opinion and Order In Matter of Unlicensed Operation in the TV Broadcast Bands, Additional Spectrum for Unlicensed Devices Below 900 MHz and in the 3 GHz Band, Document 08-260,"* Nov. 2008.

[5] UK Office of Communications (Ofcom), *"Decision to make the Wireless Telegraphy (White Space Devices),"* Dec. 2015. [Online]. Available: http://stakeholders.ofcom.org.uk/binaries/spectrum/whitespaces/regulations-2015/Statement_on_LE_regulations_draft_FINAL.pdf

[6] I. F. Akyildiz, W.-Y. Lee, M. C. Vuran, and S. Mohanty, "Next generation/dynamic spectrum access/cognitive radio wireless networks: a survey," *Computer Netw.*, vol. 50, no. 13, pp. 2127–2159, 2006.

[7] H. Sun, A. Nallanathan, C.-X. Wang, and Y. Chen, "Wideband spectrum sensing for cognitive radio networks: a survey," *IEEE Wireless Commun.*, vol. 20, no. 2, pp. 74–81, Mar. 2013.

[8] Z. Tian and G. Giannakis, "Compressed sensing for wideband cognitive radios," in *Proc. IEEE Intl. Conf. Acoust. Speech Signal Process. (ICASSP)*, Honolulu, HI, Apr. 2007, pp. 1357–1360.

[9] B. Farhang-Boroujeny, "Filter bank spectrum sensing for cognitive radios," *IEEE Trans. Signal Process.*, vol. 56, no. 5, pp. 1801–1811, May. 2008.

[10] Z. Quan, S. Cui, A. H. Sayed, and H. V. Poor, "Optimal multiband joint detection for spectrum sensing in cognitive radio networks," *IEEE Trans. Signal Process.*, vol. 57, no. 3, pp. 1128–1140, Feb. 2009.

[11] H. Sun, D. I. Laurenson, and C. X. Wang, "Computationally tractable model of energy detection performance over slow fading channels," *IEEE Commun. Lett.*, vol. 14, no. 10, pp. 924–926, Oct. 2010.

[12] R. Zhang and C. K. Ho, "MIMO broadcasting for simultaneous wireless information and power transfer," *IEEE Trans. Commun.*, vol. 12, no. 5, pp. 1989–2001, Mar. 2013.

[13] H. Landau, "Necessary density conditions for sampling and interpolation of certain entire functions," *Acta Math.*, vol. 117, no. 1, pp. 37–52, Jul. 1967.

[14] E. Candes, "Compressive sampling," in *Proc. Intl. Congress Math.*, vol. 3, Madrid, Spain, Oct. 2006, pp. 1433–1452.

[15] J. Treichler, M. Davenport, and R. Baraniuk, "Application of compressive sensing to the design of wideband signal acquisition receivers," *US/Australia Joint Work. Defense Apps. Signal Process. (DASP)*, vol. 5, Apr. 2009.

[16] A. Ghasemi and E. Sousa, "Collaborative spectrum sensing for opportunistic access in fading environments," in *Proc. IEEE Int. Symp. Dynamic Spect. Access Netw. (DYSPAN)*, Baltimore, MD, Nov. 2005, pp. 131 –136.

[17] A. Ian, L. Brandon, and B. Ravikumar, "Cooperative spectrum sensing in cognitive radio networks: A survey," *Physical Commun.*, vol. 4, no. 1, pp. 40–62, Mar. 2011.

[18] Y. Wang, Z. Tian, and C. Feng, "Collecting detection diversity and complexity gains in cooperative spectrum sensing," *IEEE Trans. Wireless Commun.*, vol. 11, no. 8, pp. 2876 –2883, Aug. 2012.

[19] V. Raghunathan, S. Ganeriwal, and M. Srivastava, "Emerging techniques for long lived wireless sensor networks," *IEEE Commun. Mag.*, vol. 44, no. 4, pp. 108–114, May. 2006.

[20] T. Le, K. Mayaram, and T. Fiez, "Efficient far-field radio frequency energy harvesting for passively powered sensor networks," *IEEE J. Solid-State Circuits*, vol. 43, no. 5, pp. 1287–1302, May. 2008.

[21] D. Donoho, "Compressed sensing," *IEEE Trans. Inf. Theory*, vol. 52, no. 4, pp. 1289 –1306, Apr. 2006.

[22] E. J. Candes, J. Romberg, and T. Tao, "Robust uncertainty principles: Exact

signal reconstruction from highly incomplete frequency information," *IEEE Trans. Inf. Theory*, vol. 52, no. 2, pp. 489–509, Feb. 2006.

[23] E. J. Candes and T. Tao, "Near-optimal signal recovery from random projections: Universal encoding strategies?" *IEEE Trans. Inf. Theory*, vol. 52, no. 12, pp. 5406–5425, Dec. 2006.

[24] R. Baraniuk, "Compressive sensing [lecture notes]," *IEEE Signal. Proc. Mag.*, vol. 24, no. 4, pp. 118–121, Jul. 2007.

[25] B. Bah and J. Tanner, "Improved bounds on restricted isometry constants for gaussian matrices," *SIAM J. Matrix Analysis Applications*, vol. 31, no. 5, pp. 2882–2898, 2010.

[26] G. Zhang, S. Jiao, X. Xu, and L. Wang, "Compressed sensing and reconstruction with bernoulli matrices," in *Proc. IEEE Intl. Conf. Info. Automation (ICIA)*, Harbin,China, Jun. 2010, pp. 455–460.

[27] E. Candes and J. Romberg, "Sparsity and incoherence in compressive sampling," *Inverse problems*, vol. 23, no. 3, p. 969, Apr. 2007.

[28] J. Tropp, J. Laska, M. Duarte, J. Romberg, and R. Baraniuk, "Beyond nyquist: Efficient sampling of sparse bandlimited signals," *IEEE Trans. Inf. Theory*, vol. 56, no. 1, pp. 520–544, Jan. 2010.

[29] M. Mishali and Y. Eldar, "From theory to practice: Sub-nyquist sampling of sparse wideband analog signals," *IEEE J. Sel. Areas Signal. Proc.*, vol. 4, no. 2, pp. 375–391, Apr. 2010.

[30] R. Venkataramani and Y. Bresler, "Perfect reconstruction formulas and bounds on aliasing error in sub-Nyquist nonuniform sampling of multiband signals," *IEEE Trans. Inf. Theory*, vol. 46, no. 6, pp. 2173–2183, Sep. 2000.

[31] S. Chen and D. Donoho, "Basis pursuit," in *Proc. Asilomar Conf. Signals Systems Comput.*, vol. 1, Oct. 1994, pp. 41–44.

[32] E. J. Candes and T. Tao, "Decoding by linear programming," *IEEE Trans. Inf. Theory*, vol. 51, no. 12, pp. 4203–4215, Dec. 2005.

[33] G. Michael and P. B. Stephen, "CVX: Matlab software for disciplined convex programming, version 2.0(beta)," Mar. 2013.

[34] K. Hayashi, M. Nagahara, and T. Tanaka, "A user's guide to compressed sensing for communications systems," *IEICE Trans. Commun.*, vol. 96, no. 3, pp. 685–712, Mar. 2013.

[35] E. Candes and J. Romberg, "l_1-magic: Recovery of sparse signals via convex programming," *URL: www. acm. caltech. edu/l1magic/downloads/l1magic. pdf*, vol. 4, Oct. 2005.

[36] S. Becker, J. Bobin, and E. J. Candès, "Nesta: A fast and accurate first-order method for sparse recovery," *SIAM J. Imaging Sciences*, vol. 4, no. 1, pp. 1–39, Jun. 2011.

[37] E. Van Den Berg and M. P. Friedlander, "Probing the pareto frontier for basis pursuit solutions," *SIAM J. Scientific Comput.*, vol. 31, no. 2, pp. 890–912, May. 2008.

[38] E. T. Hale, W. Yin, and Y. Zhang, "A fixed-point continuation method for l_1-regularized minimization with applications to compressed sensing," *CAAM TR07-07, Rice University*, Jul. 2007.

[39] W. Yin, S. Osher, D. Goldfarb, and J. Darbon, "Bregman iterative algorithms for l1 minimization with applications to compressed sensing," *SIAM J. Imaging Sciences*, vol. 1, no. 1, pp. 143–168, Mar. 2008.

[40] S. J. Wright, R. D. Nowak, and M. A. Figueiredo, "Sparse reconstruction by separable approximation," *IEEE Trans. Signal Process.*, vol. 57, no. 7, pp. 2479–2493, Jul. 2009.

[41] J. A. Tropp, "Greed is good: algorithmic results for sparse approximation," *IEEE Trans. Inf. Theory*, vol. 50, no. 10, pp. 2231–2242, Oct. 2004.

[42] Y. C. Pati, R. Rezaiifar, and P. S. Krishnaprasad, "Orthogonal matching pursuit: recursive function approximation with applications to wavelet decomposition," in *Proc. Asilomar Conf. Signals System Comput.*, Nov. 1993, pp. 40–44 vol.1.

[43] D. Needell and J. A. Tropp, "CoSaMP: Iterative signal recovery from incomplete and inaccurate samples," *Applied Comput. Harmonic Analysis*, vol. 26, no. 3, pp. 301–321, Jul. 2008.

[44] S. Kher, T. S. Ganesh, P. Ramesh, and A. K. Somani, "Greedy dynamic crossover

management in hardware accelerated genetic algorithm implementations using fpga," in *Proc. Intl. Conf. Comput. Modelling Simu. (UKSIM)*, Cambridge, UK, Mar. 2009, pp. 47–52.

[45] R. Chartrand and V. Staneva, "Restricted isometry properties and nonconvex compressive sensing," *Inverse Problems*, vol. 24, no. 3, p. 035020, May. 2008.

[46] R. Chartrand, "Exact reconstruction of sparse signals via nonconvex minimization," *IEEE Signal Process. Lett.*, vol. 14, no. 10, pp. 707–710, Oct. 2007.

[47] I. F. Gorodnitsky and B. D. Rao, "Sparse signal reconstruction from limited data using FOCUSS: a re-weighted minimum norm algorithm," *IEEE Trans. Signal Process.*, vol. 45, no. 3, pp. 600–616, Mar. 1997.

[48] R. Chartrand and W. Yin, "Iteratively reweighted algorithms for compressive sensing," in *Proc. IEEE Intl. Conf. Acoust. Speech Signal Process. (ICASSP)*, Las Vegas, NV, Mar. 2008, pp. 3869–3872.

[49] E. J. Candes, M. B. Wakin, and S. P. Boyd, "Enhancing sparsity by reweighted l_1 minimization," *J. of Fourier Analysis and Applications*, vol. 14, no. 5-6, pp. 877–905, 2008.

[50] D. Wipf and S. Nagarajan, "Iterative reweighted l_1 and l_2 methods for finding sparse solutions," *IEEE J. Sel. Areas Signal. Proc.*, vol. 4, no. 2, pp. 317–329, Apr. 2010.

[51] D. P. Wipf and B. D. Rao, "Sparse bayesian learning for basis selection," *IEEE Trans. Signal Process.*, vol. 52, no. 8, pp. 2153–2164, Aug. 2004.

[52] S. Ji, Y. Xue, and L. Carin, "Bayesian compressive sensing," *IEEE Trans. Signal Process.*, vol. 56, no. 6, pp. 2346–2356, Jun. 2008.

[53] M. B. Wakin, M. F. Duarte, S. Sarvotham, D. Baron, and R. G. Baraniuk, "Recovery of jointly sparse signals from few random projections," in *Proc. Neural Inform. Processing Systems (NIPS)*, Dec. 2005.

[54] J. A. Tropp, A. C. Gilbert, and M. J. Strauss, "Simultaneous sparse approximation via greedy pursuit," in *Proc. IEEE Intl. Conf. Acoust. Speech Signal Process. (ICASSP)*, vol. 5, Mar. 2005, pp. v/721–v/724 Vol. 5.

[55] S. F. Cotter, B. D. Rao, K. Engan, and K. Kreutz-Delgado, "Sparse solutions to

linear inverse problems with multiple measurement vectors," *IEEE Trans. Signal Process.*, vol. 53, no. 7, pp. 2477–2488, Jul. 2005.

[56] E. Candes and B. Recht, "Exact low-rank matrix completion via convex optimization," in *Proc. Allerton Conf. on Commun. Control Comput.*, Urbana-Champaign, IL, May. 2008, pp. 806–812.

[57] J.-F. Cai, E. J. Candes, and Z. Shen, "A singular value thresholding algorithm for matrix completion," *SIAM J. Optimization*, vol. 20, no. 4, pp. 1956–1982, Jan. 2010.

[58] K.-C. Toh and S. Yun, "An accelerated proximal gradient algorithm for nuclear norm regularized linear least squares problems," *Pacific J. Optimization*, vol. 6, no. 615-640, p. 15, 2010.

[59] S. Ma, D. Goldfarb, and L. Chen, "Fixed point and bregman iterative methods for matrix rank minimization," *Math. Programming*, vol. 128, no. 1-2, pp. 321–353, Jun. 2011.

[60] R. H. Keshavan and S. Oh, "A gradient descent algorithm on the grassman manifold for matrix completion," *CoRR*, vol. abs/0910.5260, Nov. 2009.

[61] K. Lee and Y. Bresler, "Admira: Atomic decomposition for minimum rank approximation," *IEEE Trans. Inf. Theory*, vol. 56, no. 9, pp. 4402–4416, Aug. 2010.

[62] Z. Wen, W. Yin, and Y. Zhang, "Solving a low-rank factorization model for matrix completion by a nonlinear successive over-relaxation algorithm," *Math. Programming Comput.*, vol. 4, no. 4, pp. 333–361, Jul. 2012.

[63] N. Boumal and P.-A. Absil, "RTRMC: A Riemannian trust-region method for low-rank matrix completion," in *Proc. Advances Neural Info. Process. Systems 24 (NIPS)*, Dec. 2011, pp. 406–414.

[64] Y. Liu, Z. Ding, M. Elkashlan, and J. Yuan, "Non-orthogonal multiple access in large-scale underlay cognitive radio networks," *IEEE Trans. Veh. Technol.*, vol. PP, no. 99, pp. 1–1, 2016.

[65] M. Nekovee, "Impact of cognitive radio on future management of spectrum," in *Proc. Intl. Conf. Cognitive Radio Oriented Wireless Netw. Commun. (CrownCom)*, Singapore, May. 2008, pp. 1–6.

[66] D. Bhargavi and C. R. Murthy, "Performance comparison of energy, matched-filter and cyclostationarity-based spectrum sensing," in *Proc. Intl. Workshop Signal Process. Advances Wireless Commun. (SPAWC)*, June 2010, pp. 1–5.

[67] G. Ganesan and Y. Li, "Cooperative spectrum sensing in cognitive radio networks," in *Proc. IEEE Int. Symp. Dynamic Spect. Access Netw. (DYSPAN)*, Baltimore, MD, Nov. 2005, pp. 137–143.

[68] A. Zakaria, M. Tahir, N. Ramli, H. Mohamad, and M. Ismail, "Performance evaluation of centralized and decentralized cooperative spectrum sensing in cognitive radio networks," in *Proc. Intl Conf. Comput. Commun. Eng. (ICCCE)*, Kuala Lumpur, Malaysia, Jul. 2012, pp. 283 –288.

[69] Federal Communications Commission (FCC), *"Second Report and Order And Memorandum Opinion and Order, FCC 08-260 ET Docket No.04-186,"* Nov. 2009.

[70] Federal Communications Commission (FCC), *"FCC Frees Up Vacant TV Airwaves for 'Super Wi-Fi,' Technologies and Other Technologies,"* Sep. 2010.

[71] UK Office of Communications (Ofcom), "Implementing TV White Spaces," Feb. 2015. [Online]. Available: http://stakeholders.ofcom.org.uk/binaries/consultations/white-space-coexistence/statement/tvws-statement.pdf

[72] S. J. Shellhammer, "A comparison of geo-location and spectrum sensing in cognitive radio," in *Proc. IEEE Intl. Conf. Comput. Commun. Netw. (ICCCN)*. IEEE, 2009, pp. 1–6.

[73] H. R. Karimi, "Geolocation databases for white space devices in the UHF TV bands: Specification of maximum permitted emission levels," in *Proc. IEEE Int. Symp. Dynamic Spect. Access Netw. (DYSPAN)*, May. 2011, pp. 443–454.

[74] V. Petrini and H. Karimi, "TV white space databases: algorithms for the calculation of maximum permitted radiated power levels," in *Proc. IEEE Int. Symp. Dynamic Spect. Access Netw. (DYSPAN)*, Bellevue, WA, Oct. 2012, pp. 552–560.

[75] U.K. Television Stations (UHF Digital System). [Online]. Available: http://www.wolfbane.com/ukdtt.htm

[76] UK Office of Communications (Ofcom), "TV white spaces- approach to coexistence," Sep, 2013. [Online]. Available: http://stakeholders.ofcom.org.uk/

consultations/white-space-coexistence/

[77] S. C. Schwartz and Y.-S. Yeh, "On the distribution function and moments of power sums with log-normal components," *Bell System Technical J.*, vol. 61, no. 7, pp. 1441–1462, Sep. 1982.

[78] Y. Wang, Z. Tian, and C. Feng, "Sparsity order estimation and its application in compressive spectrum sensing for cognitive radios," *IEEE Trans. Wireless Commun.*, vol. 11, no. 6, pp. 2116–2125, 2012.

[79] H. Sun, W.-Y. Chiu, and A. Nallanathan, "Adaptive compressive spectrum sensing for wideband cognitive radios," *IEEE Commun. Lett.*, vol. 16, no. 11, pp. 1812–1815, Nov. 2012.

[80] V. Havary-Nassab, S. Hassan, and S. Valaee, "Compressive detection for wideband spectrum sensing," in *Proc. IEEE Intl. Conf. Acoust. Speech Signal Process. (ICASSP)*, Dallas, TX, 2010, pp. 3094–3097.

[81] F. Zeng, C. Li, and Z. Tian, "Distributed compressive spectrum sensing in cooperative multihop cognitive networks," *IEEE J. Sel. Areas Signal. Proc.*, vol. 5, no. 1, pp. 37 –48, Feb. 2011.

[82] F. F. Digham, M.-S. Alouini, and M. K. Simon, "On the energy detection of unknown signals over fading channels," *IEEE Trans. Commun.*, vol. 55, no. 1, pp. 21–24, Jan. 2007.

[83] Z. Tian, "Compressed wideband sensing in cooperative cognitive radio networks," in *Proc. IEEE Global Commun. Conf. (GLOBECOM)*, New Orleans, LA, Dec. 2008, pp. 3756–3760.

[84] J. Bazerque and G. Giannakis, "Distributed spectrum sensing for cognitive radio networks by exploiting sparsity," *IEEE Trans. Signal Process.*, vol. 58, no. 3, pp. 1847–1862, Mar. 2010.

[85] Z. Li, F. R. Yu, and M. Huang, "A distributed consensus-based cooperative spectrum-sensing scheme in cognitive radios," *IEEE Trans. Veh. Technol.*, vol. 59, no. 1, pp. 383–393, Jan. 2010.

[86] W. Zhang, R. Mallik, and K. Letaief, "Optimization of cooperative spectrum sensing with energy detection in cognitive radio networks," *IEEE Trans. Wireless*

Commun., vol. 8, no. 12, pp. 5761–5766, Dec. 2009.

[87] Y. Zeng, Y.-C. Liang, A. T. Hoang, and R. Zhang, "A review on spectrum sensing for cognitive radio: Challenges and solutions," *EURASIP J. Adv. Signal Process*, vol. 2010, pp. 1–15, Jan. 2010.

[88] J. Meng, W. Yin, H. Li, E. Houssain, and Z. Han, "Collaborative spectrum sensing from sparse observations using matrix completion for cognitive radio networks," in *Proc. IEEE Intl. Conf. Acoust. Speech Signal Process. (ICASSP)*, Dallas, TX, Mar. 2010, pp. 3114 –3117.

[89] J. Meng, W. Yin, H. Li, E. Hossain, and Z. Han, "Collaborative spectrum sensing from sparse observations in cognitive radio networks," *IEEE J. Sel. Areas Commun.*, vol. 29, no. 2, pp. 327–337, Feb. 2011.

[90] Z. Ye, G. Memik, and J. Grosspietsch, "Energy detection using estimated noise variance for spectrum sensing in cognitive radio networks," in *Proc. IEEE Wireless Commun. Netw. Conf. (WCNC)*, Las Vegas, NV, Mar. 2008, pp. 711–716.

[91] N. Wang, Y. Gao, and X. Zhang, "Adaptive spectrum sensing algorithm under different primary user utilizations," *IEEE Commun. Lett.*, vol. 17, no. 9, pp. 1838–1841, Sep. 2013.

[92] RFeye Node. [Online]. Available: http://www.crfs.com/products/rf-sensor-rfeye-node/

[93] "IEEE Standard for Wireless Regional Area Networks Part 22: Cognitive Wireless RAN MAC & PHY Specifications: Policies and Procedures for Operation in the TV Bands," *IEEE Std. 802.22-2011*, 2011.

[94] Q. Ling and Z. Tian, "Decentralized support detection of multiple measurement vectors with joint sparsity," in *Proc. IEEE Intl. Conf. Acoust. Speech Signal Process. (ICASSP)*, Prague, Czech, May. 2011, pp. 2996–2999.

[95] T. Yucek and H. Arslan, "A survey of spectrum sensing algorithms for cognitive radio applications," *IEEE Commun. Surveys Tuts.*, vol. 11, no. 1, pp. 116–130, Mar. 2009.

[96] E. Candes and B. Recht, "Exact matrix completion via convex optimization," *Foundations of Comput. math.*, vol. 9, no. 6, pp. 717–772, Apr. 2009.

[97] F. Paisana, N. Marchetti, and L. DaSilva, "Radar, TV and cellular bands: Which spectrum access techniques for which bands?" *IEEE Commun. Surveys Tuts.*, vol. 16, no. 3, pp. 1193–1220, Third Quarter 2014.

[98] J. Ribeiro, J. Rodriguez, R. Dionisio, H. Esteves, P. Duarte, and P. Marques, "Testbed for combination of local sensing with geolocation database in real environments," *IEEE Wireless Commun.*, vol. 19, no. 4, pp. 59–66, Aug. 2012.

[99] J. Wang, G. Ding, Q. Wu, L. Shen, and F. Song, "Spatial-temporal spectrum hole discovery: a hybrid spectrum sensing and geolocation database framework," *Chinese Science Bulletin*, vol. 59, no. 16, pp. 1896–1902, 2014.

[100] N. Wang, Y. Gao, and B. Evans, "Database-augmented spectrum sensing algorithm for cognitive radio," in *Proc. IEEE Int. Conf. Commun. (ICC)*, London, UK, Jun. 2015, pp. 7468–7473.

[101] R. E. Carrillo and K. Barner, "Iteratively re-weighted least squares for sparse signal reconstruction from noisy measurements," in *Proc. Conf. Info. Sciences Systems (CISS)*, Baltimore, MD, Mar. 2009, pp. 448–453.

[102] R. Saab and Ö. Yılmaz, "Sparse recovery by non-convex optimization–instance optimality," *Applied and Comput. Harmonic Analysis*, vol. 29, no. 1, pp. 30–48, Jul. 2010.

[103] D. Ba, B. Babadi, P. Purdon, and E. Brown, "Convergence and stability of iteratively re-weighted least squares algorithms," *IEEE Trans. Signal Process.*, vol. 62, no. 1, pp. 183–195, Jan. 2014.

[104] O. Escoda, L. Granai, and P. Vandergheynst, "On the use of a priori information for sparse signal approximations," *IEEE Trans. Signal Process.*, vol. 54, no. 9, pp. 3468–3482, Sep. 2006.

[105] M. Friedlander, H. Mansour, R. Saab, and O. Yilmaz, "Recovering compressively sampled signals using partial support information," *IEEE Trans. Inf. Theory*, vol. 58, no. 2, pp. 1122–1134, Feb. 2012.

[106] W. Lu and N. Vaswani, "Regularized modified BPDN for noisy sparse reconstruction with partial erroneous support and signal value knowledge," *IEEE Trans. Signal Process.*, vol. 60, no. 1, pp. 182–196, Jan. 2012.

[107] C. J. Miosso, R. von Borries, M. Argaez, L. Velázquez, C. Quintero, and C. Potes, "Compressive sensing reconstruction with prior information by iteratively reweighted least-squares," *IEEE Trans. Signal Process.*, vol. 57, no. 6, pp. 2424–2431, Jun. 2009.

[108] O. Holland, S. Ping, A. Aijaz, J. Chareau, P. Chawdhry, Y. Gao, Z. Qin, and H. Kokkinen, "To white space or not to white space: That is the trial within the ofcom TV white spaces pilot," in *Proc. IEEE Int. Symp. Dynamic Spect. Access Netw. (DYSPAN)*, Stockholm, Sweden, Sep. 2015, pp. 11–22.

[109] L. Fenton, "The sum of log-normal probability distributions in scatter transmission systems," *IRE Trans. Commun. Systems*, vol. 8, no. 1, pp. 57–67, Mar. 1960.

[110] G. Ding, Q. Wu, Y.-D. Yao, J. Wang, and Y. Chen, "Kernel-based learning for statistical signal processing in cognitive radio networks: Theoretical foundations, example applications, and future directions," *IEEE Signal. Proc. Mag.*, vol. 30, no. 4, pp. 126–136, Jun. 2013.

[111] Q. Yan, M. Li, T. Jiang, W. Lou, and Y. Hou, "Vulnerability and protection for distributed consensus-based spectrum sensing in cognitive radio networks," in *Proc. IEEE Intl. Conf. Comput. Commun. (INFOCOM)*, Mar. 2012, pp. 900–908.

[112] L. Zhang, G. Ding, Q. Wu, Y. Zou, Z. Han, and J. Wang, "Byzantine attack and defense in cognitive radio networks: A survey," *IEEE Commun. Surveys Tuts.*, vol. 17, no. 3, pp. 1342–1363, Apr. 2015.

[113] W. Wang, H. Li, Y. Sun, and Z. Han, "Attack-proof collaborative spectrum sensing in cognitive radio networks," in *Proc. Conf. Info. Sciences Systems (CISS)*, Mar. 2009, pp. 130–134.

[114] ——, "Securing collaborative spectrum sensing against untrustworthy secondary users in cognitive radio networks," *EURASIP J. Adv. Signal Process.*, vol. 2010, pp. 1–15, Jan. 2010.

[115] R. Chen, J.-M. Park, and K. Bian, "Robust distributed spectrum sensing in cognitive radio networks," in *Proc. IEEE Intl. Conf. Comput. Commun. (INFOCOM)*, Phoenix, AZ, Apr. 2008, pp. 13–18.

[116] P. Kaligineedi, M. Khabbazian, and V. Bhargava, "Secure cooperative sensing

techniques for cognitive radio systems," in *Proc. IEEE Int. Conf. Commun. (ICC)*, Beijing, China, Jun. 2008, pp. 3406–3410.

[117] P. Kaligineedi, M. Khabbazian, and V. K. Bhargava, "Malicious user detection in a cognitive radio cooperative sensing system," *IEEE Trans. Wireless Commun.*, vol. 9, no. 8, pp. 2488–2497, Jun. 2010.

[118] S. Kalamkar, A. Banerjee, and A. Roychowdhury, "Malicious user suppression for cooperative spectrum sensing in cognitive radio networks using dixon's outlier detection method," in *Proc. National Conf. Commun. (NCC)*, Kharagpur, Feb. 2012, pp. 1–5.

[119] H. Li and Z. Han, "Catch me if you can: An abnormality detection approach for collaborative spectrum sensing in cognitive radio networks," *IEEE Trans. Wireless Commun.*, vol. 9, no. 11, pp. 3554–3565, Nov. 2010.

[120] W. Wang, L. Chen, K. Shin, and L. Duan, "Secure cooperative spectrum sensing and access against intelligent malicious behaviors," in *Proc. IEEE Intl. Conf. Comput. Commun. (INFOCOM)*, Toronto, ON, Apr. 2014, pp. 1267–1275.

[121] ——, "Thwarting intelligent malicious behaviors in cooperative spectrum sensing," *IEEE Trans. Mobile Commun.*, vol. 14, no. 11, pp. 2392–2405, Nov. 2015.

[122] H. Li, "Reconstructing spectrum occupancies for wideband cognitive radio networks: A matrix completion via belief propagation," in *Proc. IEEE Int. Conf. Commun. (ICC)*, Cape Town, South Africa, May 2010, pp. 1–6.

[123] M. Yan, Y. Yang, and S. Osher, "Exact low-rank matrix completion from sparsely corrupted entries via adaptive outlier pursuit," *J. Sci. Comput.*, vol. 56, no. 3, pp. 433–449, Sep. 2013.

[124] K. Huang and V. K. Lau, "Enabling wireless power transfer in cellular networks: architecture, modeling and deployment," *IEEE Trans. Wireless Commun.*, vol. 13, no. 2, pp. 902–912, Feb. 2014.

[125] Z. Ding, S. M. Perlaza, I. Esnaola, and H. V. Poor, "Power allocation strategies in energy harvesting wireless cooperative networks," *IEEE Trans. Wireless Commun.*, vol. 13, no. 2, pp. 846–860, Jan. 2014.

[126] Y. Liu, L. Wang, T. T. Duy, M. Elkashlan, and T. Q. Duong, "Relay selection for

security enhancement in cognitive relay networks," *IEEE Wirel. Commun. Lett.*, vol. 4, no. 1, pp. 46–49, Feb. 2015.

[127] Y. Liu, Z. Ding, M. Elkashlan, and H. V. Poor, "Cooperative non-orthogonal multiple access with simultaneous wireless information and power transfer," *IEEE J. Sel. Areas Commun.*, vol. 34, no. 4, pp. 938–953, Apr. 2016.

[128] X. Lu, P. Wang, D. Niyato, and E. Hossain, "Dynamic spectrum access in cognitive radio networks with RF energy harvesting," *IEEE Wireless Commun.*, vol. 21, no. 3, pp. 102–110, Jun. 2014.

[129] Y. L. Che, L. Duan, and R. Zhang, "Spatial throughput maximization of wireless powered communication networks," *IEEE J. Sel. Areas Commun.*, vol. 33, no. 8, pp. 1534–1548, Jul. 2015.

[130] S. Park, H. Kim, and D. Hong, "Cognitive radio networks with energy harvesting," *IEEE Trans. Wireless Commun.*, vol. 12, no. 3, pp. 1386–1397, Mar. 2013.

[131] S. Park and D. Hong, "Optimal spectrum access for energy harvesting cognitive radio networks," *IEEE Trans. Wireless Commun.*, vol. 12, no. 12, pp. 6166–6179, Nov. 2013.

[132] W. Chung, S. Park, S. Lim, and D. Hong, "Spectrum sensing optimization for energy-harvesting cognitive radio systems," *IEEE Trans. Wireless Commun.*, vol. 13, no. 5, pp. 2601–2613, Apr. 2014.

[133] J. Venkataraman, M. Haenggi, and O. Collins, "Shot noise models for outage and throughput analyses in wireless Ad Hoc networks," in *Proc. Military Commun. Conf. (MILCOM)*, Oct. 2006, pp. 1–7.

[134] Y. Liu, S. Mousavifar, Y. Deng, C. Leung, and M. Elkashlan, "Wireless energy harvesting in a cognitive relay network," *IEEE Trans. Wireless Commun.*, Dec. 2015.

[135] I. Krikidis, S. Sasaki, S. Timotheou, and Z. Ding, "A low complexity antenna switching for joint wireless information and energy transfer in mimo relay channels," *IEEE Trans. Commun.*, vol. 62, no. 5, pp. 1577–1587, May 2014.

[136] Y.-C. Liang, Y. Zeng, E. Peh, and A. T. Hoang, "Sensing-throughput tradeoff for cognitive radio networks," *IEEE Trans. Wireless Commun.*, vol. 7, no. 4, pp.

1326–1337, Apr. 2008.

[137] I. S. Gradshteyn and I. M. Ryzhik, *Table of Integrals, Series and Products*, 6th ed. New York, NY: Academic Press, 2000.

[138] E. J. Candè and M. B. Wakin, "An introduction to compressive sampling," *IEEE Signal. Proc. Mag.*, vol. 25, no. 2, pp. 21–30, Mar. 2008.

[139] E. J. Candes and Y. Plan, "Matrix completion with noise," *Proc. IEEE*, vol. 98, no. 6, pp. 925–936, Mar. 2010.